ISSN 2667-4211

ESKİŞEHİR TECHNICAL UNIVERSITY JOURNAL OF SCIENCE AND TECHNOLOGY

A – Applied Sciences and Engineering

Volume 24 Number 2 - June - 2023

ESKİŞEHİR TECHNICAL UNIVERSITY JOURNAL OF SCIENCE AND TECHNOLOGY
A- Applied Sciences and Engineering
Eskişehir Teknik Üniversitesi Bilim ve Teknoloji Dergisi A – Uygulamalı Bilimler ve Mühendislik

Volume: 24 / Number: 2 / June - 2023

Eskişehir Technical University Journal of Science and Technology A - Applied Sciences and Engineering (ESTUJST-A) is a peer-reviewed and refereed international journal published by Eskişehir Technical University. Since 2000, it has been regularly published and distributed biannually and it has been published quarterly and only electronically since 2016.
The journal accepts only manuscripts written in English.

The journal issues are published electronically in **March, June**, **September**, and **December**.

Eskişehir Technical University Journal of Science and Technology A - Applied Sciences and Engineering is an international peer-reviewed and refereed journal published by Eskişehir Technical University.

The journal is dedicated to the dissemination of knowledge in applied sciences and engineering disciplines.

The journal aims to publish high quality, original international scientific research articles with specific contributions to the literature in the field of engineering and applied sciences. The journal publishes research papers in the fields of applied science and technology such as Physics, Biology, Mathematics, Statistics, Chemistry and Chemical Engineering, Environmental Sciences and Engineering, Civil Engineering, Earth and Atmospheric Sciences, Electrical and Electronical Engineering, Computer Science and Informatics, Materials Sciences and Engineering, Mechanical Engineering, Mining Engineering, Industrial Engineering, Aeronautics and Astronautics, Pharmaceutical Sciences.

The journal publishes original research articles and special issue articles.
All articles are peer-reviewed and the articles that have been evaluated are ensured to meet with researchers as soon as possible.

"Anadolu Üniversitesi Bilim ve Teknoloji Dergisi A - Uygulamalı Bilimler ve Mühendislik (Anadolu University Journal of Science and Technology A - Applied Sciences and Engineering)" published within Anadolu University started to be published within Eskişehir Technical University which was established due to statute law 7141, in 2018. Hence, the name of the journal is changed to " Eskişehir Technical University Journal of Science and Technology A - Applied Sciences and Engineering (Eskişehir Teknik Üniversitesi Bilim ve Teknoloji Dergisi A - Uygulamalı Bilimler ve Mühendislik)".

Indexed by **ULAKBIM TR Dizin**

ESKİŞEHİR TECHNICAL UNIVERSITY JOURNAL OF SCIENCE AND TECHNOLOGY
A- Applied Sciences and Engineering

Eskişehir Teknik Üniversitesi Bilim ve Teknoloji Dergisi A – Uygulamalı Bilimler ve Mühendislik

Volume: 24 / Number: 2 / June– 2023

Owner / Publisher: Prof. Dr. Adnan ÖZCAN for Eskişehir Technical University

CONTACT INFORMATION
Eskişehir Technical Unıversity Journal of Science and Technology
Eskişehir Technical University, Institute of Graduate Programs, 26470 Eskişehir, TURKEY
Phone: +90 222 213 7485
e-mail : btda@eskisehir.edu.tr

ESKİŞEHİR TECHNICAL UNIVERSITY JOURNAL OF SCIENCE AND TECHNOLOGY
A- Applied Sciences and Engineering
Eskişehir Teknik Üniversitesi Bilim ve Teknoloji Dergisi A – Uygulamalı Bilimler ve Mühendislik

Volume: 24 / Number: 2 / June - 2023

ESKİŞEHİR TECHNICAL UNIVERSITY JOURNAL OF SCIENCE AND TECHNOLOGY
A- Applied Sciences and Engineering

Eskişehir Teknik Üniversitesi Bilim ve Teknoloji Dergisi A – Uygulamalı Bilimler ve Mühendislik

ABOUT

Eskişehir Technical University Journal of Science and Technology A - Applied Sciences and Engineering (ESTUJST-A) is a peer-reviewed and refereed international journal published by Eskişehir Technical University. Since 2000, it has been regularly published and distributed biannually and it has been published quarterly and only electronically since 2016.

The journal accepts only manuscripts written in English.

The journal issues are published electronically in **MARCH, JUNE, SEPTEMBER**, and **DECEMBER.**

AIM AND SCOPE

Eskişehir Technical University Journal of Science and Technology A - Applied Sciences and Engineering is an international peer-reviewed and refereed journal published by Eskişehir Technical University.

The journal is dedicated to the dissemination of knowledge in applied sciences and engineering disciplines.

The journal aims to publish high quality, original international scientific research articles with specific contributions to the literature in the field of engineering and applied sciences. The journal publishes research papers in the fields of applied science and technology such as Physics, Biology, Mathematics, Statistics, Chemistry and Chemical Engineering, Environmental Sciences and Engineering, Civil Engineering, Earth and Atmospheric Sciences, Electrical and Electronical Engineering, Computer Science and Informatics, Materials Sciences and Engineering, Mechanical Engineering, Mining Engineering, Industrial Engineering, Aeronautics and Astronautics, Pharmaceutical Sciences.

The journal publishes original research articles and special issue articles. All articles are peer-reviewed and the articles that have been evaluated are ensured to meet with researchers as soon as possible.

PEER REVIEW PROCESS

Manuscripts are first reviewed by the editorial board in terms of its its journal's style rules scientific content, ethics and methodological approach. If found appropriate, the manuscript is then send to at least two renown referees by editor. The decision in line with the referees may be an acceptance, a rejection or an invitation to revise and resubmit. Confidential review reports from the referees will be kept in archive. All submission process manage through the online submission systems.

OPEN ACCESS POLICY

This journal provides immediate open access to its content on the principle that making research freely available to the public supports a greater global exchange of knowledge.

PRICE POLICY

Eskişehir Technical University Journal of Science and Technology A - Journal of Applied Sciences and Engineering is an English, peer-reviewed, scientific, free of charge open-access-based journal. The author is not required to pay any publication fees or article processing charges (APCs) for peer-review administration and management, typesetting, and open-access. Articles also receive Digital Object Identifiers (DOIs) from the CrossRef organization to ensure they are always available.

ETHICAL RULES

You can reach the Ethical Rules in our journal in full detail from the link below:

https://dergipark.org.tr/en/pub/estubtda/policy

Ethical Principles and Publication Policy

Policy & Ethics

Assessment and Publication

As a peer-reviewed journal, it is our goal to advance scientific knowledge and understanding. We adhere to the guideline and ethical standards from the Committee on Publication Ethics (COPE) and the recommendations of ICMJE (International Committee of Medical Journal Editors) regarding all aspects of publication ethics and cases of research and publication misconduct to ensure that all publications represent accurate and original work and that our peer review process is structured without bias. We have outlined a set of ethical principles that must be followed by all authors, reviewers, and editors.

All manuscripts submitted to our journals are pre-evaluated in terms of their relevance to the scope of the journal, language, compliance with writing instructions, suitability for science, and originality, by taking into account the current legal requirements regarding copyright infringement and plagiarism. Manuscripts that are evaluated as insufficient or non-compliant with the instructions for authors may be rejected without peer review.

Editors and referees who are expert researchers in their fields assess scientific manuscripts submitted to our journals. A blind peer review policy is applied to the evaluation process. The Editor-in-Chief, if he/she sees necessary, may assign an Editor for the manuscript or may conduct the scientific assessment of the manuscript himself/herself. Editors may also assign referees for the scientific assessment of the manuscript and make their decisions based on reports by the referees. The Editor-in-Chief makes the final decision regarding the publishing of the manuscript.

Articles are accepted for publication by the Editor-in-Chief in accordance with the COPE (Committee on Publication Ethics). Authors can access this information online via the journals' websites (https://publicationethics.org/). Articles are accepted for publication on the understanding that they have not been published and are not going to be considered for publication elsewhere. Authors should certify that neither the manuscript nor its main contents have already been published or submitted for publication in another journal.

The journal adapts the COPE guidelines to satisfy the high-quality standards of ethics for authors, editors, and reviewers:

Duties of Editors-in-Chief and co-Editors

The crucial role of the journal Editor-in-Chief and co-Editors is to monitor and ensure the fairness, timeliness, thoroughness, and civility of the peer-review editorial process. The main responsibilities of Editors-in-Chief are as follows:

• Selecting manuscripts suitable for publication while rejecting unsuitable manuscripts,
• Ensuring a supply of high-quality manuscripts to the journal by identifying important,
• Increasing the journal's impact factor and maintaining the publishing schedule,
• Providing strategic input for the journal's development,

Duties of Editors

The main responsibilities of editors are as follows:

• An editor must evaluate the manuscript objectively for publication, judging each on its quality without considering the nationality, ethnicity, political beliefs, race, religion, gender, seniority, or institutional affiliation of the author(s). Editors should decline any assignment when there is a potential for conflict of interest.
• Editors must ensure the document(s) sent to the reviewers does not contain information of the author(s) and vice versa.
• Editors' decisions should be provided to the author(s) accompanied by the reviewers' comments and recommendations unless they contain offensive or libelous remarks.
• Editors should respect requests (if well reasoned and practicable) from author(s) that an individual should not review the submission.
• Editors and all staff members should guarantee the confidentiality of the submitted manuscript.
• Editors should have no conflict of interest with respect to articles they reject/accept. They must not have a conflict of interest with the author(s), funder(s), or reviewer(s) of the manuscript.
• Editors should strive to meet the needs of readers and authors and to constantly improve the journal.

Duties of Reviewers/Referees

The main responsibilities of reviewers/referees are as follows:

• Reviewers should keep all information regarding papers confidential and treat them as privileged information.
• Reviews should be conducted objectively, with no personal criticism of the author.
• Reviewers assist in the editorial decision process and as such should express their views clearly with supporting arguments.
• Reviewers should complete their reviews within a specified timeframe (maximum thirty-five (35) days). In the event that a reviewer feels it is not possible for him/her to complete the review of the manuscript within a stipulated time, then this information must be communicated to the editor so that the manuscript could be sent to another reviewer.
• Unpublished materials disclosed in a submitted manuscript must not be used in a reviewer's personal research without the written permission of the author. Information contained in an unpublished manuscript will remain confidential and must not be used by the reviewer for personal gain.
• Reviewers should not review manuscripts in which they have conflicts of interest resulting from competitive, collaborative, or other relationships or connections with any of the authors, companies, or institutions connected to the papers.

• Reviewers should identify similar work in published manuscripts that has not been cited by the author. Reviewers should also notify the Editors of significant similarities and/or overlaps between the manuscript and any other published or unpublished material.

Duties of Authors

The main responsibilities of authors are as follows:

• The author(s) should affirm that the material has not been previously published and that they have not transferred elsewhere any rights to the article.
• The author(s) should ensure the originality of the work and that they have properly cited others' work in accordance with the reference format.
• The author(s) should not engage in plagiarism or in self-plagiarism.
• On clinical and experimental humans and animals, which require an ethical committee decision for research in all branches of science;
All kinds of research carried out with qualitative or quantitative approaches that require data collection from the participants by using survey, interview, focus group work, observation, experiment, interview techniques,
Use of humans and animals (including material/data) for experimental or other scientific purposes,
• Clinical studies on humans,
• Studies on animals,
• Retrospective studies in accordance with the law on the protection of personal data, (Ethics committee approval should have been obtained for each individual application, and this approval should be stated and documented in the article.)
Information about the permission (board name, date, and number) should be included in the "Method" section of the article and also on the first/last page.
During manuscript upload, the "Ethics Committee Approval" file should be uploaded to the system in addition to the manuscript file.
In addition, in case reports, it is necessary to include information on the signing of the informed consent/ informed consent form in the manuscript.
• The author(s) should suggest no personal information that might make the identity of the patient recognizable in any form of description, photograph, or pedigree. When photographs of the patient were essential and indispensable as scientific information, the author(s) have received consent in written form and have clearly stated as much.
• The author(s) should provide the editor with the data and details of the work if there are suspicions of data falsification or fabrication. Fraudulent data shall not be tolerated. Any manuscript with suspected fabricated or falsified data will not be accepted. A retraction will be made for any publication which is found to have included fabricated or falsified data.
• The author(s) should clarify everything that may cause a conflict of interests such as work, research expenses, consultant expenses, and intellectual property.
• The author(s) must follow the submission guidelines of the journal.
• The author(s) discover(s) a significant error and/or inaccuracy in the submitted manuscript at any time, then the error and/or inaccuracy must be reported to the editor.
• The author(s) should disclose in their manuscript any financial or other substantive conflicts of interest that might be construed to influence the results or interpretation of their manuscript. All sources of financial support should be disclosed under the heading of "Acknowledgment" or "Contribution".
• The corresponding author should ensure that all appropriate co-authors and no inappropriate co-authors are included in the paper and that all co-authors have seen and approved the final version of the paper and have agreed to its submission for publication. All those who have made

significant contributions should be listed as co-authors. Others who have participated in certain substantive aspects of the research should be acknowledged or listed under the heading of "Author Contributions".

Cancellations/Returns

Articles/manuscripts may be returned to the authors in order to increase the authenticity and/or reliability and to prevent ethical breaches, and even if articles have been accepted and/or published, they can be withdrawn from publication if necessary. The Editor-in-Chief of the journal has the right to return or withdraw an article/manuscript in the following situations:

• When the manuscript is not within the scope of the journal,
• When the scientific quality and/or content of the manuscript do not meet the standards of the journal and a referee review is not necessary,
• When there is proof of ruling out the findings obtained by the research, (When the article/manuscript is undergoing an assessment or publication process by another journal, congress, conference, etc.,)
• When the article/manuscript was not prepared in compliance with scientific publication ethics,
• When any other plagiarism is detected in the article/manuscript,
• When the authors do not perform the requested corrections within the requested time (maximum twenty-one (21) days),
• When the author does not submit the requested documents/materials/data etc. within the requested time,
• When the requested documents/materials/data etc. submitted by the author are missing for the second time,
• When the study includes outdated data,
• When the authors make changes that are not approved by the editor after the manuscript was submitted,
• When an author is added/removed, the order of the authors is changed, the corresponding author is changed, or the addresses of the authors are changed without the consent of the Editor-in-Chief,
• When a statement is not submitted indicating that approval of the ethics committee permission was obtained for the following (including retrospective studies):
• When human rights or animal rights are violated,

ETHICAL ISSUES

Plagiarism

The use of someone else's ideas or words without a proper citation is considered plagiarism and will not be tolerated. Even if a citation is given, if quotation marks are not placed around words taken directly from other authors' work, the author is still guilty of plagiarism. Reuse of the author's own previously published words, with or without a citation, is regarded as self-plagiarism.

All manuscripts received are submitted to iThenticate®, which compares the content of the manuscript with a database of web pages and academic publications. Manuscripts are judged to be plagiarized or self-plagiarized, based on the iThenticate® report or any other source of information, will be rejected. Corrective actions are proposed when plagiarism and/or self-plagiarism is detected after publication. Editors should analyze the article and decide whether a corrected article or retraction needs to be published.

Open-access theses are considered as published works and they are included in the similarity checks.

iThenticate® report should have a maximum of 11% from a single source, and a maximum of 25% in total.

Conflicts of Interest

Eskişehir Technical University Journal of Science and Technology A - Applied Sciences and Engineering should be informed of any significant conflict of interest of editors, authors, or reviewers to determine whether any action would be appropriate (e.g. an author's statement of conflict of interest for a published work, or disqualifying a referee).

Financial

The authors and reviewers of the article should inform the journal about the financial information that will bring financial gain or loss to any organization from the publication of the article.

*Research funds; funds, consulting fees for a staff member; If you have an interest, such as patent interests, you may have a conflict of interest that needs to be declared.

Other areas of interest

The editor or reviewer may disclose a conflict of interest that, if known, would be embarrassing (for example, an academic affiliation or rivalry,a close relationship or dislike, or a person who may be affected by the publication of the article).

Conflict of interest statement

Please note that a conflict of interest statement is required for all submitted manuscripts. If there is no conflict of interest, please state "There are no conflicts of interest to declare" in your manuscript under the heading "Conflicts of Interest" as the last section before your Acknowledgments.

AUTHOR GUIDELINES

All manuscripts must be submitted electronically.

You will be guided stepwise through the creation and uploading of the various files. There are no page charges. Papers are accepted for publication on the understanding that they have not been published and are not going to be considered for publication elsewhere. Authors should certify that neither the manuscript nor its main contents have already been published or submitted for publication in another journal. We ask a signed copyright to start the evaluation process. After a manuscript has been submitted, it is not possible for authors to be added or removed or for the order of authors to be changed. If authors do so, their submission will be cancelled.

Manuscripts may be rejected without peer review by the editor-in-chief if they do not comply with the instructions to authors or if they are beyond the scope of the journal. After a manuscript has been accepted for publication, i.e. after referee-recommended revisions are complete, the author will not be permitted to make any changes that constitute departures from the manuscript that was accepted by the editor. Before publication, the galley proofs are always sent to the authors for corrections. Mistakes or omissions that occur due to some negligence on our part during final printing will be rectified in an errata section in a later issue.

This does not include those errors left uncorrected by the author in the galley proof. The use of someone else's ideas or words in their original form or slightly changed without a proper citation is considered plagiarism and will not be tolerated. Even if a citation is given, if quotation marks are not placed around words taken directly from another author's work, the author is still guilty of plagiarism. All manuscripts received are submitted to iThenticateR, a plagiarism checking system, which compares the content of the manuscript with a vast database of web pages and academic publications. In the received iThenticateR report; The similarity rate is expected to be below 25%. Articles higher than this rate will be rejected.

Uploading Articles to the Journal

Authors should prepare and upload 2 separate files while uploading articles to the journal. First, the Author names and institution information should be uploaded so that they can be seen, and then (using the additional file options) a separate file should be uploaded with the Author names and institution information completely closed. When uploading their files with closed author names, they will select the "Show to Referee" option, so that the file whose names are closed can be opened to the referees.

Prepatation of Manuscript

Style and Format

Manuscripts should be **single column** by giving one-spaced with 2.5-cm margins on all sides of the page, in Times New Roman font (font size 11). Every page of the manuscript, including the title page, references, tables, etc., should be numbered. All copies of the manuscript should also have line numbers starting with 1 on each consecutive page.

Manuscripts must be upload as word document (*.doc, *.docx vb.). **Please avoid uploading *texts in *.pdf format.***

Symbols, Units and Abbreviations

Standard abbreviations and units should be used; SI units are recommended. Abbreviations should be defined at first appearance, and their use in the title and abstract should be avoided. Generic names of chemicals should be used. Genus and species names should be typed in italic or, if this is not available, underlined.

Please refer to equations with capitalisation and unabbreviated (e.g., as given in Equation (1)).

Manuscript Content

Articles should be divided into logically ordered and numbered sections. Principal sections should be numbered consecutively with Arabic numerals (1. Introduction, 2. Formulation of problem, etc.) and subsections should be numbered 1.1., 1.2., etc. Do not number the Acknowledgements or References sections. The text of articles should be, if possible, divided into the following sections: Introduction, Materials and Methods (or Experimental), Results, Discussion, and Conclusion.

Title and contact information

The first page should contain the full title in sentence case (e.g., Hybrid feature selection for text classification), the full names (last names fully capitalised) and affiliations (in English) of all authors (Department, Faculty, University, City, Country, E-mail), and the contact e-mail address for the clearly identified corresponding author. The first page should contain the full title, abstract and keywords (both English and Turkish).

Abstract

The abstract should provide clear information about the research and the results obtained, and should not exceed 300 words. The abstract should not contain citations and must be written in Times New Roman font with font size 9.

Keywords

Please provide 3 to 5 keywords which can be used for indexing purposes.

Introduction

The motivation or purpose of your research should appear in the "Introduction", where you state the questions you sought to answer, and then provide some of the historical basis for those questions.

Methods

Provide sufficient information to allow someone to repeat your work. A clear description of your experimental design, sampling procedures, and statistical procedures is especially important in papers describing field studies, simulations, or experiments. If you list a product (e.g., animal food, analytical device), supply the name and location of the manufacturer. Give the model number for equipment used.

Results

Results should be stated concisely and without interpretation.

Discussion

Focus on the rigorously supported aspects of your study. Carefully differentiate the results of your study from data obtained from other sources. Interpret your results, relate them to the results of previous research, and discuss the implications of your results or interpretations.

Conclusion

This should state clearly the main conclusions of the research and give a clear explanation of their importance and relevance. Summary illustrations may be included.

Acknowledgments

Acknowledgments of people, grants, funds, etc. should be placed in a separate section before the reference list. The names of funding organizations should be written in full.

Conflict of Interest Statement

The authors are obliged to present the conflict of interest statement at the end of the article after the acknowledgments section.

Author Contributions

All authors, author contributions and contribution rates should be clearly stated.

References

Writting Style; **AMA; References Writting format** should be used in the reference writing of our journal. If necessary, at this point, the reference writings of the articles published in our article can be examined.

Citations in the text should be identified by numbers in square brackets. The list of references at the end of the paper should be given in order of their first appearance in the text. All authors should be included in reference lists unless there are 10 or more, in which case only the first 10 should be given, followed by 'et al.'. Do not use individual sets of square brackets for citation numbers that appear together, e.g., [2,3,5–9], not [2], [3], [5]–[9]. Do not include personal communications, unpublished data, websites, or other unpublished materials as references, although such material may be inserted (in parentheses) in the text. In the case of publications in languages other than English, the published English title should be provided if one exists, with an annotation such as "(article in Turkish with an abstract in English)". If the publication was not published with an English title, cite the original title only; do not provide a self-translation. References should be formatted as follows (please note the punctuation and capitalisation):

Journal articles
Journal titles should be abbreviated according to ISI Web of Science abbreviations.
Guyon I, Elisseeff A. An introduction to variable and feature selection. J Mach Learn Res 2003; 3: 1157-1182.

Izadpanahi S, Ozcınar C, Anbarjafari G, Demirel H. Resolution enhancement of video sequences by using discrete wavelet transform and illumination compensation. Turk J Elec Eng & Comp Sci 2012; 20: 1268-1276.

Books
Haupt RL, Haupt SE. Practical Genetic Algorithms. 2nd ed. New York, NY, USA: Wiley, 2004.
Kennedy J, Eberhart R. Swarm Intelligence. San Diego, CA, USA: Academic Press, 2001.

Chapters in books
Poore JH, Lin L, Eschbach R, Bauer T. Automated statistical testing for embedded systems. In: Zander J, Schieferdecker I, Mosterman PJ, editors. Model-Based Testing for Embedded Systems. Boca Raton, FL, USA: CRC Press, 2012. pp. 111-146.

Conference proceedings
Li RTH, Chung SH. Digital boundary controller for single-phase grid-connected CSI. In: IEEE 2008 Power Electronics Specialists Conference; 15–19 June 2008; Rhodes, Greece. New York, NY, USA: IEEE. pp. 4562-4568.

Theses
Boynukalın Z. Emotion analysis of Turkish texts by using machine learning methods. MSc, Middle East Technical University, Ankara, Turkey, 2012.

Tables and Figures
All illustrations (photographs, drawings, graphs, etc.), not including tables, must be labelled "Figure." Figures must be submitted in the manuscript.

All tables and figures must have a caption and/or legend and be numbered (e.g., Table 1, Figure 2), unless there is only one table or figure, in which case it should be labelled "Table" or "Figure" with no numbering. Captions must be written in sentence case (e.g., Macroscopic appearance of the samples.). The font used in the figures should be Times New Roman. If symbols such as ×, μ, η, or ν are used, they should be added using the Symbols menu of Word.

All tables and figures must be numbered consecutively as they are referred to in the text. Please refer to tables and figures with capitalisation and unabbreviated (e.g., "As shown in Figure 2…", and not "Fig. 2" or "figure 2").

The resolution of images should not be less than 118 pixels/cm when width is set to 16 cm. Images must be scanned at 1200 dpi resolution and submitted in jpeg or tiff format. Graphs and diagrams must be drawn with a line weight between 0.5 and 1 point. Graphs and diagrams with a line weight of less than 0.5 point or more than 1 point are not accepted. Scanned or photocopied graphs and diagrams are not accepted.

Figures that are charts, diagrams, or drawings must be submitted in a modifiable format, i.e. our graphics personnel should be able to modify them. Therefore, if the program with which the figure is drawn has a “save as” option, it must be saved as *.ai or *.pdf. If the “save as” option does not include these extensions, the figure must be copied and pasted into a blank Microsoft Word document as an editable object. It must not be pasted as an image file (tiff, jpeg, or eps) unless it is a photograph.

Tables and figures, including caption, title, column heads, and footnotes, must not exceed 16 × 20 cm and should be no smaller than 8 cm in width. For all tables, please use Word’s “Create Table” feature, with no tabbed text or tables created with spaces and drawn lines. Please do not duplicate information that is already presented in the figures.

Article Corrections and Uploading to the System

Authors should upload the desired edits for their articles without destroying or changing the Template file of the article, by selecting and specifying the relevant edits as Colored, and also submit the Clean version of the article in 2 separate files (using the Additional file option if necessary). * In case of submitting a corrected article, a separate File in Reply to the Referees must be prepared and the "Reply to the Referees" option in the Add additional file option should be checked and uploaded. If a separate file is not prepared in response to the referees, the Author will definitely be asked to upload the relevant file again and the evaluation will be in the pending phase.

ESKİŞEHİR TECHNICAL UNIVERSITY JOURNAL OF SCIENCE AND TECHNOLOGY
A – Applied Sciences and Engineering
Volume: 24 / Number: 2 / June - 2023

CONTENTS

RESEARCH ARTICLE

ESKİŞEHİR TECHNICAL UNIVERSITY JOURNAL OF SCIENCE AND TECHNOLOGY
A- APPLIED SCIENCES AND ENGINEERING

2023, 24(2), pp. 86-106, DOI: 10.18038/estubtda.1201120

RESEARCH ARTICLE

THE EFFECT OF SYNTHETIC FIBER TYPE ON FRESH, HARDENED AND TOUGHNESS PROPERTIES OF HSFR-SCC

Ceren KINA [1]*, Esma BALALAN [2], Kâzım TURK [2]

[1] Department of Civil Engineering, Faculty of Engineering and Natural Sciences, Malatya Turgut Ozal University, Malatya, Türkiye
2 Department of Civil Engineering, Engineering Faculty, Inonu University, Malatya, Türkiye

ABSTRACT

This study presents the experimental results about the effects of Polyvinyl-alcohol (PVA) and Polypropylene (PP) fibers on the fresh and mechanical properties including compressive, splitting tensile strength, modulus of rupture (MOR) as well as toughness of the hybrid fiber reinforced self-compacting concrete (SCC). PVA and PP fibers were added into SCC mixtures having only macro steel fiber and also having binary hybridization of both macro and micro steel fiber. The results showed that the use of micro steel fiber replaced by macro steel fiber improved the workability, compressive and splitting tensile strength, MOR and toughness and also caused reduction in the weight loss percentage compared to the use of only macro steel fiber. Moreover, it was emphasized that PVA or PP enhanced the residual flexural performance of SCC, generally, while it negatively influenced the workability and the residual strengths according to the use of single steel fiber and binary steel fiber hybridization. Compared to the effect of synthetic fibers, PP had slightly more positive effect in the view of workability while PVA enhanced the residual mechanical properties more.

Keywords: Hybrid fiber reinforced self-compacting concrete, Polypropylene fiber, Polyvinyl-alcohol fiber, Strength, Toughness

1. INTRODUCTION

Self-compacting concrete (SCC) was first developed on 20th century in Japan which is one of the countries where earthquakes were experienced most frequently. It was started to be used due to the need for concrete that can be placed into reinforced concrete elements without applying any compression process [1]. It can be classified as high-performance concrete due to having low water-binder ratio achieved by the use of hyper plasticizer additives and being more resistant against external effects. In order to classify a mixture as SCC, the limit values of the workability tests determined by EFNARC [2] committee must be achieved.

The first studies on fiber reinforced concrete (FR-C) were carried out in the mid-20th century to examine the mechanical behavior of steel FR-C [3]. FR-C is defined as concrete reinforced with randomly oriented fibers in the matrix [4]. The use of fibers into the concrete prevents the crack formation. Fibers affect the tensile, compressive and flexural strengths as well as some properties such as creep, shrinkage, impact and fatigue according to many parameters such as type, volume fraction, shape, distribution of fiber, tensile performance, etc. The most important increase in performance of FR-C compared to concrete with no fiber is the energy absorption capacity of concrete during fracture. Fiber types used in the construction industry are generally steel, plastic, synthetic and ceramic-glass fibers. Steel fiber is one of the most widely used fibers in concrete due to their excellent mechanical properties [5]. However, the service life of concrete elements reinforced with steel fiber may be limited by changes in hardened properties due to corrosion in certain specific environments [6]. On the other hand, synthetic fibers offer important benefits as they are resistant to corrosion, chemically inert

*Corresponding Author: ceren.kina@ozal.edu.tr
Received: 08.11.2022 Published:21.06.2023

and stable in alkaline environment [7]. In the past, the aim of the use of synthetic fiber was to minimize the segregation in the fresh state and to resist the stresses obtained from the volumetric change [8]. In today, in order to increase the fracture energy to the cementitious matrices, monofilament and multifilament synthetic fibers were developed. The most commonly utilized synthetic fibers in cement-based composites are PVA, PP, polyethylene (PE). These fibers can improve the ductility of the concrete and reduce cracking. PVA fiber has highest modulus elasticity and durability among all synthetic fibers so it performs well in preventing the crack propagation. Besides, the adherence formed by the matrix with PVA is so high [9]. Dong et al [10] found from their experimental work that the utilization of 0.75% PVA fiber enhanced the porosity, mechanical properties of cementitious composites. In the study of Mostofinejad et al [11] PVA and PP fibers were utilized into ultra-high performance concrete and it was found that PVA fiber enhanced the flexural performance in terms of first-crack strength, ultimate flexural strength and toughness. However, it was emphasized that the use of PP and PP as hybrid showed strain-hardening behaviour and superior mechanical characteristics. Nam et al [12] also investigated the influence of PP and PVA fiber on the cementitious composites and found that PVA fiber showed better freezing thawing resitance. Guo et al [13] observed that the incorporation of PVA and PP fibers caused maximum compressive and flexural strengths with regards to unreinforced samples.

FR-C produced from the hybridization of more than one discontinuous fiber type into traditional concrete matrix is called hybrid fiber reinforced concrete (HFR-C) [14, 15]. In the case of using synthetic and steel fibers (SFs) as hybrid, SFs provide high ductility and superior tensile strength to the matrix and delay the crack initiation and propagation, while PP can alleviate the breakdown of concrete exposed to high temperature [16]. Liu et al [17] noted that the incorporation of steel and PP as hybrid created a positive synergy by effectively improving the strength as well as flexural performance of HFR-C. In the experimental work of Dawood and Hamad [18], it was concluded that flexural toughness increased with increasing fiber volume. Besides, they noted that the best flexural performance for cement-based composite materials was achieved when the fibers were used as hybrid. Ding et al [19] used an improved topographic analysis method and argued that the use of hybrid fiber into cementitious composites will be an important solution in the future to increase the flexural toughness of concrete which is so vital for durability.

There are some experimental and theoretical studies and standards to evaluate the flexural toughness parameters of FR-composites. The most widely used methods are ASTM C1609 [20] and JSCE [21]. The study of Banthia and Trottier [22] found that there are some limitations in all methods for determining the flexural toughness of FR-composites so it makes sense to compare these different methods.

In this study, PVA and PP synthetic fibers were added into single and HSFR-SCC mixtures and thus, binary and ternary HFR-SCC mixtures were designed. As mentioned in the literature, the utilization of fibers as hybrid provides beneficial properties for concrete in terms of mechanical and durability aspects. Within this scope, the incorporation of steel fibers with synthetic fibers is also a promising way to improve the performance of concrete due to their synergies. However, different types of synthetic fibers can cause different impacts on the fresh and hardened properties of steel fiber reinforced concrete mixtures/samples. The objective of this experimental work is to investigate the effect of the use of different synthetic fibers into single and HSFR-SCC mixtures on fresh, hardened and flexural properties. Besides, flexural parameters such as toughness, ductility were also calculated based on ASTM C1609 and JSCE.

2. EXPERIMENTAL METHODS

2.1. Materials

CEM I 42.5R Portland Cement (PC) and Class-F fly ash (FA) were used as binder in the production of fiber reinforced SCC mixtures. The chemical and physical properties of these materials were given in Table 1. The aggregate groups were arranged as 0-5 mm and 5-10 mm according to the maximum aggregate size. The finer aggregate group (0-5 mm) had specific gravity of 2.49 and water absorption of 2.2%. The specific gravity and water absorption of coarse aggregate group (5-10 mm) was 2.63 and 0.3%, respectively. A polycarboxylate-based Water Reducer (WR) with the specific gravity of 1.06 was used as chemical admixture to ensure the workability of fresh SCC. A macro SF and three different micro fiber types were utilized in the fiber reinforced SCC mixtures. As micro fiber, a micro SF and two different synthetic fibers names as PVA and PP were used. The properties of these fibers were listed in Table 2.

Table 1. The physical and chemical properties of PC and FA

Binders	**Composition (%)**									**Specific Gravity**	**Surface Area (cm^2/g)**
	CaO	**SiO_2**	**Fe_2O_3**	**Al_2O_3**	**MgO**	**SO_3**	**K_2O**	**Na_2O**	**LOI**		
PC	58.85	19.41	3.67	5.58	2.12	3.16	0.69	0.61	6.07	3.06	4891
FA	1.07	63.04	6.77	21.63	-	0.10	-	-	2.60	2.30	2900

Table 2. The properties of fibers

Fiber	Type	Picture	Shape	Length (mm)	Aspect Factor	Tensile Strength (MPa)	Modulus of Elasticity (GPa)	Density (g/cm^3)
MA	Macro Steel		Hooked-end	60	65	1345	200	7.8
MI	Micro Steel		Straight	6	40	3000	200	7.2
PVA	Micro Synthetic		Straight	8	200	1600	41	1.3
PP	Micro Synthetic		Straight	6	240	350	-	0.91

2.2. Experimental Program

In the determination of the mix proportions, the workability tests (slump-flow, t_{50} and J-ring) were taken into account according to EFNARC [23] which determines the self-compacting ability conditions of the mixtures. Within this scope, binder content for all SCC mixtures was used as 600 kg/m^3 for PC and 300 kg/m^3 for FA and the water/binder ratio was kept constant as 0.23. WR was added into all SCC mixtures to ensure the limit values (650-800 mm) determined by EFNARC [23] for the slump-flow test.

A total of seven SCC mixtures were designed by using four different types and shapes of fibers including a control mixture with no fiber in this study. Table 3 shows SCC mix designations. A single FR-SCC having only 1% macro SF (MA1) and SCC mixture reinforced with binary fiber hybridization of both micro and macro SFs (MA0.75_MI0.25) were designed. In order to investigate the effect of PVA and PP fiber on SFR-SCC, these FR-SCC mixtures were also combined with both PVA and PP separately. By this way, binary blends of macro steel and synthetic fibers (MA1_PVA & MA1_PP) and ternary blends of macro steel, micro steel and synthetic fibers (MA0.75_MI0.25_PVA & MA0.75_MI0.25_PP) were obtained. The steel and synthetic fiber content of the mixtures were kept constant as 1% and 0.25% by volume, respectively.

Table 3. The proportions of mixtures

Mix Code	Binders (kg/m^3)		Water (kg/m^3)	Aggregates (kg/m^3)		Steel Fiber (%)		Synthetic Fiber (%)		WR (kg/m^3)
	PC	FA		(0-5)	(5-10)	MA	MI	PVA	PP	
Control	600	300	203	973.8	171.8	0	0	0	0	15
MA1	600	300	204	952.0	168.0	1	0	0	0	16
MA1_PVA	600	300	204	918.5	162.1	1	0	0.25	0	20
MA1_PP	600	300	204	922.6	162.8	1	0	0	0.25	18
MA0.75_MI0.25	600	300	204	949.5	167.6	0.75	0.25	0	0	19
MA0.75_MI0.25_PVA	600	300	204	914.0	161.3	0.75	0.25	0.25	0	22
MA0.75_MI0.25_PP	600	300	204	914.0	161.3	0.75	0.25	0	0.25	22

2.3. The Preparation of the Fiber Reinforced SCC Samples

Aggregates were first put, followed by SFs and 2/3 of mixing water and they were mixed for 3 minutes into the mixer. Afterwards, binders and the remaining mixing water with WR were added and mixed for additional 5 minutes. In order to prevent the clumping of synthetic fibers, they were added into the mixture little by little after 7 minutes. The prepared SCC mixtures were placed into molds without any compression process. The samples were kept for 24 hours by covering them with a nylon cover to prevent evaporation. After they were removed from the molds, they were placed in a curing pool at 23±2°C and cured for a total of 90 days.

2.4. Procedures for Testing

2.4.1. Fresh SCC tests

At first, to determine the fresh unit weight values of the mixtures, the prepared mixtures were filled into a 100x200 mm cylinder molds without applying any compression process. The measured weight was divided by the volume of the mold to calculate the fresh unit weight of the designed mixtures.

The fresh concrete properties of SCC with no fiber and FR-SCC mixtures were evaluated based on the workability test methods determined by EFNARC [23]. Within this scope, slump-flow and J-Ring tests were carried out as shown in Fig. 1. The purpose of using slump-flow test method was to measure the filling ability of concrete. In this test, without wasting time, the Abrams cone placed on a flat plate was filled with the prepared mixture without applying the compression process and lifted upwards. When the spreading of concrete is complete, the slump-flow diameter was measured by taking the average of the two perpendicular dimensions (D_s). The time elapsed from the removal of the cone until the fresh SCC reached a diameter of 500 mm was measured and recorded as t_{50} time. In order to measure the ability fresh SCC to pass through obstacles, J-ring test was performed. Unlike the slump-flow test, a 300 mm diameter ring was used, for this test procedure. Then, the heights formed in the inner and outer part of the ring were measured and the difference was taken (ΔH). Similar to slump-flow test, the flow diameter (D_J) and t_{50j} were also measured in the J-ring test.

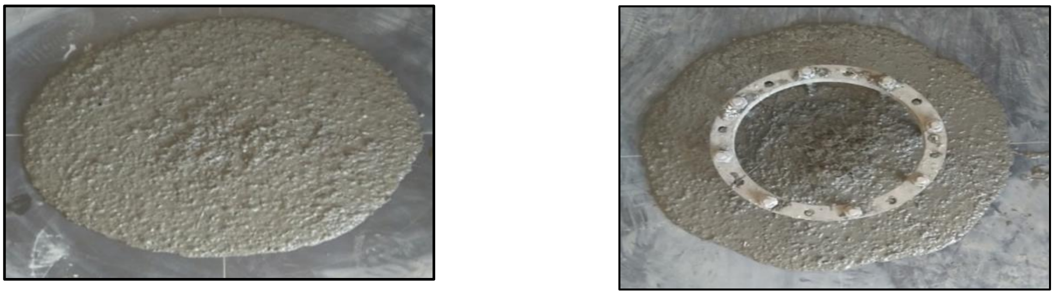

(a) (b)

Figure 1. Fresh SCC tests: (a) Slump-flow, (b) J-Ring

2.4.2. Hardened SCC tests

In order to attain the hardened properties of SCC with no fiber and FR-SCC specimens, the compressive, splitting tensile and flexural strength tests were performed on 90 days curing samples. Compressive strength (f_c) test was applied to 100x100x100 mm cubic samples based on ASTMC39 [24] and splitting tensile strength (f_{ct}) test was performed on ϕ100x200mm cylinder specimens according to ASTM C496 / C496M-17 [25]. To measure the flexural tensile strength (f_f), the four-point bending test was carried out on 400mm x 100mm x 100mm prism specimens with a loading speed of 0,003 mm/sec according to ASTM C1609 [20] with displacement control. A photo of the test equipments were provided in Fig. 2. Three specimens were produced and tested for all designed mixtures and tests and the average of the test results were calculated.

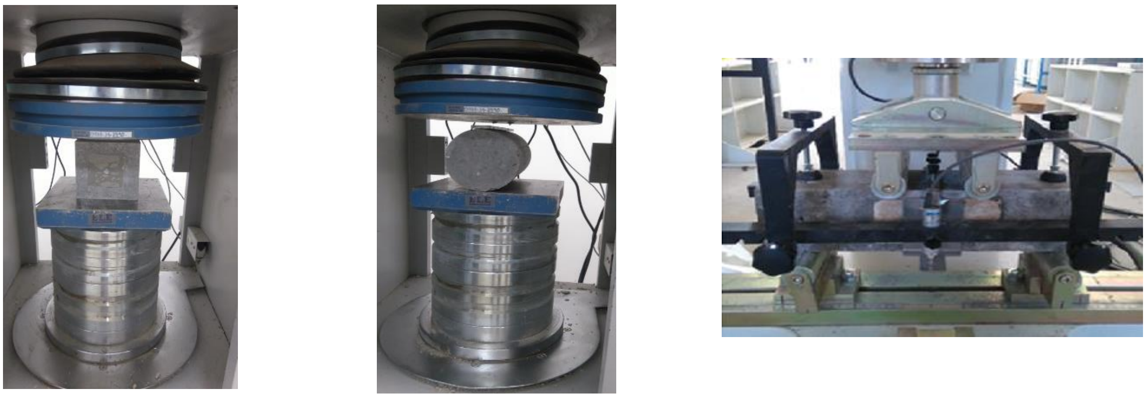

(a) (b) (c)

Figure 2. Hardened SCC tests: (a) f_c, (b) f_{ct}, (c) f_f

2.4.3. Evaluation methods of flexural toughness

Bending behavior of fiber reinforced cement based composite specimens is defined as deflection-hardening or deflection-softening. In the deflection-hardening behavior, a higher load-bearing capacity is observed after the initial crack formation, while in the deflection-softening behavior, the load-bearing capacity decreased. In ASTM C1609 [20], the first peak is used because, as proved by Kim [26], it is difficult to determine the initial peak strength of fiber reinforced concrete specimens exhibiting deflection-hardening behavior. The flexural strength of the samples were calculated using the equation given in Equation (1) according to ASTM C1609 [20].

$$f_f = \frac{F.L}{b.h^2} \tag{1}$$

where f_f is the flexural strength (MPa), F is the maximum load (N), L, b and h are the length, width and height of the specimen in mm, respectively.

The fracture modulus is defined as modulus of rupture (MOR) on the load-deflection curve observed after the limit of proportionality (LOP) point at which the first crack occurs. If the load value P_{MOR} corresponding to this point is greater than the P_{LOP} value corresponding to the LOP point where the first crack occurs, it is concluded that the deflection –hardening behavior occurs. If it is less than the P_{LOP} value, the deflection-softening behavior occurs in the specimen subjected to four-point bending. The stress value in the MOR was calculated using Equation (1). In addition, L/600 and L/150 points were determined according to ASTM C1609 [20]. L/600 and L/150 are 1/600 and 1/150 of the test span, respectively. The load and deflection values, toughness and stresses corresponding to the L/600 and L/150 points were calculated. In this study, deflection values at 0.5 mm and 2 mm points were used since the L is 300 mm. While calculating the toughness (T) values, the areas under the load-deflection curves until the L/600 and L/500 points were used. The same P, δ, T and f prefixes were used for the load, deflection, toughness and flexural strength values corresponding to the LOP, MOR, L/600 and L/150 points. The flexural toughness factor (FTF) in N/mm^2 according to JSCE [21] was calculated using Equation (2).

$$FTF = \frac{T_{\left(\frac{L}{150}\right)}.L}{\left(\frac{L}{150}\right).b.h^2} \tag{2}$$

where $T_{(L/150)}$ is the area under the load-deflection curve until 2 mm deflection in N.mm.

3. RESULTS AND DISCUSSION

In this study, PVA and PP synthetic fibers were added into single 1% macro steel FR-SCC specimens and HSFR-SCC specimens having 0.75% macro and 0.25% micro SF to investigate the effects of synthetic fibers on the properties of steel FR-SCC. For this purpose, the fresh, hardened and toughness properties of these designed mixtures were obtained as summarized in Table 4-7.

Table 4. Fresh SCC test results

Mix Code	Unit weight (kg/m^3)	Slump-Flow		J-Ring		
		D_s (mm)	t_{50} (sec)	D_J (mm)	t_{50J} (sec)	ΔH (mm)
Control	2159	770	4	780	4	0.3
MA1	2458	750	5	730	6	4.0
MA1_PVA	2296	710	7	685	10	7.0
MAK_PP	2239	718	6	690	8	6.5
MA0.75_MI0.25	2419	742	5	724	7	3.5
MA0.75_MI0.25_PVA	2368	723	6	698	9	5.0
MA0.75_MI0.25_PP	2353	730	5	700	8	4.7

3.1. Fresh SCC Properties

The fresh properties of designed mixtures were given in Table 4.

3.1.1. Fresh unit weight

Observing Fig. 3, the fresh unit weight values of all FR-SCC mixtures were higher than those of the control mixture due to the fact that they contain SFs. Besides, it was obvious that the addition of synthetic fibers into the single and HSFR-SCC mixtures induced the fresh unit weight values. In addition, the inclusion of PP into the single steel FR-SCC mixtures caused 2.3% more reduction in unit weight with regards to control mixture compared to the one with PVA while that value was 0.6% for the HSFR-SCC mixtures. It may be attributed to the lower specific gravity of synthetic fibers which was used as a replace of aggregates. Moreover, the reason of having lower unit weight of MA1_PVA and MA1_PP than MA0.75_MI0.25_PVA and MA0.75_MI0.25_PP may be due to the use of micro SF at a rate of 0.25% instead of macro SF which increases the packing density of the fibers. The similar finding was also obtained in the study of Kina [27]. Besides, the use of PP fiber decreased the unit weight of the mixtures with regards to that of the PVA fiber. It may be attributed to the fact that the same volume fractions of both fibers caused the use of different amount of fibers since their specific gravities are different from each other.

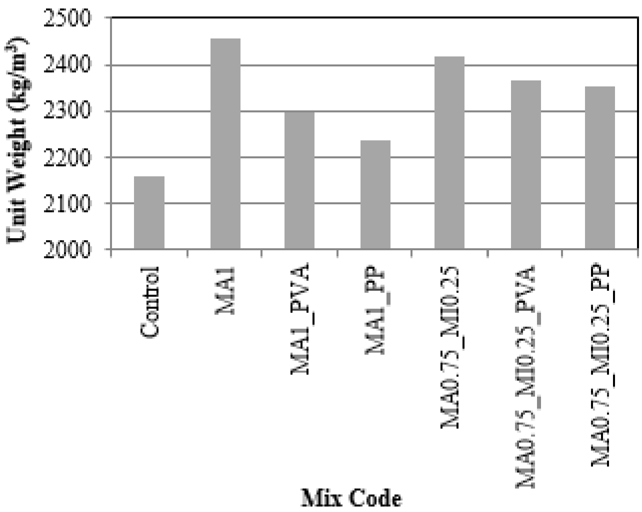

Figure 3. The fresh unit weight values of designed SCC mixtures

3.1.2. Slump-flow diameter and t_{50}

Referring to Fig. 4, the addition of PVA and PP into single SFR and HSFR-SCC caused a decrease in the slump-flow diameter (D_S) values while an increase in t_{50} values occurred. It was observed that PVA had more negative effect on the slump-flow test results than PP fiber. The addition of PVA fiber into single SFR-SCC mixtures caused 1.06% more reduction in slump-flow diameter compared to the one with PP while there was 0.94% decrease in D_S of HSFR-SCC mixture. In the studies of Ahmad and Umar [28] and Zhu et al. [29], it was found that there was a decrease in D_S with the addition of PVA fiber into the concrete. Besides, it was noted that PP synthetic fiber had less negative effect on the workability properties of mixtures. This may be due to the fact that PP fiber disperses more homogeneously and prevents agglomeration. Moreover, it may be also attributed to the hydrophilic nature and having high aspect ratio of PVA which adversely affect the fresh properties of mixtures [30]. In the study of Umar et al [31] the slump values of the SCC with no fiber decreased by 3.97% and 5.56% with the addition of 0.2% PP and 0.2% PVA fibers, respectively. This higher reduction in flowability of PVA fiber reinforced SCC was explained by the poor dispersibility of PVA fiber which's surface texture is relatively less smooth. In the literature, the similar results were also found by the other researchers [29, 32].

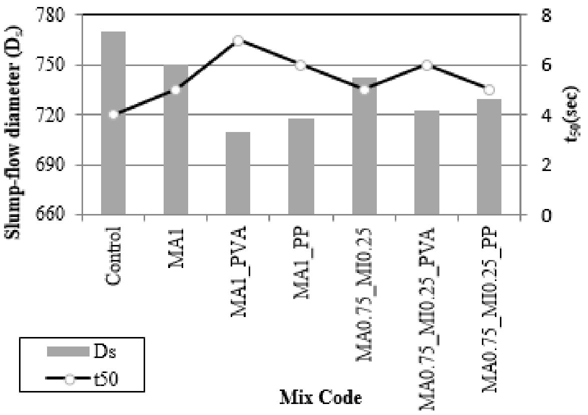

Figure 4. The slump-flow diameter and t_{50} values of designed mixtures

In this study, Visual Stability Index (VSI) values were used to evaluate the stability of FR-SCC mixtures according to ASTM C1611 [33]. When the visuals given in Fig. 5 were examined, it was seen that the VSI value of MA1 and MA0.75_MI0.25 was 0. However, the VSI values of FR-SCC mixtures became 2 by the addition of PVA and PP synthetic fibers into single and HSFR-SCC mixtures. It may be due to the formation of segregation as a result of agglomeration caused by the synthetic fibers. Observing Fig. 5, at the center part of the mixtures having PP and PVA fibers, the agglomeration appeared in the matrix because of the poor dispersion of fibers. Nevertheless, it was found that all the FR-SCC mixtures have acceptable stability.

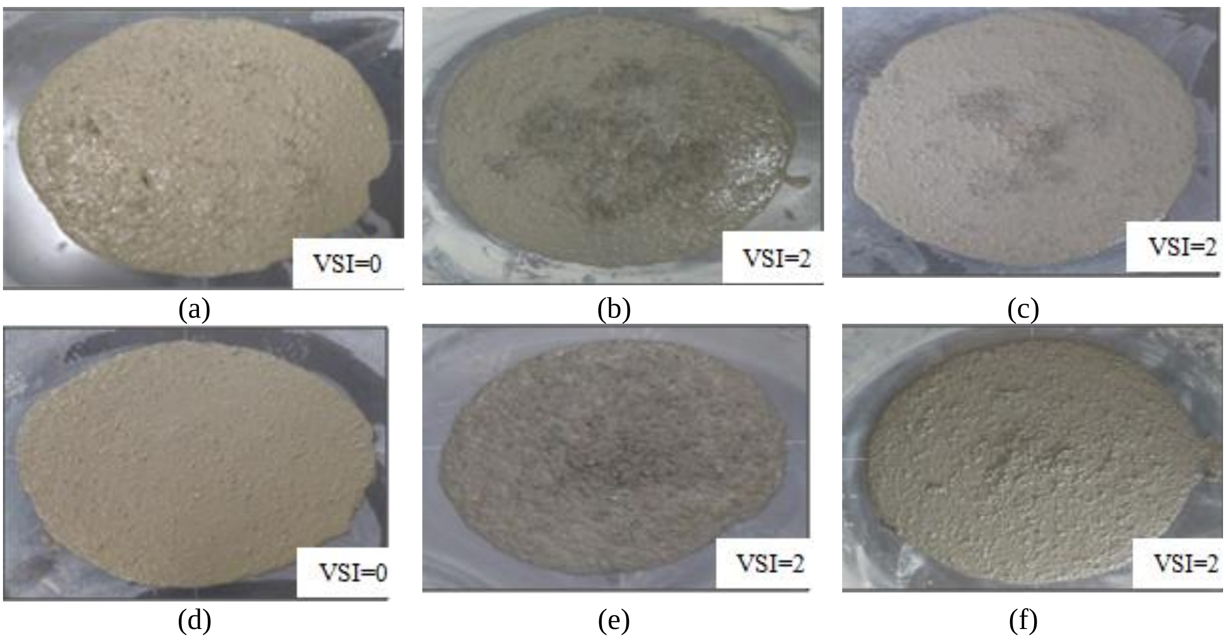

Figure 5. VSI assessments based on slump-flow diameter visuals of (a) MA1, (b) MA1_PVA, (c) MA1_PP, (d) MA0.75_MI0.25, (e) MA0.75_MI0.25_PVA, (f) MA0.75_MI0.25_PP

3.1.3. J-Ring slump-flow diameter, t_{50J} and height difference

Observing Fig. 6, the incorporation of synthetic fibers into single and hybrid SFR-SCC decreased the J-ring slump-flow diameters and increased the t_{50J} values. It was also seen that the use of PVA and PP into the SCC mixtures increased the J-Ring height difference value (ΔH) as in the case of other studies [28, 34]. When synthetic fibers were compared with each other in the J-ring test, it was determined that PVA has a more negative effect than PP fiber. The inclusion of PVA into single steel FR-SCC mixtures caused 0.68% more reduction in DJ compared to the one with PP while 0.27% decrease was observed in D_J of HSFR-SCC mixtures. That is because, PP fiber spreads more homogenously in the mixture compared to PVA and causes less agglomeration. The reason for the decrease in the DJ of the mixtures can be explained by getting stuck of aggregates and macro SFs to the obstacles on the ring, since the SFs and synthetic fibers in the FR-SCC mixture cause agglomeration. As it can be proven by the Fig. 7, in the mixture of MA1_PVA, the agglomeration in the inside part of the J-ring was more obvious than that of the mixture of MA1_PP. The inability of these solid materials in the FR-SCC mixtures to pass between the obstacles causes a height difference (ΔH) in the inner and outer parts of the ring. ΔH values increased with the addition of synthetic fibers into single and HSFR-SCC mixtures.

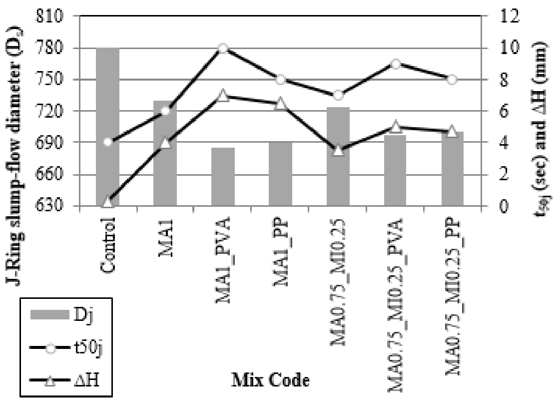

Figure 6. The J-Ring slump-flow diameter, t_{50j} and ΔH values of designed mixtures

Figure 7. The agglomeration of the mixtures (a) MA1_PVAand (b) MA1_PP

3.2. Hardened SCC Properties

The hardened properties of designed mixtures were given in Table 5.

Table 5. Hardened SCC test results

Mix Code	Statistical Values	f_c (MPa)	f_{ct} (MPa)	f_f (MPa)
Control	μ	85.1	3.2	8.3
	σ	1.98	0.07	0.28
MA1	μ	100.4	8.4	12.5
	σ	5.52	0.57	0.13
MA1_PVA	μ	92.4	8.9	20.9
	σ	3.39	0.42	1.24
MA1_PP	μ	87.9	8.8	17.6
	σ	3.11	0.42	0.11
MA0.75_MI0.25	μ	101	8.6	12.4
	σ	2.83	0.28	0.1
MA0.75_MI0.25_PVA	μ	94.9	10.2	16.4
	σ	5.3	1.06	0.13
MA0.75_MI0.25_PP	μ	93.1	10	15.7
	σ	0.42	0.57	0.07

μ : average, σ : standard deviation

3.2.1. Compressive strength

Observing Fig. 8, the use of PVA and PP synthetic fibers into SFR-SCC decreased the f_c values and PVA fiber showed less negative effect on f_c than PP fiber. The addition of PP fiber into single SFR-SCC caused 4.49% more reduction in the f_c values compared to the ones with PVA, while it was seen that it led to a 1.78% decrease in the f_c values of HSFR-SCC. This can be attributed to the inability of the synthetic fibers to be dispersed homogenously in the SCC mixture and to agglomerate due to the low shearing effect of the mixer used in the preparation of the mixtures. In some studies [35–39], it was also determined that the use of PP and PVA fibers into concrete adversely affect the fresh properties of SCC mixtures. Thus, the decrease in the filling rate of the mixtures affected the f_c of concrete negatively.

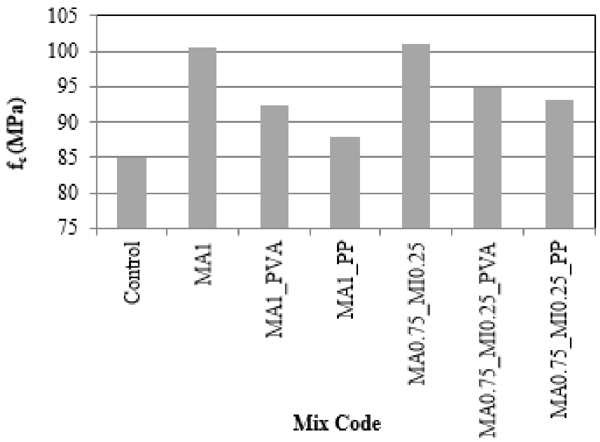

Figure 8. The f_c of designed SCC mixtures

3.2.2. Splitting tensile strength

When the effect of synthetic fibers on the f_{ct} was examined, it was observed that adding PVA and PP separately into the single and HSFR-SCC mixtures increased the f_{ct} (see Fig. 9). Besides, it was found that PVA fiber had more positive effect on the f_{ct} with regards to PP fiber. Addition of PVA into single SFR-SCC caused more enhancements with 1.07% in the f_{ct} compared to the one with PP, while it caused an increase of 1.86% for HSFRC-SCC. This situation can be explained by the fact the use of binary and more fiber hybridization can show superior performance with regards to single fiber and it can be called as synergy. In the literature, some findings obtained by the other researchers [40, 41] also support this situation.

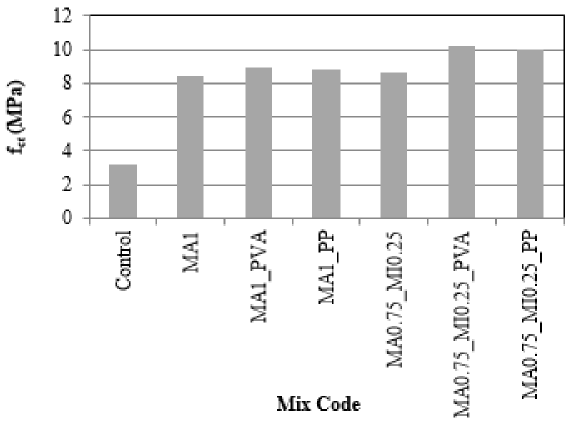

Figure 9. The f_{ct} of designed SCC mixtures

3.2.3. Flexural strength

Observing Fig. 10, when the flexural strengths of SCC specimens were examined, an increase in f_f was observed with the addition of synthetic fiber into SFR-SCC mixtures. Besides, it was observed that PVA fiber had a more positive effect on f_f compared to PP fiber, similar to splitting tensile strength. Addition of PVA fiber into single SFR-SCC caused more increase with 11.21% in f_f compared to the one with PP, while that value was 3.37% for HSFRC-SCC. This is because the use of synthetic fibers can increase the total fiber volume with regards to the SCC mixtures containing only single and hybrid SF [42]. Moreover, the hydrophilic nature of PVA fiber can be shown as the reason of its increase. In the study of Emamjomeh et al [43], the mixtures with PVA fiber also exhibited higher flexural strength compared to those of the ones with PP fiber. This fact was attributed to having higher tensile strength of PVA and higher PVA-matrix bond strength with regards to that of the PP-matrix interface. At the interface of the PVA, both frictional and chemical bonds are at work. However, the lower bond strength of PP-matrix interface is because of the frictional bonding rather than a chemical one [44]. Studies carried out by some researchers [41, 45] found that the inclusion of both PP and PVA fiber into cementitious composites has a positive effect on the f_f. Thus, for this study, it can be concluded that the synergy resulting from the addition of PVA or PP into mixtures as second or third fiber also increases the f_f.

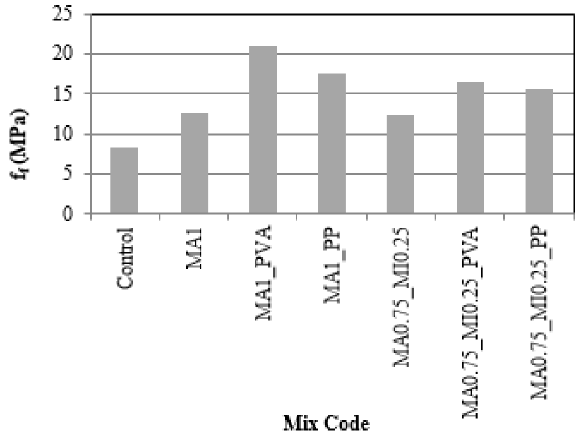

Figure 10. The f_f of designed SCC mixtures

3.2.4. Flexural performance

The flexural performance of designed mixtures was given in Table 6.

3.2.4.1. *Toughness (Energy absorption capacity)*

The flexural strength-mid span deflection curves of all FR-SCC specimens were shown in Fig. 11 and also the values obtained from the test results were given in Table 7. While the control specimen with no fiber showed a brittle fracture, as can be seen in Fig.12(a) and (b), all FR-SCC samples exhibited deflection-hardening behavior. The addition of fibers into SCC prevented brittle fracture and created the deflection-hardening behavior, thus made the concrete behave more ductile. Observing Table 6, when all samples were taken into account, it was seen that the MA1_PVA samples absorbed the most energy, while the MA0.75_MI0.25 samples had the lowest energy absorption capacity. Besides, it was found that the energy absorption capacity of the samples increased with the addition of PVA and PP synthetic fibers into SCC. On the other hand, when the area under the load-deflection curves (energy absorption capacity) of the samples consisting of a binary and ternary fiber hybridization of SF, PVA and PP fibers were examined, it was seen that the use of PVA showed higher enhancement compared to PP fiber. It may be due to the slip-hardening behaviour of PVA fiber [46] which enabled to achieve higher strain capacity. In the study of Khan and Ayub [47], PP fiber reinforced SCC also exhibited lower strain-hardening response after cracking and it was attributed to the weak bond between PP and matrix interface. Similar findings were also obtained by the study of Pakravan et al. [48].

Table 6. The flexural performance of FR-SCC specimens

Mix Code	Energy Absorption Capacity (N.m)	Failure Behavior	Ductility		
			δ_{LOP}	δ_{MOR}	D-index
MA1	72.48	Deflection hardening	0.019	0.347	18.17
MA1_PVA	119.58	Deflection hardening	0.018	0.485	26.8
MA1_PP	102.54	Deflection hardening	0.017	0.431	26.12
MA0.75_MI0.25	72.94	Deflection hardening	0.02	0.269	13.52
MA0.75_MI0.25_PVA	96.44	Deflection hardening	0.017	0.443	25.91
MA0.75_MI0.25_PP	85.01	Deflection hardening	0.022	0.483	22.05

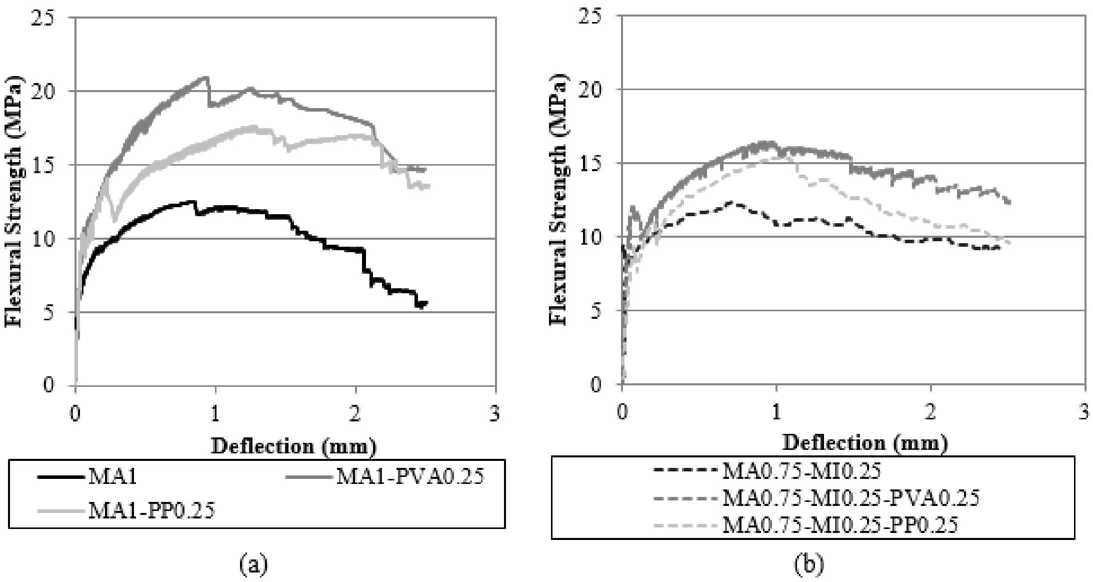

Figure 11. The flexural strength-mid span deflection curves of SFR-SCC samples containing different synthetic fiber: (a) single SFR-SCC, (b) HSFR-SCC

Table 7. The flexural properties of FR-SCC specimens

Mix Code		MA1	MA1_PVA	MA1_PP	MA0.75_MI0.25	MA0.75_MI0.25_PVA	MA0.75_MI0.25_PP
L/600	$\delta_{L/600}$	0.5	0.5	0.5	0.5	0.5	0.5
	$f_{L/600}$	11.42	17.92	14.53	11.62	14.53	13.26
	$T_{L/600}$	15.72	22.95	19.82	17.27	20.06	18.84
L/150	$\delta_{L/150}$	2	2	2	2	2	2
	$f_{L/150}$	9.13	18.05	16.98	9.83	14.03	10.9
	$T_{L/150}$	72.48	119.58	102.54	72.94	96.44	85.01
MOR	δ_{MOR}	0.84	0.93	1.28	0.71	0.93	0.96
	f_{MOR}	12.49	20.96	17.58	12.44	16.27	16.35
	T_{MOR}	29.42	50.98	62.26	26.25	33.52	44.17

The effect of the addition of synthetic fiber into SFR-SCC mixtures on the load carrying capacity was shown in Fig. 12 for different deflection points. Flexural strength values were calculated using Equation (1) for these three different deflection points determined based on [20]. These deflection points are the deflection points corresponding to L/600, L/150 and MOR for ASTM C1609 [20]. When the findings were examined it was seen that the effects of the fibers became more pronounced as the deflection point increased. As seen in Fig. 11, the flexural strength increased for all deflection points by the addition of synthetic fibers into SFRC-SCC and it was observed that the MA1_PVA specimen exhibited the best performance in terms of flexural performance. Moreover, the samples having synthetic fiber showed higher increase in the resistance against the bending load before the peak load than those of the samples with single and hybrid SF. In fact, it was observed that the increase in resistance to bending load of the samples containing PVA fiber was much more pronounced. As a result, when the effect of the addition of synthetic fiber into the single and HSFR-SCC samples on the flexural performance was investigated, it was found that PVA fiber caused a greater increase in flexural strength for all deflection points compared to PP fiber.

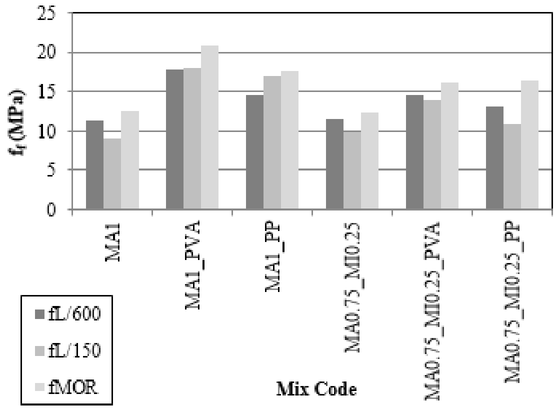

Figure 12. f_f values of FR-SCC samples for some deflection points

3.2.4.2. *Toughness values based on ASTM C1609*

The toughness values of all FR-SCC samples calculated according to ASTM C1609 [20] were given in Fig. 13. In this method, the toughness values at L/600 and L/150 points are taken into account. For this reason, the behavior before and after the peak load in the load-deflection curves could be examined. Observing Fig. 13, the addition of synthetic fibers into single and HSFR-SCC caused an increase in the toughness values. It was determined that the use of PVA as synthetic fiber into SFR-SCC had a more positive effect on toughness values compared to PP fiber.

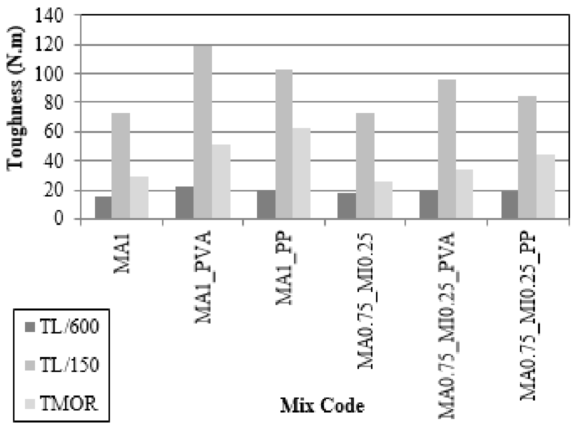

Figure 13. Toughness values of FR-SCC samples for some deflection points

3.2.4.3. *Flexural toughness factors values based on JSCE*

In Fig. 14, flexural toughness factor (FTF) values of all FR-SCC samples were given in order to examine the effect of adding different synthetic fibers into single and HSFR-SCC according to JSCE [21]. Similar to ASTM C1609, the use of synthetic fiber into single and HSFR-SCC caused an increase in the FTF values. When the synthetic fibers were compared among themselves, it was found that the FTF values of the FR-SCC with PVA were higher than the FTF values of the FR-SCC with PP. In this method, only the area under the curve up to the deflection point L/150 was used. Therefore, analysis of the range of load-deflection curves before and after the peak load could not be performed.

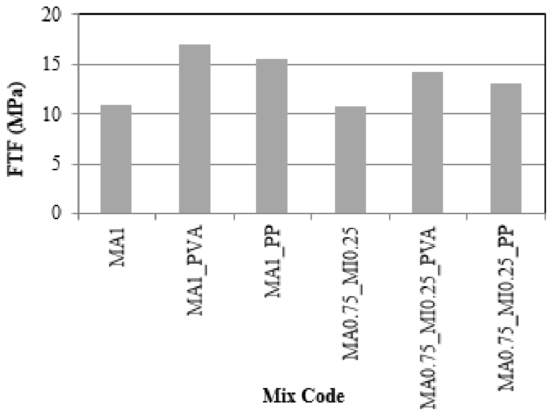

Figure 14. Flexural toughness factor values of FR-SCC samples based on JSCE

3.2.4.4. *Comparison of ASTM C1609 and JSCE*

Considering the above-mentioned results, it was found that the flexural toughness parameters showed similar trends according to both ASTM C1609 and JSCE. However, the important point is to determine which method is suitable for evaluating the flexural performance of fiber reinforced cement based composites. In the ASTM C1609 [20] method, the effect of fiber on the behavior of FR-SCC samples before and after the peak load on the load-deflection curves were determined and also, the flexural strengths of the samples could be calculated. On the other hand, the FTF in JSCE method is only related to the linear function of $T_{L/150}$ [49]. Therefore, the FTF according to JSCE [21] is calculated based on the area under the load-deflection curve up to the specified deflection (L/150=2). In this regard, it was considered that the effect of fiber on the pre-peak load behavior of FR-SCC samples on the load-deflection curve using the JSCE method is insufficient.

3.2.4.5. *Ductility*

The deflection capacity obtained from the four-point bending tests of the samples produced from FR-SCC mixtures is an important parameter in terms of ductility. The ductility index (D-index) values of the SFR-SCC specimens containing different synthetic fibers were shown in Table 6 and Fig. 15. In this study, the ductility index was calculated by Equation (3) as follows;

$$D - index = \frac{\delta_{\mathrm{MOR}}}{\delta_{LOP}} \quad (3)$$

Observing Fig. 15, the highest and lowest D-index values were obtained from MA1_PVA with 26.80 and MA0.75_MI0.25 with 13.52, respectively. However, D-index increased with the addition of synthetic fibers into SCC mixtures. It was found that the use of PVA into SCC mixtures caused more increase with 2% in the D-index of the single SFR-SCC, while the D-index values of the HSFR-SCC samples increased by 9.1% compared to the addition of PP. For all samples, PVA fiber performed better than PP fiber among synthetic fibers.

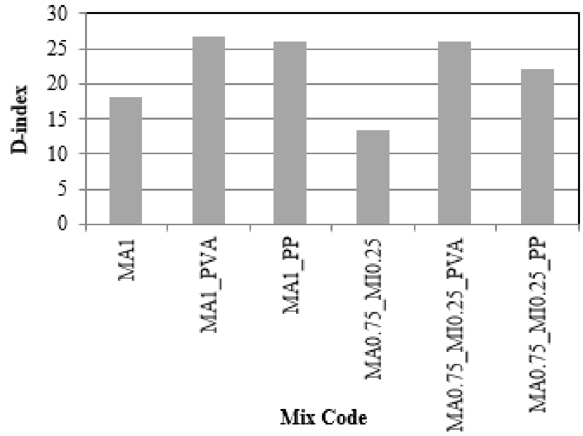

Figure 15. Ductility index values of FR-SCC samples

3.2.4.6 *Crack characterization*

Observing Fig. 16 (a-f), when synthetic fibers were added into SFR-SCC mixtures, a multiple cracking formation was observed due to the branching of cracks. Besides, it was seen that PVA fiber caused more crack branching than PP fiber in the binary and ternary HFR-SCC samples. Large amount of cracks occurred in the mid-span region of the samples due to the branching of cracks resulting in a deflection-hardening behavior [50–53]. It was observed that the use of PVA into single SF-SCC mixtures (MA1_PVA) exhibited highest multiple cracking behavior which is consistent with the energy absorption capacity findings. Another point observed from the bending test was the differences in the crack width on the tension side of the specimens. It was too small in the PVA fiber reinforced SCC specimens while in the PP fiber reinforced SCC specimens, the cracks were larger which could be due to the higher slippage distance of PP fiber. In the study of [43], it was found that the limited slippage distance of PVA fibers might be the main reason underlying the higher energy absorption capacity and crack formation with less width.

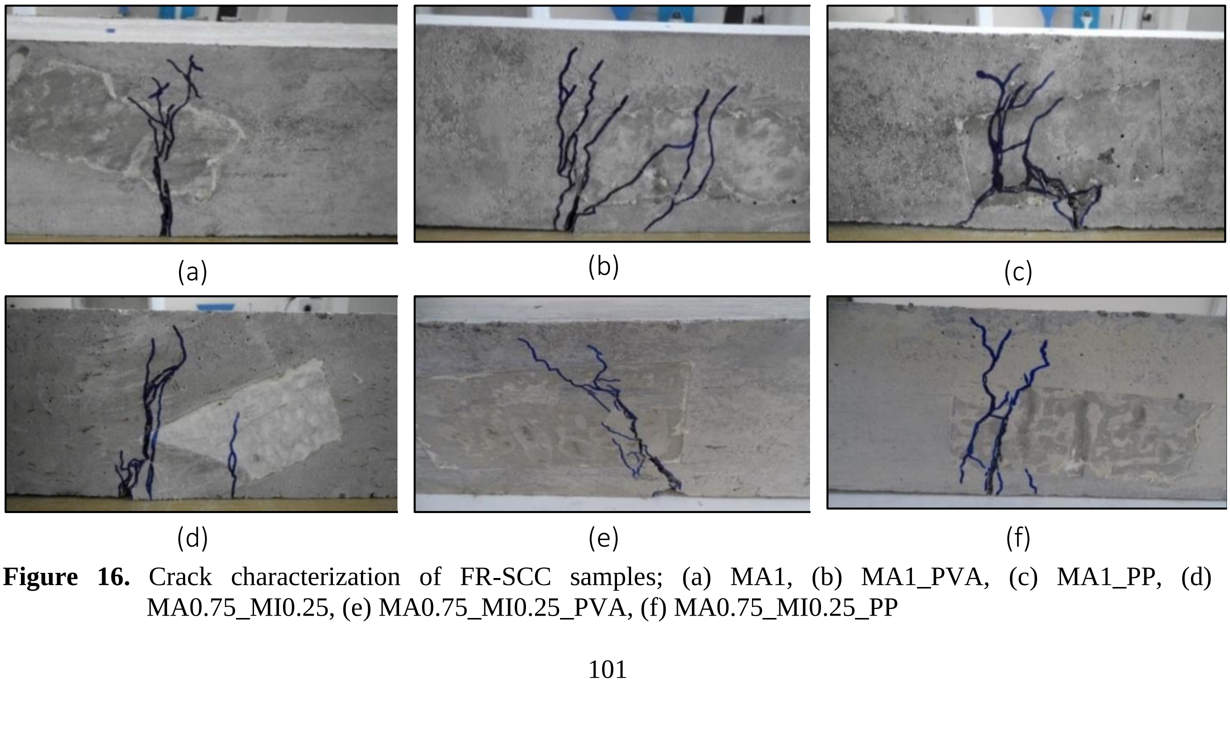

(a) (b) (c) (d) (e) (f)

Figure 16. Crack characterization of FR-SCC samples; (a) MA1, (b) MA1_PVA, (c) MA1_PP, (d) MA0.75_MI0.25, (e) MA0.75_MI0.25_PVA, (f) MA0.75_MI0.25_PP

4. CONCLUSION

Considering the results obtained from the experimental studies carried out within the scope of this study, the following conclusions can be reached;

- The addition of PVA or PP into SFR-SCC mixtures negatively affected the fresh properties of SCC. Besides, among synthetic fiber, it was found that PP influenced the workability of SCC less negatively than PVA.
- The use of synthetic fibers into SFR-SCC mixtures reduced the f_c but PVA fiber had less negative effect on f_c compared to PP.
- The splitting tensile and flexural strength of SFR-SCC samples were enhanced by the use of synthetic fiber and it was seen that PVA fiber had more positive effect than PP fiber.
- All SFR-SCC samples showed deflection- hardening behavior. Besides, it was found that the use of synthetic fiber into single (MA1) and HSFR-SCC (MA0.75_MI0.25) samples improved the energy absorption capacity and it was more pronounced in the SFR-SCC samples with PVA.
- It was found that the flexural toughness parameters showed similar trends based on ASTM C1609 and JSCE. The addition of PVA into single SFR-SCC caused the highest enhancement in the toughness values.
- The inclusion of synthetic fibers in SFR-SCC caused more multiple cracking behavior while more pronounced crack branching was observed in the single SFR-SCC containing PVA.

To sum up, it was found that the addition of synthetic fibers improved the flexural strength and performance of the SFR-SCC mixtures to a high extent. Especially, single SFR-SCC samples with PVA showed superior performance. It is obvious that this feature can provide great advantages in structures which are exposed to dynamic loads such as earthquakes as well as external environmental effects such as infrastructure and industry.

ACKNOWLEDGEMENTS

In this study, Scientific Research Projects Committee of Inonu University provided the financial support in Turkey (Project No: FYL-2017-844). Their support was gratefully acknowledged.

CONFLICT OF INTEREST

The author(s) stated that there are no conflicts of interest regarding the publication of this article.

AUTHORSHIP CONTRIBUTIONS

Ceren Kina: Formal analysis, Writing - original draft, Visualization, Conceptualization. **Esma Balalan:** Formal analysis, Investigation, Conceptualization. **Kazim Turk:** Supervision, Visualization, Conceptualization.

REFERENCES

[1] Okamura and Quchi. Self-Compacting Concrete. Development Present Use and Future. Proceedings of the First International RILEM Symposium, 1999, p. 3–14.

[2] EFNARC - EUROPEAN FEDERATION FOR SPECIALIST CONSTRUCTION CHEMICALS AND CONCRETE SYSTEMS (EFNARC). The European Guidelines for Self-

Compacting Concrete. The European Guidelines for Self Compacting Concrete 2005.

[3] Hannant DJ. Fibre cements and fibre concretes. Building and Environment 1980;15:200. https://doi.org/10.1016/0360-1323(80)90041-4.

[4] Bentur A. Fiber-reinforced cementitious materials. In Material Science of Concrete. Westerville,Ohio: The American Ceramic Society; 1989.

[5] Pakravan HR, Ozbakkaloglu T. Synthetic fibers for cementitious composites: A critical and in-depth review of recent advances. Construction and Building Materials 2019;207:491–518. https://doi.org/10.1016/j.conbuildmat.2019.02.078.

[6] Carpinteri A, Fortese G, Ronchei C, Scorza D, Vantadori S. Mode I fracture toughness of fibre reinforced concrete. Theoretical and Applied Fracture Mechanics 2017;91:66–75. https://doi.org/10.1016/j.tafmec.2017.03.015.

[7] González-Aviña J V., Juárez-Alvarado CA, Terán-Torres BT, Mendoza-Rangel JM, Durán-Herrera A, Rodríguez-Rodríguez JA. Influence of fibers distribution on direct shear and flexural behavior of synthetic fiber-reinforced self-compacting concrete. Construction and Building Materials 2022;330. https://doi.org/10.1016/j.conbuildmat.2022.127255.

[8] Kovar M, Foglar M. An analytical description of the force-deflection diagram of FRC. Composites Part B: Engineering 2015;69:550–61. https://doi.org/10.1016/j.compositesb.2014.10.021.

[9] Horikoshi T, Ogawa A, Saito T, Hoshiro H. Properties of polyvinyl alcohol fiber as reinforcing materials for cementitious composites. International RILEM Workshop on High Performance Fiber Reinforced Cementitious Composites in Structural Applications, 2006, p. 145–53.

[10] Dong P, Ahmad MR, Chen B, Munir MJ, Kazmi SMS. A study on magnesium phosphate cement mortars reinforced by polyvinyl alcohol fibers. Construction and Building Materials 2021;302. https://doi.org/10.1016/j.conbuildmat.2021.124154.

[11] Mostofinejad D, Moosaie I, Eftekhar M, Hesami E. Ultra-High Performance Hybrid Polyvinyl Alcohol-Polypropylene Fiber-Reinforced Cementitious Composites with Augmented Toughness and Strain-Hardening Behavior. Iranian Journal of Science and Technology - Transactions of Civil Engineering 2022;46:1997–2009. https://doi.org/10.1007/s40996-021-00815-4.

[12] Nam J, Kim G, Lee B, Hasegawa R, Hama Y. Frost resistance of polyvinyl alcohol fiber and polypropylene fiber reinforced cementitious composites under freeze thaw cycling. Composites Part B: Engineering 2016;90:241–50. https://doi.org/10.1016/j.compositesb.2015.12.009.

[13] Guo L, Wu Y, Xu F, Song X, Ye J, Duan P, et al. Sulfate resistance of hybrid fiber reinforced metakaolin geopolymer composites. Composites Part B: Engineering 2020;183. https://doi.org/10.1016/j.compositesb.2019.107689.

[14] Ding Y, You Z, Jalali S. Hybrid fiber influence on strength and toughness of RC beams. Composite Structures 2010;92:2083–9. https://doi.org/10.1016/j.compstruct.2009.10.016.

[15] Sukontasukkul P, Jamsawang P. Use of steel and polypropylene fibers to improve flexural performance of deep soil-cement column. Construction and Building Materials 2012;29:201–5.

https://doi.org/10.1016/j.conbuildmat.2011.10.040.

[16] Rodrigues JPC, Laím L, Correia AM. Behaviour of fiber reinforced concrete columns in fire. Composite Structures 2010;92:1263–8. https://doi.org/10.1016/j.compstruct.2009.10.029.

[17] Liu X, Wu T, Yang X, Wei H. Properties of self-compacting lightweight concrete reinforced with steel and polypropylene fibers. Construction and Building Materials 2019;226:388–98. https://doi.org/10.1016/j.conbuildmat.2019.07.306.

[18] Dawood ET, Hamad AJ. Toughness behaviour of high-performance lightweight foamed concrete reinforced with hybrid fibres. Structural Concrete 2015;16:496–507. https://doi.org/10.1002/suco.201400087.

[19] Ding Y, Zeng W, Wang Q, Zhang Y. Topographical analysis of fractured surface roughness of macro fiber reinforced concrete and its correlation with flexural toughness. Construction and Building Materials 2020;235. https://doi.org/10.1016/j.conbuildmat.2019.117466.

[20] ASTM C1609/C1609M. Standard Test Method for Flexural Performance of Fiber-Reinforced Concrete (Using Beam With Third-Point Loading). 2019.

[21] JCI Standard SF4. Method of Tests for Flexural Strength and Flexural Toughness of Steel Fiber Reinforced Concrete. Japan Concrete Institute Standards for Test Methods of Fiber Reinforced Concrete 1984:58–61.

[22] Banthia N, Trottier JF. Test methods for flexural toughness characterization of fiber reinforced concrete: some concerns and a proposition. ACI Materials Journal 1995;92:48–57. https://doi.org/10.14359/1176.

[23] EFNARC. Specification and Guidelines for Self-Compacting Concrete. vol. 44. 2002.

[24] ASTM C39 / C39M-20. Standard Test Method for Compressive Strength of Cylindrical Concrete Specimens, 2020. https://doi.org/10.1520/C0039_C0039M-20.

[25] ASTM C496 / C496M-17. Standard Test Method for Splitting Tensile Strength of Cylindrical Concrete Specimens, 2017. https://doi.org/10.1520/C0496_C0496M-17.

[26] Kim D joo, Naaman AE, El-Tawil S. Comparative flexural behavior of four fiber reinforced cementitious composites. Cement and Concrete Composites 2008;30:917–28. https://doi.org/10.1016/j.cemconcomp.2008.08.002.

[27] Kina C. Yüksek performanslı karma lif takviyeli beton geliştirilmesi. İnönü Üniversitesi, Malatya, Türkiye, 2019.

[28] Ahmad S, Umar A. Rheological and mechanical properties of self-compacting concrete with glass and polyvinyl alcohol fibres. Journal of Building Engineering 2018;17:65–74. https://doi.org/10.1016/j.jobe.2018.02.002.

[29] Zhu C, Zhang J, Peng J, Cao W, Liu J. Physical and mechanical properties of gypsum-based composites reinforced with PVA and PP fibers. Construction and Building Materials 2018;163:695–705. https://doi.org/10.1016/j.conbuildmat.2017.12.168.

[30] Yang E, Li VC. A Micromechanical Model for Fiber Cement Optimization and Component

Tailoring. 10th Int. Inorganic-Bonded Fiber Composites Conf. (IIBFCC), 2006, p. 1–13.

[31] Umar HA, Zeng X, Long G, Li Y, Zhao H. The combined effect of fiber and asphalt emulsion on properties of self-compacting concrete. Structural Concrete 2023. https://doi.org/10.1002/suco.202200252.

[32] Mahapatra CK, Barai S V. Temperature impact on residual properties of self-compacting based hybrid fiber reinforced concrete with fly ash and colloidal nano silica. Construction and Building Materials 2019;198:120–32. https://doi.org/10.1016/j.conbuildmat.2018.11.155.

[33] ASTM Committee C09.47. ASTM C1611-09 Standard Test Method for Slump Flow of Self-Consolidating Concrete. Annual Book of ASTM Standards Volume 04.02, 2009, p. 1–6.

[34] Öz A. The investigation of some properties of self compacting hybrid fiber concrete containing fly ash. Atatürk University, 2014.

[35] Chen B, Liu J. Contribution of hybrid fibers on the properties of the high-strength lightweight concrete having good workability. Cement and Concrete Research 2005;35:913–7. https://doi.org/10.1016/j.cemconres.2004.07.035.

[36] Wang JY, Banthia N, Zhang MH. Effect of shrinkage reducing admixture on flexural behaviors of fiber reinforced cementitious composites. Cement and Concrete Composites 2012;34:443–50. https://doi.org/10.1016/j.cemconcomp.2011.12.004.

[37] Atahan HN, Pekmezci BY, Tuncel EY. Behavior of PVA Fiber-Reinforced Cementitious Composites under Static and Impact Flexural Effects. Journal of Materials in Civil Engineering 2013;25:1438–45. https://doi.org/10.1061/(asce)mt.1943-5533.0000691.

[38] Hossain KMA, Lachemi M, Sammour M, Sonebi M. Strength and fracture energy characteristics of self-consolidating concrete incorporating polyvinyl alcohol, steel and hybrid fibres. Construction and Building Materials 2013;45:20–9. https://doi.org/10.1016/j.conbuildmat.2013.03.054.

[39] Başsürücü M, Fenerli C, Kına C & Akbas Ş. Effect of fiber type, shape and volume fraction on mechanical and flexural properties of concrete. Journal of Sustainable Construction Materials and Technologies 2022;7:158–171.

[40] Hsie M, Tu C, Song PS. Mechanical properties of polypropylene hybrid fiber-reinforced concrete. Materials Science and Engineering A 2008;494:153–7. https://doi.org/10.1016/j.msea.2008.05.037.

[41] Blunt J, Ostertag CP. Performance-Based Approach for the Design of a Deflection Hardened Hybrid Fiber-Reinforced Concrete. Journal of Engineering Mechanics 2009;135:978–86. https://doi.org/10.1061/(asce)0733-9399(2009)135:9(978).

[42] Yazici Ş, Inan G, Tabak V. Effect of aspect ratio and volume fraction of steel fiber on the mechanical properties of SFRC. Construction and Building Materials 2007;21:1250–3. https://doi.org/10.1016/j.conbuildmat.2006.05.025.

[43] Emamjomeha H, Behfarnia K, Raji A, Almohammad-albakkar M. Influence of PVA and PP fibers addition on the durability and mechanical properties of engineered cementitious composites blended with silica fume and zeolite. Research on Engineering Structures and

Materials 2023. https://doi.org/10.17515/resm2022.491me0804.

[44] Ananthi A, Karthikeyan J. Combined Performance of Polypropylene Fibre and Weld Slag in High Performance Concrete. Journal of The Institution of Engineers (India): Series A 2017;98:405–12. https://doi.org/10.1007/s40030-017-0248-5.

[45] Mazaheripour H, Ghanbarpour S, Mirmoradi SH, Hosseinpour I. The effect of polypropylene fibers on the properties of fresh and hardened lightweight self-compacting concrete. Construction and Building Materials 2011;25:351–8. https://doi.org/10.1016/j.conbuildmat.2010.06.018.

[46] Khan SU, Ayub T. Modelling of the pre and post-cracking response of the PVA fibre reinforced concrete subjected to direct tension. Construction and Building Materials 2016;120:540–57. https://doi.org/10.1016/j.conbuildmat.2016.05.130.

[47] Khan SU, Ayub T. Mechanical Properties of Hybrid Self-Compacting Fibre-Reinforced Concrete (SCC-FRC) Containing PVA and PP Fibres. Iranian Journal of Science and Technology - Transactions of Civil Engineering 2022;46:2677–95. https://doi.org/10.1007/s40996-021-00652-5.

[48] Pakravan HR, Latifi M, Jamshidi M. Hybrid short fiber reinforcement system in concrete: A review. Construction and Building Materials 2017;142:280–94. https://doi.org/10.1016/j.conbuildmat.2017.03.059.

[49] Wang J, Dai Q, Si R, Guo S. Investigation of properties and performances of Polyvinyl Alcohol (PVA) fiber-reinforced rubber concrete. Construction and Building Materials 2018;193:631–42. https://doi.org/10.1016/j.conbuildmat.2018.11.002.

[50] Yoo DY, Kang ST, Yoon YS. Enhancing the flexural performance of ultra-high-performance concrete using long steel fibers. Composite Structures 2016;147:220–30. https://doi.org/10.1016/j.compstruct.2016.03.032.

[51] Turk K, Kina C, Oztekin E. Effect of macro and micro fiber volume on the flexural performance of hybrid fiber reinforced SCC. Advances in Concrete Construction 2020;10:257–69. https://doi.org/10.12989/acc.2020.10.3.257.

[52] Turk K, Bassurucu M, Bitkin RE. Workability, strength and flexural toughness properties of hybrid steel fiber reinforced SCC with high-volume fiber. Construction and Building Materials 2021;266. https://doi.org/10.1016/j.conbuildmat.2020.120944.

[53] Kina C, Turk K. Bond strength of reinforcing bars in hybrid fiber-reinforced SCC with binary, ternary and quaternary blends of steel and PVA fibers. Materials and Structures/Materiaux et Constructions 2021;54. https://doi.org/10.1617/s11527-021-01733-7.

ESKİŞEHİR TECHNICAL UNIVERSITY JOURNAL OF SCIENCE AND TECHNOLOGY
A- APPLIED SCIENCES AND ENGINEERING

2023, 24(2), pp. 107-120, DOI: 10.18038/estubtda.1025092

RESEARCH ARTICLE

CLINICAL DECISION SUPPORT SYSTEM FOR EARLY DIAGNOSIS OF HEART ATTACK USING MACHINE LEARNING METHODS

Burçin KURT [1], **İlknur BUÇAN KIRKBİR** [1, 2]

[1] Department of Biostatistics and Medical Informatics, Karadeniz Technical University, Trabzon, Turkey
[2] Department of Public Health Nursing, Karadeniz Technical University, Trabzon, Turkey

ABSTRACT

Heart attack which is the main cause of death for both men and women is the leader among deaths due to heart diseases. Therefore, early diagnosis is very important for patients who are having a heart attack. Therefore, the study aimed to develop a clinical decision support system for the diagnosis of a heart attack to help physicians. In the study, variables were obtained accompanied by physicians by statistical analysis methods, where the optimum variables were selected from these variables considering the patient's unconscious state in some cases. Different decision models were developed using probit regression, decision tree, SVM, and ANN methods. As a result, the developed clinical decision support models for heart attack diagnosis were compared and evaluated. Consequently, the best diagnosis model was obtained using ANN with selected variables. In addition to these, the proposed study is significantly noticed with a sensitivity of 98% and specificity of 93.7% for heart attack diagnosis with optimum variables compared to similar studies in the literature. By using the proposed decision support system, it is possible to determine whether a patient has a heart attack or not and help the physician in the process of diagnosis of a heart attack.

Keywords: Heart attack, Machine learning, Clinical decision support system

1. INTRODUCTION

Cardiovascular diseases are the leading cause of death among all causes of death, especially ischemic heart diseases, and cerebrovascular diseases constitute the first two causes of death [1]. In 2012, 38 million deaths out of 56 million des in worldwide were caused by non-contagious diseases, especially heart and vascular diseases, cancer, and chronic airway diseases. In 2012, 46.2% (17.5 million) of non-contagious diseases worldwide were caused by cardiovascular disease. Of these deaths, 7.4 million depend on heart attacks [1]. Cardiovascular diseases are responsible for 37% of those under 70 deaths due to non-contagious diseases. It seems that cardiovascular diseases will continue to be the number one cause of death globally for a long time.

Myocardial infarction (MI) occurs when the heart muscle cells cannot get enough oxygen because of not getting enough blood, and is also called a heart attack. As a result, damage may occur and even death may result if the heart muscle is left without oxygen for a long time. While 50% of deaths due to heart attacks occur in the first hour, this rate rises to 80% in the first 24 hours [2]. Duration of diagnosis and treatment of patients play a big role in deaths which are from heart attacks. Computer programs or machine learning techniques can be used to reduce the mortality rate, improve the accuracy of disease diagnosis and mainly reduce the diagnosis time. Therefore, it aimed to develop a clinical decision support system to help physicians for prediction of a heart attack, in the study.

Doğan et al. developed a system for the diagnosis of heart attack using the decision tree method with different biochemical variables [3]. LDH, CK, CKMB, AST, and ALT enzymes were used as input to predict MI+ or MI-, and the proposed system has been evaluated on 61 patients. The developed system has performed 100% success on the patient data of 50 heart attacks and 11 non-diagnosed heart attacks

*Corresponding Author: burcinnkurt@gmail.com
Received: 17.11.2021 Published: 21.06.2023

diagnosed by physicians. In another study conducted in the literature [4], the clinical symptoms; myoglobin, mass concentration, CG, creatine kinase MB activity, creatinine kinase, and cardiac troponin T values were compared and used with the decision tree method for heart attack diagnosis. 91% sensitivity and 90% specificity values were obtained on 69 test dataset for the heart attack diagnosis system which was developed the using decision tree method.

In a study conducted by Dangare et al. in 2012, a model was developed that can predict the risk of heart disease by using artificial neural networks and data mining methods. A Heart Disease Prediction system (HDPS) was developed using a neural network classifying as “has heart disease” and “has no heart disease”. The HDPS system used 13 variables such as sex, cholesterol, and blood pressure to predict the likelihood of a patient getting heart disease. Nearly 100% success was obtained on 270 test data [5].In a similar study in 2011, two different models were developed that can diagnose heart disease using radial-based (RBF) artificial neural networks (ANN) and support vector machine (SVM) methods. The dataset has 214 records with 19 variables and the outcome values are 0-Myalgia, 1-Myocardial Infarction (MI), 2- Ischemic Heart Disease (IHand D), and 3- Unstable Angina (UA). 84.66% sensitivity and 88.5%specificity values were obtained for the ANN model on the 214 test data, and 82.4% sensitivity and 82.10% were obtained ned for the SVM model [6].

In this study, we have developed clinical decision support models for early diagnosis of heart attack using probit regression and machine learning methods which are decision tree, SVM, and ANN with biochemical, ECG, and demographic variables which are given in the below section. Furthermore, we have compared the performance of models using statistical scales and selected the best model for clinical decision support. Using the selected model with these variables for a patient, it can be diagnosed as a heart attack or not.

2. METHODS AND MATERIALS

2.1. Dataset

In the study, the data of 350 patients who came to Karadeniz Technical University Faculty of Medicine Farabi Hospital Emergency Medicine Service with chest pain between the years September 2013 and April 2016, with or without a heart attack diagnosis were used. The data were obtained retrospectively with the ethical approval dated 09 May 2016 and numbered 2016/45, which was given in Figure A1 in Appendix. The parameters in the data set were obtained by examining documents such as laboratory test results, epicrisis reports, and angiography results under the supervision of a specialist physician. Conditions with false positive results for CK-MB and troponin (polymyositis/dermatomyositis (inflammation of the muscles), muscular dystrophies (muscle disease), chronic renal failure, and chronic hemodialysis patients, patients who have received intramuscular (intramuscular) injections in the last 24 hours, Patients who had trauma or skeletal muscle damage during the day, patients with a hemolytic blood disease, and patients with shock were excluded from the study.

The patients were divided into two groups those with a heart attack (experimental group) and without a heart attack (control group). The diagnosis of heart attack was made according to the World Health Organization (WHO) criteria. 192 and 158 of them were diagnosed with heart attack and not heart attack respectively. The data was collected during a heart attack episode. The variables proposed by the physicians to diagnose a heart attack are given in Table 1.

The descriptive statistics of the categorical and numerical variables for patients diagnosed with heart attack and not heart attack are given in Appendix Table A1 and A2 respectively (using R software). The analyzes were implemented using open-source R 3.3. and 3.6 versions programming language ("C50", "neuralnetwork", "e1071", "caret", "pROC", "ggplot2", and "stats" packages).

Table 1. The variables for heart attack diagnosis (proposed by the physicians)

	Variable	Description
1	Sex	Male/Female
2	Ecg Change	Yes/No
3	St Segment Change	Yes/No
4	Chronical Disease	Yes/No
5	Heart Disease	Yes/No
6	Patient Pedigree	Yes/No
7	Ck-Mb (Creatine Kinase)	Iu/L
8	Hs Troponin (High Sensitivity Troponin)	Ng/Ml

The flow diagram of the study is given in Figure 1.

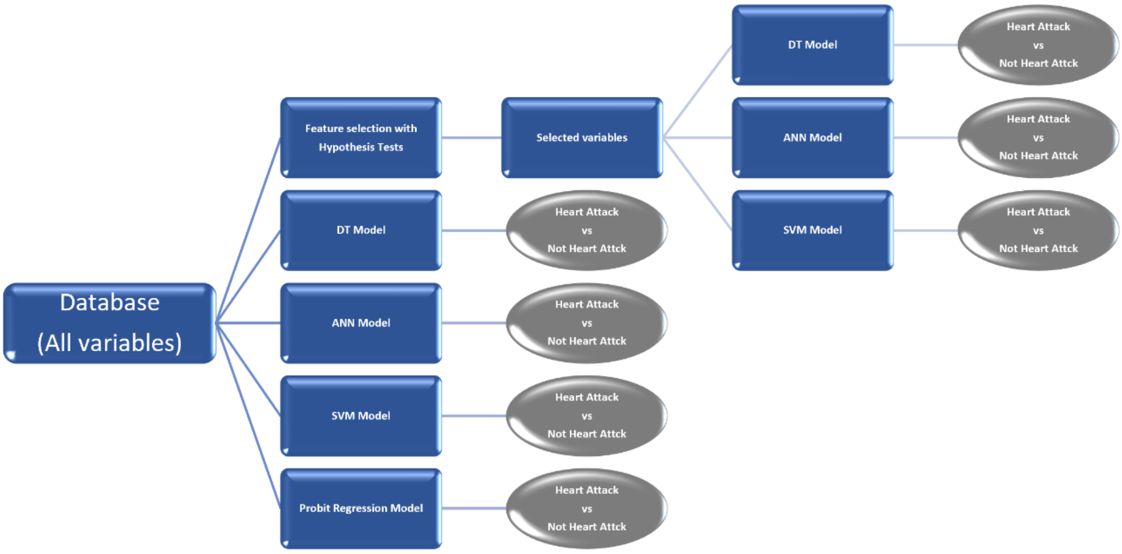

DT: Decision Tree, SVM: Support Vector Machine, ANN: Artificial Neural Networks

Figure 1. The flow diagram of the study

2.2. Probit regression (Probit model)

Probit regression is used to model dichotomous or binary dependent variables whose distribution is assumed to be a proxy for a true underlying continuous normal distribution [7]. It is a binary classification model which classifies samples according to their predicted probabilities for each class.

The probit model uses a similar approach to logistic regression and is also a popular method for an ordinal or a binary response model. It has a probit link function which uses the inverse of the cumulative distribution function of the standard normal distribution to transform probabilities to the standard normal variable and is most often estimated using the standard maximum likelihood procedure, such an estimation being called a probit regression [8]. Thus,

$$\Phi^{-1}(\pi_i) = x_i\beta + \varepsilon_i \quad (1)$$

where

$$\Phi(z) = \int_{-\infty}^{z} \frac{1}{\sqrt{2\pi}} e^{-\frac{1}{2}t^2} dt \quad , \quad (2)$$

Φ, x_i and β are the cumulative distribution function of the standard normal distribution, the ith row of the X matrix (n × p data matrix), that i, the ith record in the dataset and $\beta = (\beta_1, \beta_2, \ldots, \beta_p)^T$ respectively.

We implemented probit regression for our dataset using R open-source software and obtained the output as given in Table 2. The coefficients, z-statistic (sometimes called a Wald z-statistic), standard errors, and the associated p-values are presented as an output. As seen in Table 2; Sex(Male), Hs.Troponin, ECG.Change(No), Chronical.Disease(No) and Patient.Pedigree(No) is statistically significant. The probit regression coefficients show the change in the z-score or probit index for a one-unit change in the predictor. For example, for a one-unit increase in Hs.Troponin, the z-score increases by 4.742e-04. Furthermore, we obtained confidence intervals for the coefficient estimates, created by profiling the likelihood function [9, 10].

Table 2. The statistical output of the probit regression model for variables

	Estimate	Std. Error	z Value	Pr(<|z|)	2.5%	97.5%
(Intercept)	0.006	137.700	0.045	0.964	1.011	55.400
Sex.Male	-0.761	0.197	-3.874	***<0.001***	-1.161	-0.376
CK-MB	<-0.001	<0.001	-0.242	0.809	<-0.001	<0.001
Hs.Troponin	<0.001	<0.001	2.423	***0.015***	<0.001	<0.001
ECG Change.No	-1.271	0.178	-7.127	***<0.001***	-1.624	-0.925
ST.Segment Change.No	-4.880	-137.700	-0.035	0.972	-58.429	-0.492
Chronical.Disease.No	-0.620	0.190	-3.264	***0.001***	-0.992	-0.252
Heart.Disease.No	0.352	0.202	1.740	0.082	-0.037	0.745
Patient.Pedigree.No	-0.539	0.249	-2.162	***0.031***	-1.036	-0.058

* z value is the ratio of the *Estimate* to the *Std. Error [11]*

Goodness-of-fit (GOF) measure indicates the fitness of the data to the regression model and there are also many alternative metrics such as measures based on the variance decomposition of the predicted probabilities, measures based on the predicted probabilities, and log-likelihood-based measures. These pseudo-R2 metrics are used as the GOF measures for binary regression models [12]. Furthermore, the pseudo-R2 of McFadden measure uses the two log-likelihood values suggested by Aldrich–Nelson [13] and takes a value between 0 and 1. The obtained Pseudo-R2 of McFadden value is 0.411 for the developed probit model, which can be evaluated as a good model fit [14, 15] and the prediction results are given in the third section. Furthermore, the predicted probabilities of heart attack for statistically significant variables in the probit model are given in Appendix Figure A2.

2.3. Feature Selection and Classification with Machine Learning Methods

In the first step, the feature selection process was implemented using statistical analysis tests and considering some cases. In the statistical analyses for the study, the α of 0.05 was used as the cut-off for significance. If the P value is less than 0.05, we reject the null hypothesis, which means that there is a difference between the means, and decide that a significant difference does exist. Then, in the second step, diagnosis models were developed using three machine learning methods, for the selected variables.

2.3.1. Feature selection using statistical analysis

For the feature selection process, the normal distribution of quantitative data was tested using the Kolmogorov–Smirnov test, and the Mann-Whitney U test was performed to determine whether the values of the variables HS Troponin and CK-MB were significantly different from the patients was who diagnosed with heart attack and not heart attack groups. The results of the Mann-Whitney U test are given in Table 3.

Table 3. The Mann Whitney U test analysis results for HS Troponin and CK-MB variables of patients who were diagnosed with heart attack and not heart attack

HS-Troponin	N	Mean rank (SO)	Sum of ranks (ST)	U	z	p
Heart Attack	192	230.91	44334.5	4529.5	-11.296	**<0.001**
Not Heart Attack	158	108.17	17090.5			
Total	350					
CK-MB	**N**	**Mean rank (SO)**	**Sum of ranks (ST)**	**U**	**z**	**p**
Heart Attack	158	107.48	16982	4421	-11.409	**<0.001**
Not Heart Attack	192	231.47	44443			
Total	350					

As seen in Table 3, p values for HS Troponin ($p<0.001$) and CK-MB ($p<0.001$) were smaller than 0.05, which means that these values were significantly different between heart attack and not heart attack groups. Furthermore, categorical variables were analyzed using the Chi-square test for the feature selection process. According to the results, the categorical variables, which are sex, ECG change, ST segment change, chronical disease, and patient pedigree were obtained significantly different from the patients who were diagnosed with heart attack and not heart attack except heart disease. The Chi-square test results are given in Table 4.

Table 4. The Chi-square test analysis results for categorical variables of patients who were diagnosed with heart attack and not heart attack

Variable	Chi-square	p
Sex	21,18	**<0.001**
ECG change	118,16	**<0.001**
ST segment change	34,09	**<0.001**
Chronic Disease	23,78	**<0.001**
Patient Pedigree	24,28	**<0.001**
Heart Disease	0,005	0.95

*p <0,05

The test gives a Chi-squared statistic, which is a prediction of the goodness of fit of one category relative to the other and can be observed from the frequency of a variable with the expected frequency. The Chi-square test can estimate the role of the random effects in the results and gives a P value which is the probability that the samples have come from the same population. According to the statistical analysis results for the feature selection process; HS Troponin, CK-MB, sex, ECG change, ST segment change, chronical disease, and patient pedigree variables have been selected due to the significant difference. However, chronical disease, heart disease, and patient pedigree information cannot be obtained considering the patient's unconscious state in some cases. Therefore, two different decision system models have been developed and compared. One of them used all 8 variables while the other one used 5 variables except chronical disease, heart disease, and patient pedigree. The distributions of numerical and categorical variables are given in Figure 2.

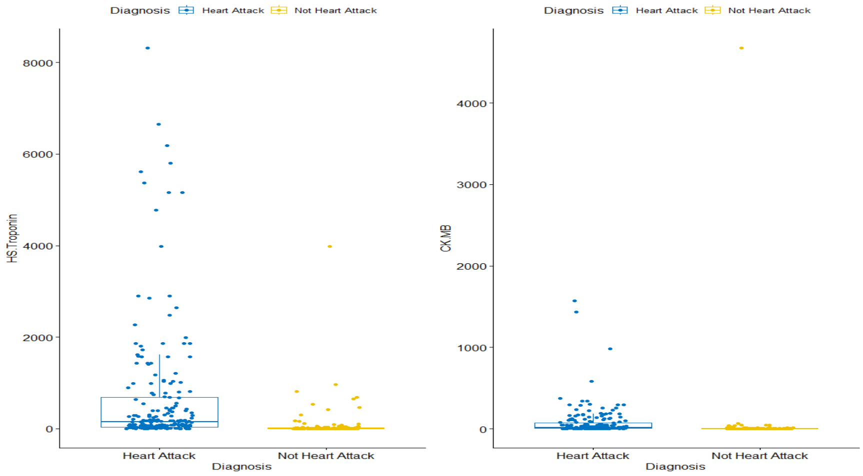

(a)

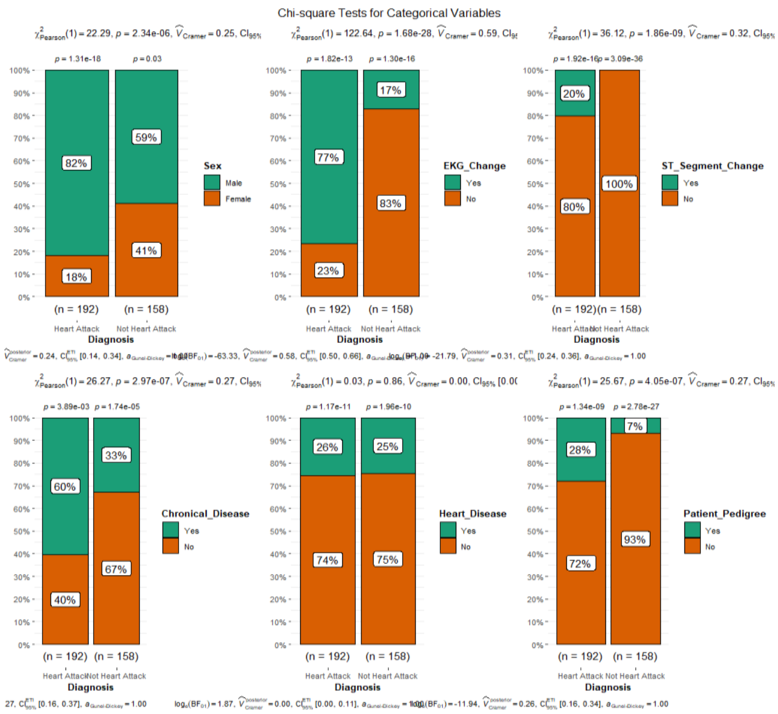

(b)

Figure 2. The distribution of (a) numerical and (b) categorical variables of patients who were diagnosed with heart attack and not a heart attack

As seen in Figure 2, the mean, standard deviation, and range values of Hs-Troponin and CK-MB variables for the "heart attack group" seems higher than the "not heart attack group". Furthermore, for categorical variables, only the "Heart Disease" variable is not significantly different between the "heart attack and "not heart attack groups due to the close distribution of the "Heart disease/yes" and "Heart disease/no" frequencies according to the dependent variable.

2.3.2. Classification using machine learning methods

For the second step, developing diagnosis models train and test sets were created. The distribution of train and test sets is given in Table 5.

Table 5. The distribution of train and test sets

	Train Set	Test Set
Heart Attack	95	97
Not Heart Attack	95	63
Total	190	160

192 and 158 patients of the dataset were diagnosed with heart attack and not heart attack respectively. To balance the patient number of each class in the training set, 60% of patients with no heart attack (as it is a minor class), which was 95 patients, and 95 patients with a heart attack (as it is equal to the number of patients with no heart attack), have been used for training. Therefore, in the development of the models, 190 of the 350 data were used as a training set and the remaining 160 were used as the test set for validation. With these train and test sets, three prediction models were developed using SVM [14,16-19], decision tree [20-22], and ANN [23, 24] methods which give successful results for clinical decision support systems in the literature.

3. RESULTS

In this study, heart attack, which is one of the serious diseases of today was handled. For this purpose, decision models were developed using probit regression, SVM, decision tree, and ANN. Furthermore, a feature selection process has been implemented for machine learning methods, whereas the probit regression method has done that by itself. Therefore, two approaches were used for each SVM, ANN, and decision tree model using selected and all features. The optimum parameter values and comparison of performance results of all these approaches are given in Table 6 and Table 7, respectively.

Table 6. The optimum parameter values for the developed machine learning models

	SVM (Sigmoid)	SVM (Radial)	SVM (Linear)	SVM (Polynomial)	DT	ANN
Optimum Parameter Values	Cost=1 Gamma=0.2 Coef.0=0	Cost=1 Gamma=0.17	Cost=1 Gamma=0.2	Cost=1 Gamma=0.2 Degree=3 Coef.0=0	Tree size=6	Hidden layer number=2 Hidden_layer1_neuronnumber=5 Hidden_layer2_neuronnumber=2 Epoch=1000 Threshold=0.01 Activation function=logistic

Table 7. The performance results of developed diagnosis models

Machine Learning Based Models			
With all 8 parameters	**SVM (Radial)**	**DT**	**ANN**
Sensitivity (%)	83.5	93.8	100
Specificity (%)	85.4	93.7	4.2
Accuracy (%)	84	93.8	68.3
With selected 5 parameters	**SVM (Radial)**	**DT**	**ANN**
Sensitivity (%)	79	91.7	**98**
Specificity (%)	83	97.9	**93.7**
Accuracy (%)	81	93.8	**96.5**
Probit Regression Model			
Sensitivity (%)	81.3		
Specificity (%)	81.7		
Accuracy (%)	81.4		

For the developed SVM models, four different kernel functions were applied. Although the performance results of these kernels were almost equal, the best SVM model was obtained with a radial-based kernel function. As seen in Table 7, the best results were obtained with ANN (MLP) using selected 5 variables considering the patient's unconscious state in some cases. Therefore, it is possible to determine whether automatically diagnosed with a heart attack or not, by using the optimum 5 variables of a patient which are ECG change, ST segment change, gender, HS-troponin, and CK-MB. Furthermore, the ROC curve performance comparison of the machine learning-based heart attack decision models using selected variables is given in Figure 3.

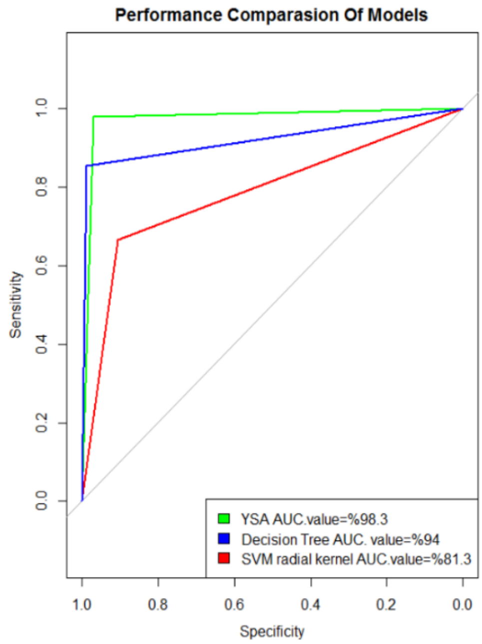

Figure 3. ROC curves of developed diagnosis models

4. DISCUSSION

According to the statistical analysis results for the feature selection process; HS Troponin, CK-MB, sex, ECG change, ST segment change, chronical disease, and patient pedigree variables have been selected due to the significant difference. However, chronical disease, heart disease, and patient pedigree information cannot be obtained considering the patient's unconscious state in some cases. Therefore, two different decision system models were developed and compared one of which used all 8 variables, while the other one used 5 variables except chronical disease, heart disease, and patient pedigree. As a result, a satisfactory successful decision support model has been developed for heart attack diagnosis using the optimum 5 variables.

For the machine learning-based models, the selected variables were obtained using statistical analysis methods and optimum variables were selected from these variables considering the patient's unconscious state in some cases. On the other hand, for the probit model, variables have been determined by the regression approach through model development. When compared to similar studies in the literature, this study is stand out by using a different approach based on probit regression and comparison with machine learning methods. In this study, classification models were implemented for heart attack decisions using probit regression, SVM, ANN, and decision tree methods. Consequently, the best decision support model was obtained using ANN with selected variables. In addition to these, the proposed study is significantly noticed with the high number of test data for heart attack classification with a sensitivity of 98% and specificity of 93.7% compared to similar studies in the literature, which can be seen in Table 8.

Table 7. Comparison of the proposed study with similar studies in the literature

Literature Studies	Method	Sens. (%)	Spec. (%)	Acc. (%)	Patients (Test Samples)	Data set Information	Variables
Doğan et al. (2007) [3]	Decision Tree (Heart attack)	100	100	100	50MI(+), 11 MI(-)	Not given in the paper	CK, CKMB, LDH, AST and ALT
Mair et al. (1995) [4]	Decision Tree (Heart attack)	91	90	90	45 MI(+), 49 unstable angina pectoris, 20 chest pain caused by other diseases	Emergency room of a Department of Internal Medicine (University Hospital)	ECG, creatine kinase, creatine kinase MB activity and mass concentration, myoglobin, and cardiac troponin T
Ghumbre et al. (2011) [6]	RBF network, SVM (Heart disease)	82.4 84.06	82.1 88.5	82.24 85.05	78 Myalgia (Normal), 139 Heart disease	Not given in the paper	Chest pain types (Left or Right side), Arm pain, Backache, Sweating, Breathlessness, Addiction, Diabetic, MAP, Pulse rate, ECG: ST elevation, ST depression, T elevation, T depression, Q waves, BSL, CKMB test
Soni et al. (2011) [25]	Decision Tree, Naive Bayes, ANN (Heart disease)	-	-	89 86.53 85.53	454	Machine Learning Repository of UCI	Sex, Chest Pain Type, Fasting Blood Sugar, Restecg, Exang, Slope, CA, Thal, Trest Blood Pressure, Serum Cholesterol, Thalach, Oldpeak, Age, Heart disease
Hazra et al. (2017) [26] Review study	RBF network **(Hannan et al.)**	-	-	90-97	75	Sahara Hospital, Aurangabad	Age, P1(Previous History), P2(Present History), P3(personnel History), P4(Physical Examination), CVS(Cardio Vascular System), RS(Respiratory System), PA(Per Abdomen), CNS (Central Nervous System), ECG (Electrocardiography) and BI (Blood Investigation)
	Learning Vector Quantization (LVQ) **(Chen et al.)** (Heart disease)	85	70	80	150	Machine Learning Repository of UCI	Age, sex, chest pain type, trestbps, cholesterol, fasting blood sugar, resting ecg, max heart rate, exercise induced angina, old peak, slope, number of vessels colored, and thal
Mujawar et al. (2015) [27]	Naive Bayes& Modified K-Means (Heart disease)	93	89	91	100 Heart disease 100 Not heart disease	Cleveland Heart Disease database	Sex, Chest Pain Type, Fasting Blood Sugar, Restecg, Exang, Slope, CA , Thal, Trest Blood Pressure, Serum Cholesterol, Thalach, Oldpeak, Age, Heart disease
Aydın et al. (2016) [28]	Bagging AdaBoostM1 Random Forest Naive Bayes RBF Network IBK NNge (Heart disease)	11.1 22.2 33.3 44.4 33.3 44.4 33.3	-	67.5 67.5 72.5 77.5 82.5 72.5 70	40 40	Long Beach VA Hospital Long Beach VA Hospital	Age, Sex, Chest Pain Type, Resting Blood Pressure, Serum Cholesterol, Fasting Blood Sugar, Resting Electrocardiographic Results, Maximum Heart Rate, Exercise induced angina, ST depression induced by exercise relative to rest,The Slope of The Peak Exercise St Segment, Number of Major Vessels, Defect Type, Heart disease
Florence et al. (2014) [29]	Decision Tree Neural Network (Heart attack)	98	53	-	76	Machine Learning Repository of UCI	Sex, Age, Cardiac Duration, Cholesterol, Signal Leval, Posibility of Attack (Yes/No)
Proposed Study	ANN SVM Decision Tree	**98** 79 91.7	**93.7** 83 97.9	**96.5** 81 93.8	145 97 MI(+), 48 MI(-)	Karadeniz Technical University Farabi Hospital	Sex, ECG change, ST Segment change, CK-MB (creatine kinase), HS Troponin (high sensitivity troponin)
	Probit Regression	81.3	81.7	81.4	-	Karadeniz Technical University Farabi Hospital	Sex, ECG change, HS Troponin (high sensitivity troponin), Chronical disease, Patient Pedigree

By using the proposed heart attack decision support model, it is aimed to reduce the number of repeated laboratory tests and ECG measurements to assist the physician in the process of deciding the probability of having a heart attack in patients who apply to the emergency department with chest pain and to make a definitive diagnosis. In addition to these, the proposed model can be used as a pilot decision support system in clinics after taking the required permissions. So, it can be developed and widened based on the evaluation results.

5. CONCLUSION

The proposed heart attack decision support system can be used as software by entering required variables or it can be integrated with the patient's tracking system in the hospital. By using the developed heart attack decision support system, it is possible to help the physician in the process of diagnosis of heart attack for patients who apply to the emergency service with chest pain compliment. Furthermore, it is aimed to reduce the number of repeated laboratory tests and ECG measurements so that a definite diagnosis can be made. Therefore, the proposed prediction model could assist in the diagnosis of MI quickly. In addition to these, if the proposed variables can be obtained with the help of portable devices in the future, the patient will be pre-diagnosed with a heart attack while being ambulance, and able to intervene first without wasting time. This will help to reduce the mortality due to heart attacks.

ACKNOWLEDGEMENTS

All necessary permissions such as ethics committee, hospital permit were obtained for the conducted study. No funding to declare.

CONFLICT OF INTEREST

The authors confirmed that there are no conflicts of interest regarding the publication of this article.

AUTHORSHIP CONTRIBUTIONS

Burçin Kurt; Contributed data or analysis tools; Performed the analysis; Wrote the paper.
İlknur Buçan Kırkbir; Collected the data; Performed the analysis.

APPENDIX

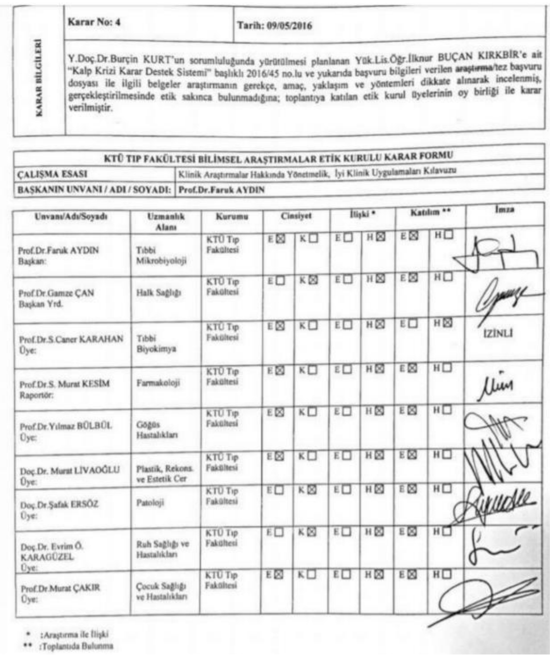

KARAR BİLGİLERİ

Karar No: 4 | Tarih: 09/05/2016

Y.Doç.Dr.Burçin KURT'un sorumluluğunda yürütülmesi planlanan Yük.Lis.Öğr.İlknur BUÇAN KIRKBİR'e ait "Kalp Krizi Karar Destek Sistemi" başlıklı 2016/45 no.lu ve yukarıda başvuru bilgileri verilen ~~araştırma~~/tez başvuru dosyası ile ilgili belgeler araştırmanın gerekçe, amaç, yaklaşım ve yöntemleri dikkate alınarak incelenmiş, gerçekleştirilmesinde etik sakınca bulunmadığına; toplantıya katılan etik kurul üyelerinin oy birliği ile karar verilmiştir.

KTÜ TIP FAKÜLTESİ BİLİMSEL ARAŞTIRMALAR ETİK KURULU KARAR FORMU

ÇALIŞMA ESASI	Klinik Araştırmalar Hakkında Yönetmelik, İyi Klinik Uygulamaları Kılavuzu
BAŞKANIN UNVANI / ADI / SOYADI:	Prof.Dr.Faruk AYDIN

Unvanı/Adı/Soyadı	Uzmanlık Alanı	Kurumu	Cinsiyet		İlişki *		Katılım **		İmza
Prof.Dr.Faruk AYDIN Başkan:	Tıbbi Mikrobiyoloji	KTÜ Tıp Fakültesi	E ☒	K ☐	E ☐	H ☒	E ☒	H ☐	
Prof.Dr.Gamze ÇAN Başkan Yrd.	Halk Sağlığı	KTÜ Tıp Fakültesi	E ☐	K ☒	E ☐	H ☒	E ☒	H ☐	
Prof.Dr.S.Caner KARAHAN Üye:	Tıbbi Biyokimya	KTÜ Tıp Fakültesi	E ☒	K ☐	E ☐	H ☒	E ☐	H ☒	İZİNLİ
Prof.Dr.S. Murat KESİM Raportör:	Farmakoloji	KTÜ Tıp Fakültesi	E ☒	K ☐	E ☐	H ☒	E ☒	H ☐	
Prof.Dr.Yılmaz BÜLBÜL Üye:	Göğüs Hastalıkları	KTÜ Tıp Fakültesi	E ☒	K ☐	E ☐	H ☒	E ☒	H ☐	
Doç.Dr. Murat LİVAOĞLU Üye:	Plastik, Rekons. ve Estetik Cer	KTÜ Tıp Fakültesi	E ☒	K ☐	E ☐	H ☒	E ☒	H ☐	
Doç.Dr.Şafak ERSÖZ Üye:	Patoloji	KTÜ Tıp Fakültesi	E ☐	K ☒	E ☐	H ☒	E ☒	H ☐	
Doç.Dr. Evrim Ö. KARAGÜZEL Üye:	Ruh Sağlığı ve Hastalıkları	KTÜ Tıp Fakültesi	E ☐	K ☒	E ☐	H ☒	E ☒	H ☐	
Prof.Dr.Murat ÇAKIR Üye:	Çocuk Sağlığı ve Hastalıkları	KTÜ Tıp Fakültesi	E ☒	K ☐	E ☐	H ☒	E ☒	H ☐	

* :Araştırma ile İlişki
** :Toplantıda Bulunma

Figure A1. The ethical approval

Table A1. The descriptive statistics of categorical variables for each group

Variable	Valid	Frequency	Percent	CumPercent
Sex	Female	35	18.23	18.23
Sex	Male	157	81.77	100.00
Sex	TOTAL	192	NA	NA
EKG_Change	No	45	23.44	23.44
EKG_Change	Yes	147	76.56	100.00
EKG_Change	TOTAL	192	NA	NA
ST_Segment_Change	No	153	79.69	79.69
ST_Segment_Change	Yes	39	20.31	100.00
ST_Segment_Change	TOTAL	192	NA	NA
Chronical_Disease	No	76	39.58	39.58
Chronical_Disease	Yes	116	60.42	100.00
Chronical_Disease	TOTAL	192	NA	NA
Heart_Disease	No	143	74.48	74.48
Heart_Disease	Yes	49	25.52	100.00
Heart_Disease	TOTAL	192	NA	NA
Patient_Pedigree	No	138	71.88	71.88
Patient_Pedigree	Yes	54	28.12	100.00
Patient_Pedigree	TOTAL	192	NA	NA

(a) Heart Attack group

Variable	Valid	Frequency	Percent	CumPercent
Sex	Female	65	41.14	41.14
Sex	Male	93	58.86	100.00
Sex	TOTAL	158	NA	NA
EKG_Change	No	131	82.91	82.91
EKG_Change	Yes	27	17.09	100.00
EKG_Change	TOTAL	158	NA	NA
Chronical_Disease	No	106	67.09	67.09
Chronical_Disease	Yes	52	32.91	100.00
Chronical_Disease	TOTAL	158	NA	NA
Heart_Disease	No	119	75.32	75.32
Heart_Disease	Yes	39	24.68	100.00
Heart_Disease	TOTAL	158	NA	NA
Patient_Pedigree	No	147	93.04	93.04
Patient_Pedigree	Yes	11	6.96	100.00
Patient_Pedigree	TOTAL	158	NA	NA

b) Not Heart Attack group

Table A2. The descriptive statistics of numerical variables for patients for each group

	Heart Attack.CK.MB	Heart Attack.HS.Troponin	Not Heart Attack.CK.MB	Not Heart Attack.HS.Troponin
nbr.val	192.00	192.00	158.00	158.00
nbr.null	0.00	0.00	0.00	0.00
nbr.na	0.00	0.00	0.00	0.00
min	1.03	0.01	0.30	0.01
max	1570.00	8315.00	4675.00	3985.00
range	1568.97	8314.99	4674.70	3984.99
sum	14762.69	134426.97	5487.77	11933.29
median	14.80	153.80	2.16	6.46
mean	76.89	700.14	34.73	75.53
SE.mean	13.28	97.95	29.57	27.71
CI.mean.0.95	26.20	193.20	58.40	54.74
var	33877.62	1842101.00	138110.20	121347.51
std.dev	184.06	1357.24	371.63	348.35
coef.var	2.39	1.94	10.70	4.61
skewness	5.68	3.09	12.32	9.26
skew.2SE	16.20	8.81	31.91	23.99
kurtosis	38.41	10.15	150.84	98.08
kurt.2SE	55.01	14.53	196.51	127.78
normtest.W	0.40	0.55	0.06	0.20
normtest.p	0.00	0.00	0.00	0.00

*nbr.val : Number of instances, nbr.null: Number of missing values, nbr.na: Number of NA value

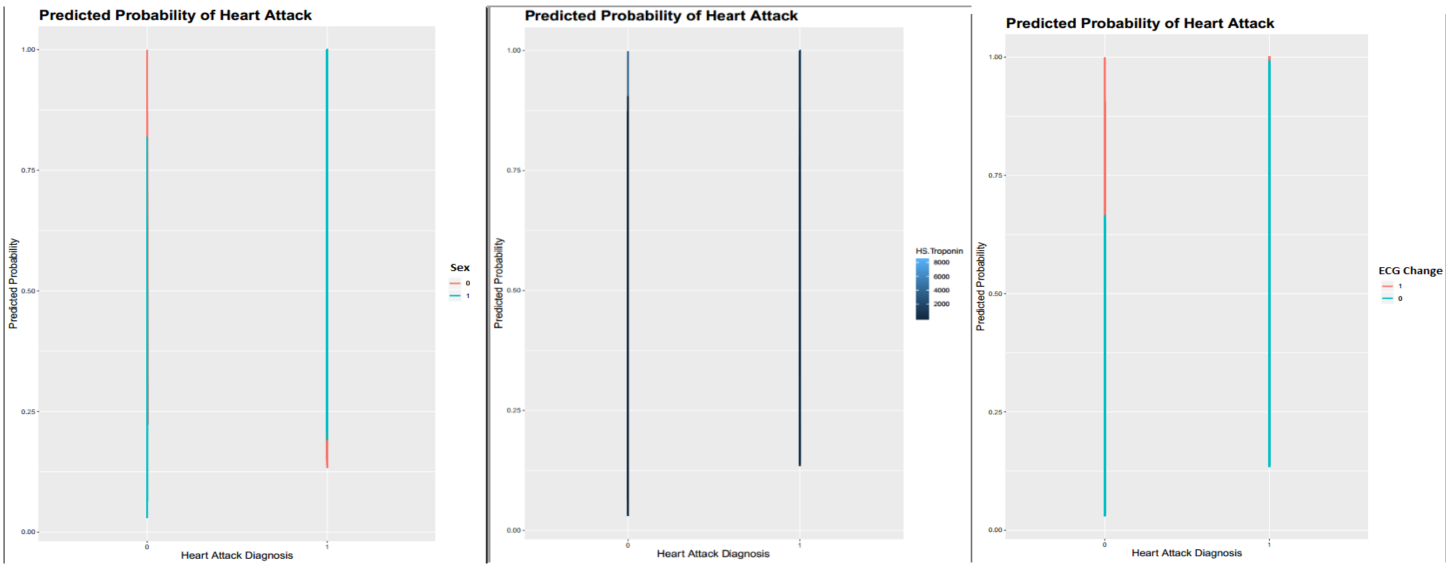

(a)Sex=0, Male and Sex=1, Female (b) Hs. Troponin (c) ECG.change=0,No and ECG.change=1, Yes

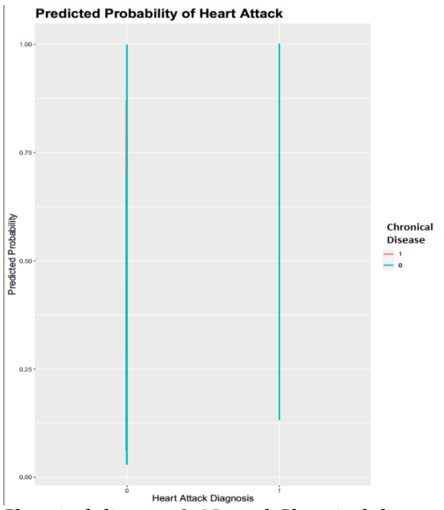

(d) Chronical.disease=0, No and Chronical.disease =1, Yes

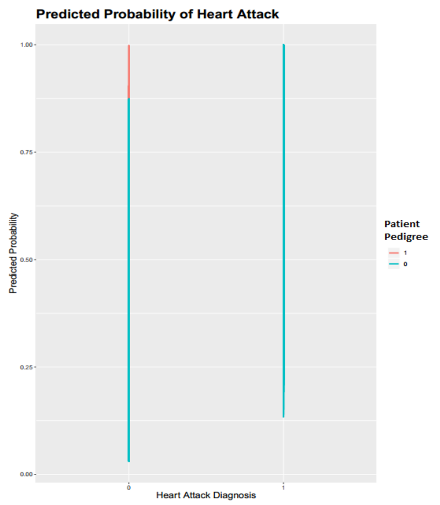

(e) Patient.pedigree=0, No and Patient.pedigree =1, Yes

Figure A2. The predicted probabilities of heart attack for statistically significant variables in the developed probit model (Heart attack diagnosis=0, No and Heart attack diagnosis =1, Yes)

REFERENCES

[1] Türkiye cardiovascular disease prevention and control program action plan. Ministry of Health, Public Health Institution of Türkiye, 988, 2015.

[2] Storrow AB, Gibler WB. Chest pain centers: diagnosis of acute coronary syndromes. Ann Emerg Med 2000; 35: 449-461.

[3] Doğan Ş, Türkoğlu İ, Yavuzkır M. Heart attack detection from cardiac by using decision trees. eJournal of New World Sciences Academy 2007; 2: 39-50.

[4] Mair J, Smidt J, Lechleitner P, Dienstl F, Puschendorf B. A decision tree for the early diagnosis of acute myocardial infarction in nontraumatic chest pain patients at hospital admission. The Journal of Emergency Medicine 1995; 14: 1502-1509.

[5] Dangare CS, Apte SS. A data mining approach for prediction of heart disease using neural networks. International Journal of Computer Engineering and Technology 2012; 3: 30-40.

[6] Ghumbre S, Patil C, Ghatol A. Heart disease diagnosis using support vector machine. International Conference on Computer Science and Information Technology (ICCSIT'2011) 17-18 December 2011; Pattaya, Thailand, 84-88.

[7] Garson GD. Probit Regression and Response Models. Statistical Associates Publishers, 2013.

[8] Razzaghi M. The probit link function in generalized linear models for data mining applications. Journal of Modern Applied Statistical Methods 2013; 12(1): 164-169.

[9] Hosmer D, Lemeshow S. Applied Logistic Regression (Second Edition). New York: John Wiley & Sons, Inc, 2000.

[10] Long JS. Regression Models for Categorical and Limited Dependent Variables. Thousand Oaks, CA: Sage Publications, 1997.

[11] Smithson M, Merkle EC. Generalized Linear Models for Categorical and Continuous Limited Dependent Variables. New York, USA: CRC Press, 2013.

[12] Yazıcı B, Alpu Ö, Yang Y. Comparison of goodness-of-fit measures in probit regression model. Communications in Statistics-Simulation and Computation 2007; 36: 1061–1073.

[13] Aldrich J.H., Nelson F.D.. Probability, logit, and probit models (Quantitative Applications in the Social Sciences). California, US: Sage Publications, 1984.

[14] McFadden D. Quantitative methods for analyzing travel behavior of individuals: some recent developments. London, England: D. Hensher and P. Stopher (eds.), Behavioural Travel Modeling, 1978.

[15] Veall MR., Zimmerman KF. Evaluating pseudo-R2's for binary probit models. Quality and Quantity 1994; 28: 151–164.

[16] Güner N, Çomak E. Predicting the success of engineering students in mathematics lessons using support vector machines. Pamukkale University Journal of Engineering Sciences 2011; 2: 87-96.

[17] Kavzoğlu T, Çölkesen İ. Investigation of the effects of kernel functions on the classification of satellite images with support vector machines. Map Journal 2010; 144: 73-82.

[18] Yılmaz Akşehirli Ö, Ankaralı H, Aydın D, Saraçlı Ö. An alternative approach to medical prediction: Support vector machines. Türkiye Clinics Journal of Biostatistics 2013; 1: 19-28.

[19] Ma Y, Guo G. Support Vector Machines Applications. MN, USA: Springer, 2014.

[20] Berry MJA, Linoff GS. Mastering Data Mining: The Art and Science of Customer Relationship. 1st ed. New York, US: Wiley Computer Publishing, 2000.

[21] Balaban ME, Kartal E. Data mining and machine learning basic algorithms and applications with R language. Istanbul, Türkiye: Caglayan Bookstore, 2015.

[22] Çalış A, Kayapınar S, Çetinyokuş T. An application on computer and internet security with decision tree algorithms in data mining. Journal of Industrial Engineering 2014; 2-19.

[23] Öztemel E. Artificial neural networks. Third edition. İstanbul, Türkiye: Papatya Publishing Education Inc. 2012.

[24] Gönül Y, Ulu Ş, Bucak A. Artificial neural networks and their use in clinical research. Journal of General Medicine 2015; 25: 104-111.

[25] Soni J, Ansari U, Sharma D, Soni S. Predictive data mining for medical diagnosis: An overview of heart disease prediction. International Journal of Computer Applications 2011; 17: 43-48.

[26] Hazra A, Mandal SK, Gupta A, Mukherjee A and Mukherjee A. Heart disease diagnosis and prediction using machine learning and data mining techniques: a review. Advances in Computational Sciences and Technology 2017; 10 (7): 2137-2159.

[27] Mujawar SH, Devale PR. Prediction of heart disease using modified k-means and by using naive bayes. International Journal of Innovative Research in Computer and Communication Engineering 2015; 3(10): 10265-10273.

[28] Aydın S, Ahanpanjeh M, Mohabbatiyan S. Comparison and evaluation of data mining techniques in the diagnosis of heart disease. International Journal on Computational Science & Applications (IJCSA) 2016; 6(1): 1-15.

[29] Florence S, Bhuvaneswari Amma NG, Annapoorani G and Malathi K, "Predicting The Risk of Heart Attacks using Neural Network and Decision Tree", International Journal of Innovative Research In Computer and Communication Engineering, ISSN (Online): 2320-9801, November 2014; Vol. 2, Issue 11, pp. 7025-7028.

ESKİŞEHİR TECHNICAL UNIVERSITY JOURNAL OF SCIENCE AND TECHNOLOGY
A- APPLIED SCIENCES AND ENGINEERING

2023, 24(2), pp. 121-140, DOI: 10.18038/estubtda.1162963

RESEARCH ARTICLE

NUMERICAL SOLUTIONS OF REACTION-DIFFUSION EQUATION SYSTEMS WITH TRIGONOMETRIC QUINTIC B-SPLINE COLLOCATION ALGORITHM

Aysun TOK ONARCAN [1], Nihat ADAR [2], Idiris DAG [2]

[1] Department of Informatics, Eskişehir Osmangazi University, Eskişehir, Türkiye
[2] Department of Computer Engineering, Eskişehir Osmangazi University, Eskişehir, Türkiye

ABSTRACT

In this study, trigonometric quintic B-spline collocation method is constructed for computing numerical solutions of the reaction-diffusion system (RDS). Schnakenberg, Gray-Scott and Brusselator models are special cases of reaction-diffusion systems considered as examples in this paper. Crank-Nicolson formulae is used for the time discretization of the generalized RDS and the nonlinear terms in time-discretized form of RDS are linearized using the Taylor expansion. The fully integration of the generalized system is carried out using the collocation method based on the trigonometric quintic B-splines. The method is tested on different problems to illustrate the accuracy. The error norms are calculated for the linear problem whereas the relative error is given for nonlinear problems. Both simple and easy B-spline algorithms are illustrated to give the solutions of RDS and also the graphical representation of the efficient solutions are presented for the nonlinear RDSs. Combination of the quintic B-splines and the collocation method is shown to present numerical solutions of the RDS successfully. With the presented method, it is possible to get approximate solutions as well as their derivatives up to an order of four on the problem domain.

Keywords: Reaction-diffusion; Collocation; B-spline; Finite element method, Brusselator, Schnakenberg, Gray-Scott

1. INTRODUCTION

In various disciplines, phenomena such as pattern formation, autocatalytic chemical reactions and population dynamics are modelled by the reaction-diffusion (RD) equation systems. These RDSs are mathematical models of chemical exchange reactions some of which of them also generates various patterns in biology, geology, physics and ecology. RDSs exhibit very rich dynamics behavior including periodic and quasi-periodic solutions. Theoretical studies have been developed to describe such dynamic behaviors. Most diffusion systems include the nonlinear reaction term making it difficult to solve analytically. Attempts have been made to look for the numerical solutions to reveal more dynamic behaviors of RDSs. Various numerical methods also have been used to find the numerical solutions of RDSs.

In the past, implicit-explicit method was designed to obtain some type of patterns, as a solution of RD equations by Ruuth [1]. An adaptive moving mesh method and a moving grid finite element method were produced for the numerical solutions of RDS respectively [2, 3]. Operator splitting methods were set up to solve RDSs in the studies [4, 5]. Both a Crank-Nicholson method with a Multi-Grid solver (CN-MG) and the implicit integration factor method were presented in the study [6]. Galerkin finite element method was constructed for getting numerical solutions of the RDSs [7]. Additionally, the differential quadrature (DQ) method was constructed for calculating numerical solutions of RDSs by Mittal et all. [8] and Jiwari et all. [9]. Recently, Jiwari presented a kind of DQ method for capturing various patterns [10].

*Corresponding Author: atonarcan@ogu.edu.tr
Received: 16.08.2022 Published: 21.06.2023

The spline functions of various degrees are accompanied to construct numerical methods for solving differential equations of certain order. Since the resulting matrix obtained for application of the spline related numerical method to the differential equation is always diagonal, it can be solved easily. High order continuous differentiable approximate solutions can be produced by way of using high order spline functions for solutions of the differential equations. B-splines are defined as a basis of the spline space[11]. Polynomial B-splines are extensively used for finding numerical solutions of differential equations, function approximation and computer-aided design. The numerical procedure based on the B-spline collocation method has been increasingly applied for nonlinear evolution equations in various fields of science [12]-[16]. The numerical methods for solving types of ordinary differential equations with trigonometric quadratic and cubic B-spline were given by A. Nikolis [17, 18]. Numerical solutions of RD systems with polynomial B-spline collocation method (PQBCM) was presented in the work of Sahin [19]. Exponential cubic B-spline algorithm for the system of RD equations was presented by Ersoy O. and Dag I.[20] and trigonometric cubic B-spline algorithm was studied by Onarcan et all [21]. Specific RDS models were studied with finite element methods by the researchers [22, 23]. Very recently Hepson O.E. and others applied quartic trigonometric tension B-spline collocation method to get some numerical simulations of RDS [24].

In this study, we use the fifth degree trigonometric B-spline termed as trigonometric quintic B-spline (TQB) to establish a collocation method to find numerical solutions of a reaction-diffusion equation systems. In the literature review, it has been found that few studies have been done with trigonometric quintic of B-spline [25]-[28]. With the TQB based collocation method that we presented, it is possible to get approximate solutions as well as its derivatives up to an order of four at each point of the problem domain. Linear problem and nonlinear Brusselator [29], Schnakenberg [30] and Gray-Scott [31] models are studied with the proposed TQB collocation method.

One dimensional time-dependent reaction-diffusion equation systems can be defined as follows:

$$\begin{aligned} \frac{\partial U}{\partial t} &= D_u \frac{\partial^2 U}{\partial x^2} + F(U,V) \\ \frac{\partial V}{\partial t} &= D_v \frac{\partial^2 V}{\partial x^2} + G(U,V) \end{aligned} \tag{1}$$

where $U = U(x,t), V = V(x,t)$ and $\Omega \subset R^2$ is the problem domain, D_u is the diffusion coefficient of U and D_v is the diffusion coefficients of V also F and G indicates the growth and interaction functions that represent the reactions of the system. F and G are, in general, nonlinear functions. A general one dimensional RD equation system which includes all test problems mentioned in this paper, is expressed as:

$$\begin{aligned} \frac{\partial U}{\partial t} &= a_1 \frac{\partial^2 U}{\partial x^2} + b_1 U + c_1 V + d_1 U^2 V + e_1 UV + m_1 UV^2 + n_1 \\ \frac{\partial V}{\partial t} &= a_2 \frac{\partial^2 V}{\partial x^2} + b_2 U + c_2 V + d_2 U^2 V + e_2 UV + m_2 UV^2 + n_2 \end{aligned} \tag{2}$$

For computational purpose, solution space of the problems $(-\infty, \infty)$ should be limited to interval (x_0, x_N). In this case, system (2)'s initial conditions are either the homogenous boundary conditions of Dirichlet

$$U(x_0,t) = U(x_N,t) = 0, \qquad V(x_0,t) = V(x_N,t) = 0, \tag{3}$$

or homogeneous Neumann boundary conditions

$$U_x(x_0,t) = U_x(x_N,t) = 0, \qquad V_x(x_0,t) = V_x(x_N,t) = 0 \tag{4}$$

The coefficients of the system (2) are depicted in Table 1, matching the coefficients of the test problems appropriately according to the characteristics of each test problem.

Table 1: Matching the coefficients of test problems with the model system

Test Problem	a_1	a_2	b_1	b_2	c_1	c_2	d_1	d_2	e_1	e_2	m_1	m_2	n_1	n_2
Linear	d	d	$-a$	0	1	$-b$	0	0	0	0	0	0	0	0
Brusselator	ε_1	ε_2	$-(B+1)$	B	0	0	1	-1	0	0	0	0	A	0
Schnakenberg	1	d	$-\zeta$	0	0	0	ζ	$-\zeta$	0	0	0	0	ζa	ζb
Gray-Scott	ε_1	ε_2	$-f$	0	0	$-k$	0	0	0	0	-1	1	f	0

2. TRIGONOMETRIC QUINTIC B-SPLINE METHOD

Consider the solution domain of the differential problem $[a = x_0, b = x_N]$ is partitioned into a mesh of uniform length $h = x_{m+1} - x_m$ by knots x_m, where $m = -2, \dots, N+2$. On this partition, together with additional knots $x_{N-2}, x_{N-1}, x_{N+1}, x_{N+2}$ outside the problem domain, the trigonometric quintic B-spline $T_m^5(x)$ basis functions at knots are given as:

$$T_m^5(x) = \frac{1}{\theta}\begin{cases} \rho^5(x_{m-3}), & x \in [x_{m-3}, x_{m-2}] \\ -\rho^4(x_{m-3})\rho(x_{m-1}) - \rho^3(x_{m-3})\rho(x_m)\rho(x_{m-3}) & \\ -\rho^2(x_{m-3})\rho(x_{m+1})\rho^2(x_{m-2}) - \rho(x_{m-3})\rho(x_{m+2})\rho^3(x_{m-2}) & \\ -\rho(x_{m+3})\rho^4(x_{m-2}), & x \in [x_{m-2}, x_{m-1}] \\ \rho^3(x_{m-3})\rho^2(x_m) + \rho^2(x_{m-3})\rho(x_{m+1})\rho(x_{m-2})\rho(x_m) & \\ +\rho^2(x_{m-3})\rho^2(x_{m+1})\rho(x_{m-1}) + \rho(x_{m+3})\rho(x_{m+2})\rho^2(x_{m-2})\rho(x_m) & \\ +\rho(x_{m-3})\rho(x_{m+2})\rho(x_{m-2})\rho(x_{m+1})\rho(x_{m-1}) + \rho(x_{m-3})\rho^2(x_{m+2})\rho^2(x_{m-1}) & \\ +\rho(x_{m+3})\rho^3(x_{m-2})\rho(x_m) + \rho(x_{m+3})\rho^2(x_{m-2})\rho(x_{m+1})\rho(x_{m-1}) & \\ +\rho(x_{m+3})\rho(x_{m-2})\rho(x_{m+2})\rho^2(x_{m-1}) + \rho^2(x_{m+3})\rho^3(x_{m-1}), & x \in [x_{m-1}, x_m] \\ -\rho^2(x_{m-3})\rho^3(x_{m+1}) - \rho(x_{m-3})\rho(x_{m+2})\rho(x_{m-2})\rho^2(x_{m+1}) & \\ -\rho(x_{m-3})\rho^2(x_{m+2})\rho(x_{m-1})\rho(x_{m+1}) - \rho(x_{m-3})\rho^3(x_{m+2})\rho(x_m) & \\ -\rho(x_{m+3})\rho^2(x_{m-2})\rho^2(x_m) - \rho(x_{m+3})\rho(x_{m-2})\rho(x_{m+2})\rho(x_{m-1})\rho(x_{m+1}) & \\ -\rho(x_{m+3})\rho(x_{m-2})\rho^2(x_{m+2})\rho(x_m) - \rho^2(x_{m+3})\rho^2(x_{m-3}) & \\ -\rho^2(x_{m+3})\rho(x_{m-1})\rho(x_{m+2})\rho(x_m) - \rho^3(x_{m+3})\rho^2(x_m), & x \in [x_m, x_{m+1}] \\ \rho(x_{m-3})\rho^4(x_{m+2}) & \\ +\rho(x_{m+3})\rho(x_{m-2})\rho^3(x_{m+2}) + \rho^2(x_{m+3})\rho(x_{m-1})\rho^2(x_{m+2}) & \\ +\rho^3(x_{m+3})\rho(x_m)\rho(x_{m+2}) + \rho^4(x_{m+3})\rho(x_{m+1}), & x \in [x_{m+1}, x_{m+2}] \\ -\rho^5(x_{m+3}), & x \in [x_{m+2}, x_{m+3}] \\ 0, & otherwise \end{cases} \tag{5}$$

where $\rho(x_m)$, θ and m are;

$$\rho(x_m) = sin(\frac{x-x_m}{2}),$$

$$\theta = sin(\frac{5h}{2})sin(2h)sin(\frac{3h}{2})sin(h)sin(\frac{h}{2}),$$

$$m = O(1)N.$$

The $T_m^5(x)$ functions and its principle derivatives vanish outside the region $[x_{m-3}, x_{m+3}]$. The set of those B-splines $T_m^5(x)$ $, m = -2, \ldots, N+2$ are a basis for the trigonometric spline space. An approximate solution $U_N(x,t)$ and $V_N(x,t)$ to the unknown solution $U(x,t)$ and $V(x,t)$ can be assumed as the forms

$$U_N(x,t) = \sum_{i=-2}^{N+2} T_i^5(x)\delta_i(t), \quad V_N(x,t) = \sum_{i=-2}^{N+2} T_i^5(x)\gamma_i(t) \tag{6}$$

Where δ_i and γ_i are time dependent parameters to be determined using the collocation method on the points $x_i,\ i = 0, \ldots, N$ together with boundary and initial conditions. $T_m^5(x)$ trigonometric quintic B-spline functions are zero outside the interval $[x_{m-3}, x_{m+3}]$ and $T_m^5(x)$ functions sequentially covers six elements in the interval $[x_{m-3}, x_{m+3}]$ so that, each $[x_m, x_{m+1}]$ finite element is covered by the six $T_{m-2}^5, T_{m-1}^5, T_m^5, T_{m+1}^5, T_{m+2}^5$, and T_{m+3}^5 trigonometric quintic B-spline. In this case the approach (6) can be written as ;

$$\begin{aligned} U_N(x,t) &= \sum_{i=m-2}^{m+3} T_i^5(x)\delta_i = T_{m-2}^5(x)\delta_{m-2} + T_{m-1}^5(x)\delta_{m-1} + T_m^5(x)\delta_m + T_{m+1}^5(x)\delta_{m+1} \\ &\quad + T_{m+2}^5(x)\delta_{m+2} + T_{m+3}^5(x)\delta_{m+3} \\ V_N(x,t) &= \sum_{i=m-2}^{m+3} T_i^5(x)\gamma_i = T_{m-2}^5(x)\gamma_{m-2} + T_{m-1}^5(x)\gamma_{m-1} + T_m^5(x)\gamma_m + T_{m+1}^5(x)\gamma_{m+1} \\ &\quad + T_{m+2}^5(x)\gamma_{m+2} + T_{m+3}^5(x)\gamma_{m+3} \end{aligned} \tag{7}$$

In these numerical approaches, the approximate solutions and its first, second, third and fourth derivative at the knots can be written in terms of the time parameters using $T_m^5(x)$ and Eq.(6) as given in the following relationships:

$$\begin{aligned} U_m &= \alpha_1\delta_{m-2} + \alpha_2\delta_{m-1} + \alpha_3\delta_m + \alpha_2\delta_{m+1} + \alpha_1\delta_{m+2} \\ U_m' &= -\alpha_4\delta_{m-2} - \alpha_5\delta_{m-1} + \alpha_5\delta_{m+1} - \alpha_4\delta_{m+2} \\ U_m'' &= \alpha_6\delta_{m-2} + \alpha_7\delta_{m-1} + \alpha_8\delta_m + \alpha_7\delta_{m+1} + \alpha_6\delta_{m+2} \\ U_m''' &= -\alpha_9\delta_{m-2} + \alpha_{10}\delta_{m-1} - \alpha_{10}\delta_{m+1} - \alpha_9\delta_{m+2} \\ U_m'''' &= \alpha_{11}\delta_{m-2} + \alpha_{12}\delta_{m-1} + \alpha_{13}\delta_m + \alpha_{12}\delta_{m+1} + \alpha_{11}\delta_{m+2} \\ V_m &= \alpha_1\gamma_{m-2} + \alpha_2\gamma_{m-1} + \alpha_3\gamma_m + \alpha_2\gamma_{m+1} + \alpha_1\gamma_{m+2} \\ V_m' &= -\alpha_4\gamma_{m-2} - \alpha_5\gamma_{m-1} + \alpha_5\gamma_{m+1} + \alpha_4\gamma_{m+2} \\ V_m'' &= \alpha_6\gamma_{m-2} + \alpha_7\gamma_{m-1} + \alpha_8\gamma_m + \alpha_7\gamma_{m+1} + \alpha_6\gamma_{m+2} \\ V_m''' &= -\alpha_9\gamma_{m-2} + \alpha_{10}\gamma_{m-1} - \alpha_{10}\gamma_{m+1} + \alpha_9\gamma_{m+2} \\ V_m'''' &= \alpha_{11}\gamma_{m-2} + \alpha_{12}\gamma_{m-1} + \alpha_{13}\gamma_m + \alpha_{12}\gamma_{m+1} + \alpha_{11}\gamma_{m+2} \end{aligned} \tag{8}$$

where the coefficients are:

$$
\begin{aligned}
\alpha_1 &= \frac{sin^5(\frac{h}{2})}{\theta} \\
\alpha_2 &= \frac{2sin^5(\frac{h}{2})cos(\frac{h}{2})(16cos^2(\frac{h}{2}) - 3)}{\theta} \\
\alpha_3 &= \frac{2(1 + 48cos^4(\frac{h}{2}) - 16cos^2(\frac{h}{2})sin^5(\frac{h}{2}))}{\theta} \\
\alpha_4 &= \frac{\frac{5}{2}sin^4(\frac{h}{2})cos(\frac{h}{2})}{\theta} \\
\alpha_5 &= \frac{5sin^4(\frac{h}{2})cos^2(\frac{h}{2})(8cos^2(\frac{h}{2}) - 3)}{\theta} \\
\alpha_6 &= \frac{\frac{5}{4}sin^3(\frac{h}{2})(5cos^2(\frac{h}{2}) - 1)}{\theta} \\
\alpha_7 &= \frac{\frac{5}{2}sin^3(\frac{h}{2})(cos(\frac{h}{2})(-15cos^2(\frac{h}{2}) + 3 + 16cos^4(\frac{h}{2}))}{\theta} \\
\alpha_8 &= \frac{-\frac{5}{2}sin^3(\frac{h}{2})(16cos^6(\frac{h}{2}) - 5cos^6(\frac{h}{2}) + 1)}{\theta} \\
\alpha_9 &= \frac{\frac{5}{8}sin^2(\frac{h}{2})cos(\frac{h}{2})(25cos^2(\frac{h}{2}) - 13)}{\theta} \\
\alpha_{10} &= \frac{-\frac{5}{4}sin^2(\frac{h}{2})(cos^2(\frac{h}{2})(8cos^4(\frac{h}{2}) - 35cos^2(\frac{h}{2}) + 15)}{\theta} \\
\alpha_{11} &= \frac{\frac{5}{16}(125cos^4(\frac{h}{2}) - 114cos^2(\frac{h}{2}) + 13)sin(\frac{h}{2}))}{\theta} \\
\alpha_{12} &= \frac{-\frac{5}{8}sin(\frac{h}{2})cos(\frac{h}{2})(176cos^6(\frac{h}{2}) - 137cos^4(\frac{h}{2}) - 6cos^2(\frac{h}{2}) + 15)}{\theta} \\
\alpha_{13} &= \frac{\frac{5}{8}(92cos^6(\frac{h}{2}) - 117cos^4(\frac{h}{2}) + 62cos^2(\frac{h}{2}) - 13)(-1 + 4cos^2(\frac{h}{2})sin(\frac{h}{2}))}{\theta}
\end{aligned}
\tag{9}
$$

The Crank–Nicholson formulas are used for time discretization.

$$
U_t = \frac{U^{n+1} - U^n}{\Delta t}, \quad U = \frac{U^{n+1} + U^n}{2}, \quad V_t = \frac{V^{n+1} - V^n}{\Delta t}, \quad V = \frac{V^{n+1} + V^n}{2} \tag{10}
$$

The unknown U and V functions and their derivatives are discretized to yield time integrated reaction-diffusion system:

$$\frac{U^{n+1}-U^{n}}{\Delta t}-a_1\frac{U_{xx}^{n+1}+U_{xx}^{n}}{2}-b_1\frac{U^{n+1}+U^{n}}{2}-c_1\frac{V^{n+1}+V^{n}}{2}-d_1\frac{(U^2V)^{n+1}+(U^2V)^{n}}{2}-e_1\frac{(UV)^{n+1}+(UV)^{n}}{2}-m_1\frac{(UV^2)^{n+1}+(UV^2)^{n}}{2}-n_1=0$$
$$\frac{V^{n+1}-V^{n}}{\Delta t}-a_2\frac{V_{xx}^{n+1}+V_{xx}^{n}}{2}-b_2\frac{U^{n+1}+U^{n}}{2}-c_2\frac{V^{n+1}+V^{n}}{2}-d_2\frac{(U^2V)^{n+1}+(U^2V)^{n}}{2}-e_2\frac{(UV)^{n+1}+(UV)^{n}}{2}-m_2\frac{(UV^2)^{n+1}+(UV^2)^{n}}{2}-n_2=0 \quad (11)$$

where $U^{n+1}=U(x,t)^{n+1}$ and $V^{n+1}=V(x,t)^{n+1}$ are solutions of the equations at the $(n+1)$th time level. Here $t^{n+1}=t^{n}+\Delta t$ and Δt is the time step, superscripts denote the n th level $t^{n}=n\Delta t$.

The nonlinear terms $(U^2V)^{n+1}$, $(UV^2)^{n+1}$and $(UV)^{n+1}$ in equation (11) are linearized by using the Rubin-Graves [33] forms:

$$(U^2V)^{n+1}=U^{n+1}U^{n}V^{n}+U^{n}U^{n+1}V^{n}+U^{n}U^{n}V^{n+1}-2U^{n}U^{n}V^{n}$$
$$(UV^2)^{n+1}=U^{n+1}V^{n}V^{n}+U^{n}V^{n+1}V^{n}+U^{n}V^{n}V^{n+1}-2U^{n}V^{n}V^{n} \quad (12)$$
$$(UV)^{n+1}=U^{n+1}V^{n}+U^{n}V^{n+1}-U^{n}V^{n}$$

Then we substitute (12) in (11) and the linearized model of the equation system (2) results in the following form:

$$-\frac{a_1}{2}U_{xx}^{n+1}+\beta_{m1}U^{n+1}+\beta_{m2}V^{n+1}=\frac{a_1}{2}U_{xx}^{n}+\beta_{m3}U^{n}+\beta_{m4}V^{n}+n_1$$
$$-\frac{a_2}{2}V_{xx}^{n+1}+\beta_{m5}U^{n+1}+\beta_{m6}V^{n+1}=\frac{a_2}{2}V_{xx}^{n}+\beta_{m7}U^{n}+\beta_{m8}V^{n}+n_2 \quad (13)$$

where

$$\beta_{m1}=\frac{1}{\Delta t}-\frac{b_1}{2}-d_1U^{n}V^{n}-\frac{e_1}{2}V^{n}-\frac{m_1}{2}(V^{n})^2$$
$$\beta_{m2}=\frac{1}{\Delta t}-\frac{c_1}{2}-\frac{d_1}{2}(U^{n})^2-\frac{e_1}{2}U^{n}-m_1U^{n}V^{n}$$
$$\beta_{m3}=\frac{1}{\Delta t}+\frac{b1}{2}-\frac{m1}{2}(V^{n})^2$$
$$\beta_{m4}=\frac{c1}{2}-\frac{d1}{2}(U^{n})^2$$
$$\beta_{m5}=-\frac{b_2}{2}-d_2U^{n}V^{n}-\frac{e_2}{2}V^{n}-\frac{m_2}{2}(V^{n})^2 \quad (14)$$
$$\beta_{m6}=\frac{1}{\Delta t}-\frac{c_2}{2}-\frac{d_2}{2}(U^{n})^2-\frac{e_2}{2}U^{n}-m_2U^{n}V^{n}$$
$$\beta_{m7}=\frac{b_2}{2}-\frac{m_2}{2}(V^{n})^2$$
$$\beta_{m8}=\frac{1}{\Delta t}+\frac{c_2}{2}-\frac{d_2}{2}(U^{n})^2.$$

We substitute the approximate solutions (8) into (13) which yields the fully-discretized equations in space.

$$\begin{aligned}
&\mu_{m1}\delta_{m-2}^{n+1}+\mu_{m2}\gamma_{m-2}^{n+1}+\mu_{m3}\delta_{m-1}^{n+1}+\mu_{m4}\gamma_{m-1+}^{n+1}+\mu_{m5}\delta_{m}^{n+1}+\mu_{m6}\gamma_{m}^{n+1}+\\
&\qquad\mu_{m7}\delta_{m+1}^{n+1}+\mu_{m8}\gamma_{m+1}^{n+1}+\mu_{m9}\delta_{m+2}^{n+1}+\mu_{m10}\gamma_{m+2}^{n+1}=\\
&\mu_{m11}\delta_{m-2}^{n}+\mu_{m12}\gamma_{m-2}^{n}+\mu_{m13}\delta_{m-1}^{n}+\mu_{m14}\gamma_{m-1}^{n}+\mu_{m15}\delta_{m}^{n}+\mu_{m16}\gamma_{m}^{n}+\\
&\qquad\mu_{m17}\delta_{m+1}^{n}+\mu_{m18}\gamma_{m+1}^{n}+\mu_{m19}\delta_{m+2}^{n}+\mu_{m20}\gamma_{m+2}^{n}+n_1\\
&\mu_{m21}\delta_{m-2}^{n+1}+\mu_{m22}\gamma_{m-2}^{n+1}+\mu_{m23}\delta_{m-1}^{n+1}+\mu_{m24}\gamma_{m-1}^{n+1}+\mu_{m25}\delta_{m}^{n+1}+\mu_{m26}\gamma_{m}^{n+1}+\\
&\qquad\mu_{m27}\delta_{m+1}^{n+1}+\mu_{m28}\gamma_{m+1}^{n+1}+\mu_{m29}\delta_{m+2}^{n+1}+\mu_{m30}\gamma_{m+2}^{n+1}=\\
&\mu_{m31}\delta_{m-2}^{n}+\mu_{m32}\gamma_{m-2}^{n}+\mu_{m33}\delta_{m-1}^{n}+\mu_{m34}\gamma_{m-1}^{n}+\mu_{m35}\delta_{m}^{n}+\mu_{m36}\gamma_{m}^{n}+\\
&\qquad\mu_{m37}\delta_{m+1}^{n}+\mu_{m38}\gamma_{m+1}^{n}+\mu_{m39}\delta_{m+2}^{n}+\mu_{m40}\gamma_{m+2}^{n}+n_2
\end{aligned}\tag{15}$$

where the μ_m coefficients are:

$$\begin{array}{llll}
\mu_{m1}=\beta_{m1}\alpha_1-\frac{a_1}{2}\alpha_6 & \mu_{m11}=\beta_{m3}\alpha_1+\frac{a_1}{2}\alpha_6 & \mu_{m21}=\beta_{m5}\alpha_1 & \mu_{m31}=\beta_{m7}\alpha_1\\
\mu_{m2}=\beta_{m2}\alpha_1 & \mu_{m12}=\beta_{m4}\alpha_1 & \mu_{m22}=\beta_{m6}\alpha_1+\frac{a_2}{2}\alpha_6 & \mu_{m32}=\beta_{m8}\alpha_1-\frac{a_2}{2}\alpha_6\\
\mu_{m3}=\beta_{m1}\alpha_2-\frac{a_1}{2}\alpha_7 & \mu_{m13}=\beta_{m3}\alpha_2+\frac{a_1}{2}\alpha_7 & \mu_{m23}=\beta_{m5}\alpha_2 & \mu_{m33}=\beta_{m7}\alpha_2\\
\mu_{m4}=\beta_{m2}\alpha_2 & \mu_{m14}=\beta_{m4}\alpha_2 & \mu_{m24}=\beta_{m6}\alpha_2+\frac{a_2}{2}\alpha_7 & \mu_{m34}=\beta_{m8}\alpha_2-\frac{a_2}{2}\alpha_7\\
\mu_{m5}=\beta_{m1}\alpha_3-\frac{a_1}{2}\alpha_8 & \mu_{m15}=\beta_{m3}\alpha_3+\frac{a_1}{2}\alpha_8 & \mu_{m25}=\beta_{m5}\alpha_3 & \mu_{m35}=\beta_{m7}\alpha_3\\
\mu_{m6}=\beta_{m2}\alpha_3 & \mu_{m16}=\beta_{m4}\alpha_3 & \mu_{m26}=\beta_{m6}\alpha_3+\frac{a_2}{2}\alpha_8 & \mu_{m36}=\beta_{m8}\alpha_3-\frac{a_2}{2}\alpha_8\\
\mu_{m7}=\beta_{m1}\alpha_2-\frac{a_1}{2}\alpha_7 & \mu_{m17}=\beta_{m3}\alpha_2+\frac{a_1}{2}\alpha_7 & \mu_{m27}=\beta_{m5}\alpha_2 & \mu_{m37}=\beta_{m7}\alpha_2\\
\mu_{m8}=\beta_{m2}\alpha_2 & \mu_{m18}=\beta_{m4}\alpha_2 & \mu_{m28}=\beta_{m6}\alpha_2+\frac{a_2}{2}\alpha_7 & \mu_{m38}=\beta_{m8}\alpha_2-\frac{a_2}{2}\alpha_7\\
\mu_{m9}=\beta_{m1}\alpha_1-\frac{a_1}{2}\alpha_6 & \mu_{m19}=\beta_{m3}\alpha_1+\frac{a_1}{2}\alpha_6 & \mu_{m29}=\beta_{m5}\alpha_1 & \mu_{m39}=\beta_{m7}\alpha_1\\
\mu_{m10}=\beta_{m2}\alpha_1 & \mu_{m20}=\beta_{m4}\alpha_1 & \mu_{m30}=\beta_{m6}\alpha_1+\frac{a_2}{2}\alpha_6 & \mu_{m40}=\beta_{m8}\alpha_1-\frac{a_2}{2}\alpha_6
\end{array}\tag{16}$$

The system (15) can be written in the following form of a ten banded matrix system:

$$A\boldsymbol{x}^{n+1}=B\boldsymbol{x}^{n}+F \tag{17}$$

$$A = \begin{bmatrix} \mu_{m1} & \mu_{m2} & \mu_{m3} & \mu_{m4} & \mu_{m5} & \mu_{m6} & \mu_{m7} & \mu_{m8} & \mu_{m9} & \mu_{m10} & & & & \\ \mu_{m21} & \mu_{m22} & \mu_{m23} & \mu_{m24} & \mu_{m25} & \mu_{m26} & \mu_{m27} & \mu_{m28} & \mu_{m29} & \mu_{m30} & & & & \\ & & \mu_{m1} & \mu_{m2} & \mu_{m3} & \mu_{m4} & \mu_{m5} & \mu_{m6} & \mu_{m7} & \mu_{m8} & \mu_{m9} & \mu_{m10} & & \\ & & \mu_{m21} & \mu_{m22} & \mu_{m23} & \mu_{m24} & \mu_{m25} & \mu_{m26} & \mu_{m27} & \mu_{m28} & \mu_{m29} & \mu_{m30} & & \\ & & & \cdots & \cdots & \cdots & \cdots & \cdots & \cdots & \cdots & \cdots & \cdots & \cdots & \cdots \\ & & & & \mu_{m1} & \mu_{m2} & \mu_{m3} & \mu_{m4} & \mu_{m5} & \mu_{m6} & \mu_{m7} & \mu_{m8} & \mu_{m9} & \mu_{m10} \\ & & & & \mu_{m21} & \mu_{m22} & \mu_{m23} & \mu_{m24} & \mu_{m25} & \mu_{m26} & \mu_{m27} & \mu_{m28} & \mu_{m29} & \mu_{m30} \end{bmatrix}$$

$$B = \begin{bmatrix} \mu_{m11} & \mu_{m12} & \mu_{m13} & \mu_{m14} & \mu_{m15} & \mu_{m16} & \mu_{m17} & \mu_{m18} & \mu_{m19} & \mu_{m20} & & & & \\ \mu_{m31} & \mu_{m32} & \mu_{m33} & \mu_{m34} & \mu_{m35} & \mu_{m36} & \mu_{m37} & \mu_{m38} & \mu_{m39} & \mu_{m40} & & & & \\ & & \mu_{m11} & \mu_{m12} & \mu_{m13} & \mu_{m14} & \mu_{m15} & \mu_{m16} & \mu_{m17} & \mu_{m18} & \mu_{m19} & \mu_{m20} & & \\ & & \mu_{m31} & \mu_{m32} & \mu_{m33} & \mu_{m34} & \mu_{m35} & \mu_{m36} & \mu_{m37} & \mu_{m38} & \mu_{m39} & \mu_{m40} & & \\ & & & \cdots & \cdots & \cdots & \cdots & \cdots & \cdots & \cdots & \cdots & \cdots & \cdots & \cdots \\ & & & & \mu_{m11} & \mu_{m12} & \mu_{m13} & \mu_{m14} & \mu_{m15} & \mu_{m16} & \mu_{m17} & \mu_{m18} & \mu_{m19} & \mu_{m20} \\ & & & & \mu_{m31} & \mu_{m32} & \mu_{m33} & \mu_{m34} & \mu_{m35} & \mu_{m36} & \mu_{m37} & \mu_{m38} & \mu_{m39} & \mu_{m40} \end{bmatrix} \quad (18)$$

The system (17) contains $2N + 2$ equations and $2N + 10$ unknowns with the vectors x^{n+1}, x^n and F as:

$$\boldsymbol{x}^{n+1} = [\delta_{-2}^{n+1}, \gamma_{-2}^{n+1}, \delta_{-1}^{n+1}, \gamma_{-1}^{n+1}, \delta_0^{n+1}, \gamma_0^{n+1} \ldots, \delta_{N+1}^{n+1}, \gamma_{N+1}^{n+1}, \delta_{N+2}^{n+1}, \gamma_{N+2}^{n+1}]^T \quad (19)$$

$$\boldsymbol{x}^{n} = [\delta_{-2}^{n}, \gamma_{-2}^{n}, \delta_{-1}^{n}, \gamma_{-1}^{n}, \delta_0^{n}, \gamma_0^{n} \ldots, \delta_{N+1}^{n}, \gamma_{N+1}^{n}, \delta_{N+2}^{n}, \gamma_{N+2}^{n}]^T \quad (20)$$

$$F = [n_1, n_2, n_1, n_2, \ldots, n_1, n_2]^T \quad (21)$$

To make the above system solvable, we need additional eight constraints. On the system (17), by imposing both Dirichlet and Neumann boundary conditions helps us to eliminate parameters: δ_{-2}, $\delta_{-1}, \delta_{N+1}, \delta_{N+2}, \gamma_{-2}, \gamma_{-1}, \gamma_{N+1}, \gamma_{N+2}$. So that, resulting $(2N + 2) \times (2N + 2)$ matrix system will be solvable with Matlab program by the Gauss elimination algorithm.

In order to begin the iteration process for calculating the numerical solution, the initial parameters; $\boldsymbol{x}^0 = (\delta_{-2}^0, \gamma_{-2}^0, \delta_{-1}^0, \gamma_{-1}^0, \delta_0^0, \gamma_0^0, \ldots, \delta_{N+1}^0, \gamma_{N+1}^0, \delta_{N+2}^0, \gamma_{N+2}^0)$ must be found once by using both initial and boundary conditions. The recurrence relationship (17) gives the time evolution of vector $\boldsymbol{x}^n$. Thus the nodal values $U_N(x,t)$ and $V_N(x,t)$ can be computed via the equations (8).

3. RESULTS OF THE NUMERICAL SOLUTIONS

The aim of this section is to show the efficiency of the algorithm by studying on four different RDS and comparing the accuracy of the suggested method on the selected problems. The accuracy of the suggested method is measured with the discrete error norm for the problems which have an analytical solution:

$$L_2 = |U - U_N|_2 = \sqrt{h \sum_{j=0}^{N} (U_j - (U_N)_j^n)} \;, \quad (22)$$

$$L_\infty = |U - U_N|_\infty = \max_j |U_j - (U_N)_j^n|. \quad (23)$$

Also, the relative error is used to measure the error if there is no analytic solution of the system.

$$RE = \sqrt{\frac{\sum_{j=0}^{N} |U_j^{n+1} - U_j^n|^2}{\sum_{j=0}^{N} |U_j^{n+1}|^2}} \tag{24}$$

The efficiency of the algorithm is exhibited by studying four different RD mechanism. For the purpose of observing the stability of the recursive system (17), the matrix stability analysis is performed and system (17) is written as in the converted matrix form as below:

$$\boldsymbol{x}^{n+1} = W\boldsymbol{x}^n + Q \tag{25}$$

Here, the iterative converted matrix is $W = A^{-1}$ and its eigenvalues λ_i are expected to be $max|\lambda_i| < 1$ to satisfy the criteria for the stability. Accordingly, eigenvalues $|\lambda_i|$ of W are computed and depicted in Figures 1-2 for the nonlinear problems; Brusselator and Schnakenberg Models.

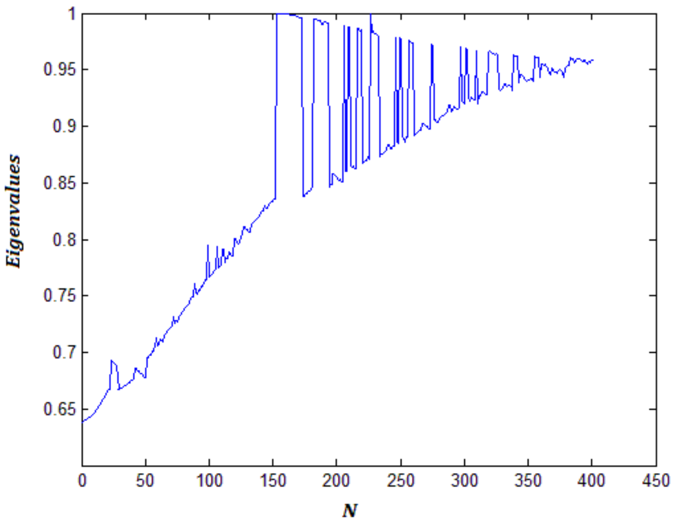

Figure 1. Eigenvalues of *W* obtained for Brusselator model when $N = 400$, $\Delta t = 0.01$, $t = 15$.

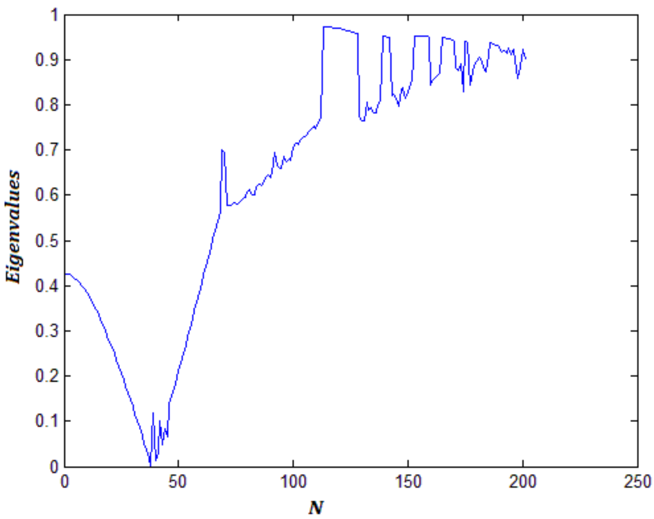

Figure 2. Eigenvalues of *W* obtained for Schnakenberg model when $N = 200$, $\Delta t = 5 \times 10^{-6}$, $t = 2.5$

During the run of the algorithm, we have observed that the absolute values of the eigenvalues are almost less than 1 at all time steps. Therefore the demonstrated eigenvalues in the Figs.1-2 are calculated at a specific time step. When similar treatments are performed for other test problems, it is observed that the absolute values of the eigenvalues are less than 1. In this way, the solution scheme of the recursive formula is unconditionally stable.

3.1. Linear Problem

It is stated that the terms $F(U,V)$ and $G(U,V)$ are nonlinear in the system (1). However it is not possible to calculate the error norms due to the limitations of the analytical solutions of the nonlinear system. Here, the linear problem with known analytical solutions is selected and has the form

$$\begin{aligned} \frac{\partial U}{\partial t} &= d\frac{\partial^2 U}{\partial x^2} - aU + V \\ \frac{\partial V}{\partial t} &= d\frac{\partial^2 V}{\partial x^2} - bV. \end{aligned} \tag{26}$$

and the known analytical exact solutions are;

$$U(x,t) = \left(e^{-(a+d)t} + e^{-(b+d)t}\right)cos(x), \qquad V(x,t) = (a-b)(e^{-(b+d)t})cos(x). \tag{27}$$

The (26) system's initial conditions are induced from the analytical solution by taking $\mathrm{t} = 0$ in the solutions of (27). Solution space is taken as $[0,\frac{\pi}{2}]$ and the set of boundary conditions which is used for eliminating the unknown parameters are:

$$\begin{aligned} &U_x(0,t) = 0, \qquad U\left(\frac{\pi}{2},t\right) = 0, \qquad V_x(0,t) = 0, \qquad V\left(\frac{\pi}{2},t\right) = 0, \\ &U_{xxx}(0,t) = 0, \qquad U_{xx}\left(\frac{\pi}{2},t\right) = 0, \qquad V_{xxx}(0,t) = 0, \qquad V_{xx}(\pi/2,t) = 0. \end{aligned} \tag{28}$$

To analyze the dominance of reaction or diffusion, three different cases are considered. The reaction-diffusion mechanism (26) is numerically calculated with different values of parameters a, b, and d. Respectively, considered cases and parameters are;

- Case of diffusion dominated ($a = 0.1$, $b = 0.01$ and $d = 1$)
- Case of reaction dominated ($a = 2, b = 1, d = 0.001$)
- Case of reaction dominated with stiff reaction ($a = 100$, $b = 1$, $d = 0.001$)

To get numerical results, software program is run up to time level $t = 1$ for various N and Δt. The boundary and initial conditions are chosen to coincide with the PQBCM [19]. The obtained results for U and V in terms of L_2 and L_∞ norms are given in Tables 2, 3 and 4 also with comparison of the results [19] and [6] when $N = 512$ and Δt. It is observed that the accuracy of the obtained results for function V are slightly efficient than results for function U. The proposed method has a better accuracy than the ones given in Tables 2, 3 ,4 under the same conditions. In conclusion presented algorithm produces similar error norms with those of the polinomial quintic B-spline collocation [19] and Implicit integrator factor and Multi-grid solver[6].

Table 2. Error norms L_2 and L_∞ for the case of diffusion dominated when $a = 0.1$, $b = 0.01$, $d = 1$, $N = 512$

	$U(TQB)$		$V(TQB)$		$U(PQBCM)$		$V(PQBCM)$	
Δt	$L_2 \times 10^4$	$L_\infty \times 10^4$	$L_2 \times 10^6$	$L_\infty \times 10^6$	$L_2 \times 10^4$	$L_\infty \times 10^4$	$L_2 \times 10^6$	$L_\infty \times 10^6$
0.005	0.008090	0.009120	0.029344	0.033079	0.015123	0.017048	0.062416	0.070361
0.01	0.053460	0.060265	0.216594	0.244162	0.060493	0.068193	0.249667	0.281444
0.02	0.234949	0.264853	0.965627	1.088530	0.241983	0.272782	0.998702	1.125815
0.04	0.961033	1.083353	3.962253	4.466566	0.968068	1.091283	3.995334	4.503855
	$U(CN-MG\ method)$							
0.005		0.0116						
0.01		0.0627						
0.02		0.267						
0.04		1.09						

Table 3. Error norms L_2 and L_∞ for the case of reaction dominated when $a = 2$, $b = 1$, $d = 0.001$, $N = 512$

	$U(TQB)$		$V(TQB)$		$U(PQBCM)$		$V(PQBCM)$	
Δt	$L_2 \times 10^4$	$L_\infty \times 10^4$	$L_2 \times 10^5$	$L_\infty \times 10^5$	$L_2 \times 10^4$	$L_\infty \times 10^4$	$L_2 \times 10^3$	$L_\infty \times 10^3$
0.005	0.026827	0.030241	0.068087	0.076753	0.026832	0.030247	0.068124	0.076795
0.01	0.107324	0.120984	0.272462	0.307141	0.107329	0.120989	0.272499	0.307183
0.02	0.429339	0.483984	1.089996	1.228729	0.429344	0.483990	1.090033	1.228771
0.04	1.717837	1.936481	4.360663	4.915683	1.717842	1.936487	4.360700	4.915725
	$U(CN-MG\ method)$							
0.005		0.0302						
0.01		0.121						
0.02		0.484						
0.04		1.94						

Table 4. Error norms L_2 and L_∞ for the case of diffusion dominated with stiff reaction when $a = 100$, $b = 1$, $d = 0.001$, $N = 512$

	$U(TQB)$		$V(TQB)$		$U(PQBCM)$		$V(PQBCM)$	
Δt	$L_2 \times 10^5$	$L_\infty \times 10^5$	$L_2 \times 10^3$	$L_\infty \times 10^3$	$L_2 \times 10^5$	$L_\infty \times 10^5$	$L_2 \times 10^3$	$L_\infty \times 10^3$
0.005	0.068087	0.076753	0.067406	0.075986	0.068124	0.076795	0.067443	0.076027
0.01	0.272462	0.307141	0.269738	0.304070	0.272499	0.307183	0.269774	0.304111
0.02	1.089996	1.228729	1.079096	1.216442	1.090033	1.228771	1.079133	1.216484
0.04	4.360663	4.915684	4.317057	4.866527	4.360700	4.915725	4.317093	4.866568
			$V(CN-MG\ method)$					
0.005				0.0760				
0.01				0.304				
0.02				1.22				
0.04				4.87				

3.2. Brusselator Model

Brusselator model is mainly defined to get a kinetic model having a limit cycle. It was also shown to represents steady state, oscillatory and chaotic solutions and mentioned by Prigogine and Lefever in the study [29]. This type of RD mechanism exhibits Turing instability and large-scale studies have been conducted on this model being investigated both analytically and numerically. The general 1D reaction-diffusion equation system for this type of model is given as [3]

$$\frac{\partial U}{\partial t} = \varepsilon_1 \frac{\partial^2 U}{\partial x^2} + A + U^2 V - (B+1)U$$
$$\frac{\partial V}{\partial t} = \varepsilon_2 \frac{\partial^2 V}{\partial x^2} + BU - U^2 V \qquad (29)$$

where $\varepsilon_1, \varepsilon_2$ are diffusion parameters, x is the spatial coordinate and U, V are functions of x and t representing concentrations. Initial conditions are specified as in the reference [3];

$$\mathrm{U}(x,0) = 0.5, \qquad V(x,0) = 1 + 5x. \qquad (30)$$

Following boundary conditions are considered at the end points of the problem domain:

$$U_x(x_0,t) = 0, \qquad U_x(x_N,t) = 0, \qquad V_x(x_0,t) = 0, \qquad V_x(x_N,t) = 0.$$
$$U_{xx}(x_0,t) = 0, \qquad U_{xx}(x_N,t) = 0, \qquad V_{xx}(x_0,t) = 0 \qquad V_{xx}(x_N,t) = 0. \qquad (31)$$

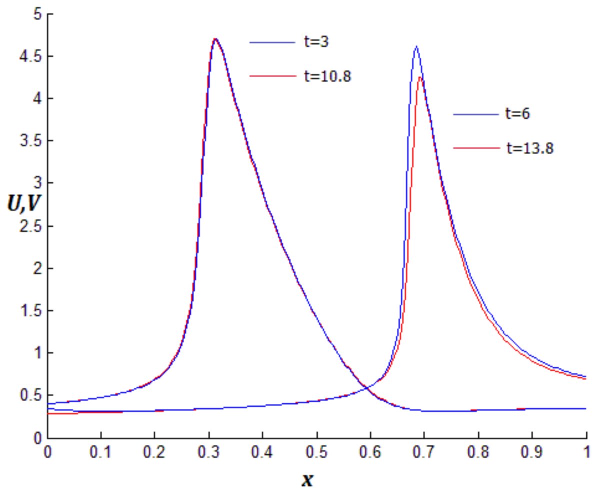

Figure 3: Periodic wave motion of *U* for Brusselator model when $N = 200$, $\Delta t = 0.01$

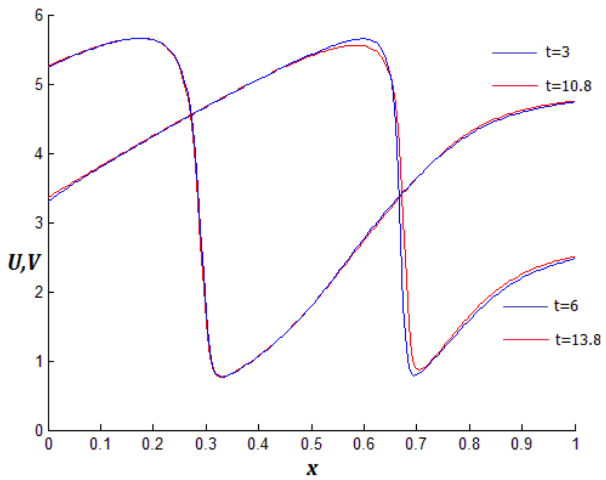

Figure 4. Periodic wave motion for *V* for Brusselator model when $N = 200$, $\Delta t = 0.01$

Suggested algorithm is performed for the equation system (29), taking the parameters as $\varepsilon_1 = \varepsilon_2 = 10^{-4}$, $A = 1$, $B = 3.4$, over the region $x \in [0,1]$. Computation is carried out until $t = 15$. Split points

$N = 200$, time step $\Delta t = 0.01$ are used for space and time discretization respectively. Obtained solutions are depicted in Figure 3 and Figure 4. They show changes of the density of the functions of U and V. It has been observed that both U and V wave motions exhibits periodic waves under these conditions.

Obtained density values for periodic motion are presented in Table 5. We found that the period of this wave action is about 7.8 with the proposed method, whereas the period 7.7 is found when the PQBCM [19] is implemented which is shown in the Tables 5- 6. Proposed method produces equivalent patterns with the references [9,19, 20].

Table 5. Density values of periodic motion when TQB is implemented.

Density	t	$x = 0.0$	$x = 0.2$	$x = 0.4$	$x = 0.6$	$x = 0.8$	$x = 1.0$
U	3	0.284595	0.317799	0.377380	0.604709	1.623703	0.691906
	10.8	0.344555	0.321243	0.376194	0.605486	1.715194	0.716792
	6	0.400865	0.687572	2.884364	0.549937	0.323697	0.348838
	13.8	0.398971	0.680057	2.911740	0.533798	0.322405	0.347582
V	3	3.363723	4.250910	5.066610	5.546754	1.650507	2.507119
	10.8	3.309473	4.240150	5.062313	5.651837	1.591938	2.473710
	6	5.258678	5.632343	1.073700	2.739517	4.300681	4.755329
	13.8	5.241915	5.634312	1.065232	2.769906	4.269058	4.737755

Table 6. Density values of periodic motion when PQBCM [19] is implemented.

Density	t	$x = 0.0$	$x = 0.2$	$x = 0.4$	$x = 0.6$	$x = 0.8$	$x = 1.0$
U	3	0.284657	0.317966	0.377959	0.612881	1.519483	0.648434
	10.7	0.347747	0.321168	0.376204	0.611218	1.626310	0.680742
	6	0.401741	0.706734	2.716642	0.510302	0.326204	0.352411
	13.7	0.398904	0.691408	2.769059	0.500480	0.324523	0.350579
V	3	3.363896	4.251219	5.066734	5.537413	1.732740	2.580615
	10.7	3.299664	4.233913	5.056668	5.637796	1.659946	2.534846
	6	5.257254	5.606791	1.137215	2.825295	4.355469	4.798749
	13.7	5.234725	5.613815	1.119445	2.846165	4.317357	4.774541

3.3. Schnakenberg Model

The Schnakenberg model is used to model autocatalytic chemical reaction with possible oscillatory behaviors and it is a relatively easy system for modelling the reaction-diffusion mechanism. Firstly it was put forward by Schakenberg [30] and can be stated as follows:

$$\begin{aligned} \frac{\partial U}{\partial t} &= \frac{\partial^2 U}{\partial x^2} + \zeta(a - U + U^2 V) \\ \frac{\partial V}{\partial t} &= d\frac{\partial^2 V}{\partial x^2} + \zeta(b - U^2 V) \end{aligned} \tag{32}$$

Here, U and V represent the concentration of activator and inhibitor respectively, d is a diffusion coefficient, ζ, a and b are rate parameters of the biochemical reactions. The results of the proposed method were obtained by studying the oscillation problem in the Schnakenberg Model. Accordingly, the parameters are taken as $a = 0.126779$, $b = 0.792366$, $d = 10$ and $\zeta = 10^4$ for system (32). Graphical solutions are obtained on the interval $[-1,1]$ and the initial conditions are taken as:

$$U(x,0) = 0.919145 + 0.001\sum_{j=1}^{25}\frac{cos(2\pi jx)}{j} \tag{33}$$

$$V(x,0) = 0.937903 + 0.001 \sum_{j=1}^{25} \frac{cos(2\pi jx)}{j}$$

The boundary conditions are taken as:

$$\begin{aligned} &U_x(x_0,t) = 0, \quad U_x(x_N,t) = 0, \quad V_x(x_0,t) = 0 \quad V_x(x_N,t) = 0, \\ &U_{xxx}(x_0,t) = 0, \quad U_{xxx}(x_N,t) = 0, \quad V_{xxx}(x_0,t) = 0, \quad V_{xxx}(x_N,t) = 0. \end{aligned} \tag{34}$$

Computations are performed until $t = 2.5$ for space/time combinations. Obtained relative errors are depicted in Table 7 together with the errors results of the PQBCM [19].

Table 7. Obtained values of relative errors for Schnakenberg model when $N = 100$ and $t = 2{,}5$.

Δt	Nu. of step	U	U[19]	V	V[19]
5×10^{-6}	500000	0	5.7160×10^{-14}	5.4418×10^{-17}	5.4564×10^{-14}
5×10^{-5}	50000	6.2202×10^{-17}	1.5653×10^{-10}	1.6794×10^{-16}	1.1105×10^{-10}
1×10^{-4}	25000	1.7593×10^{-16}	9.8744×10^{-10}	2.4423×10^{-16}	8.8599×10^{-10}
1.20×10^{-4}	20833	1.5668×10^{-16}	1.5055×10^{-09}	2.2996×10^{-16}	1.3790×10^{-09}
1.32×10^{-4}	18939	1.4610×10^{-16}	1.0564×10^{-01}	2.9664×10^{-16}	1.0301×10^{-01}
1×10^{-3}	2500	2.5895×10^{-14}	-	2.0341×10^{-14}	-
2×10^{-3}	1250	5.4591×10^{-09}	-	3.9448×10^{-09}	-
5×10^{-3}	500	5.4960×10^{-06}	-	4.7003×10^{-06}	-

The algorithm produces quite accurate results even when the time step is larger as observed in Table 7. Small error values are achieved even for a Δt as large as one with method of TQB. PQBCM needs time steps that are a factor of 200 times smaller than TQB to achieve the same accuracy. TQB method is more efficient than PQBCM method in terms of Schnakenberg Model. Graphics of Figure 5 show the oscillation movements for time increment $\Delta t = 5 \times 10^{-5}$ and split points of $N = 100$ and $N = 200$ respectively. The functions U and V make 9 oscillations when $N = 100$ and $N = 200$ as depicted in Figure 5. This result and the references [1] and [2] show that a finer mesh is necessary for accurate solutions.

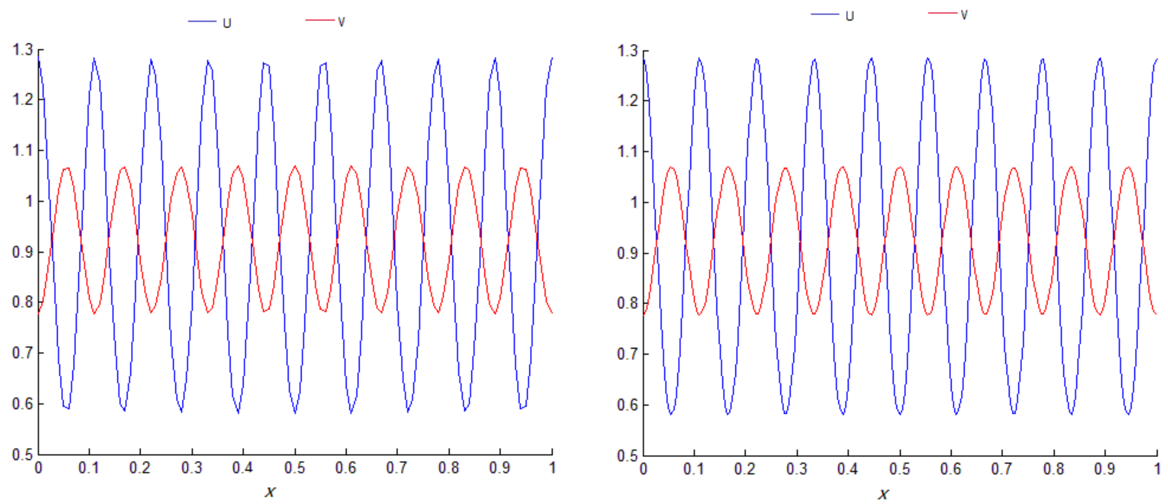

(a) (b)

Figure 5. The oscillation waves of U and V for Schnakenberg model, when (a) $N = 100$, $t = 2.5$ (b) $N = 200$, $t = 2.5$

3.4. Gray-Scott Model

The Gray-Scott model is a widely known type of reaction-diffusion system which models some spatial patterns to be formed by several chemical species in nature. Formerly it was presented by Gray and Scott [31] and defined:

$$\begin{aligned}\frac{\partial U}{\partial t} &= \varepsilon_1 \frac{\partial^2 U}{\partial x^2} - U^2 V + f(1-U),\\ \frac{\partial V}{\partial t} &= \varepsilon_2 \frac{\partial^2 V}{\partial x^2} + U^2 V - kV\end{aligned} \tag{35}$$

The proposed method is implemented on the repeating spot patterns exhibited by the Gray-Scott model. The parameters are selected in accordance with the reference [32] for the system (35)

$$\varepsilon_1 = 1, \quad \varepsilon_2 = 0.01, \quad a = 9, \quad b = 0.4, \quad f = \varepsilon_2 a, \quad k = \varepsilon_2^{1/3} b \tag{36}$$

Also the initial conditions of the system (35) are selected as:

$$U(x,0) = 1 - \frac{1}{2} sin^{100}\left(\pi \frac{(x-L)}{2L}\right), \quad V(x,0) = \frac{1}{4} sin^{100}(\pi \frac{(x-L)}{2L}) \tag{37}$$

Space discretization $N = 400$ and time discretization $\Delta t = 0.2$ are taken and solutions are computed in $L \in [-50,50]$. Dirichlet and additional Neuman boundary conditions

$$\begin{aligned}&U(x_0,t) = 1, \quad U(x_N,t) = 1, \quad V(x_0,t) = 0, \quad V(x_N,t) = 0,\\ &U_x(x_0,t) = 0, \quad U_x(x_N,t) = 0, \quad V_x(x_0,t) = 0, \quad V_x(x_N,t) = 0.\end{aligned} \tag{38}$$

are applied. The self replicating waves are obtained when the program is run until to the time level $t = 1000$. Under these initial conditions, primarily two pulses are created and separated from each other, then each pulse at the edges are being split into two again to form four pulses, as shown in Figure 6 until time $t = 1000$, as time evolved. These self-replicating process goes on to cover the spatial domain. The replicating process of U and V functions due to time and space are presented in Figures 6(a)(b)(c).

The intensity changes of functions U and V due to time and space are presented respectively in Figure 7 and Figure 8. These spatial patterns, which are kind of growing Turing patterns, initially starting with two waves of splitting movement, seem to cover the whole domain with branching over time. The obtained patterns are similar and compatible with [19, 32]

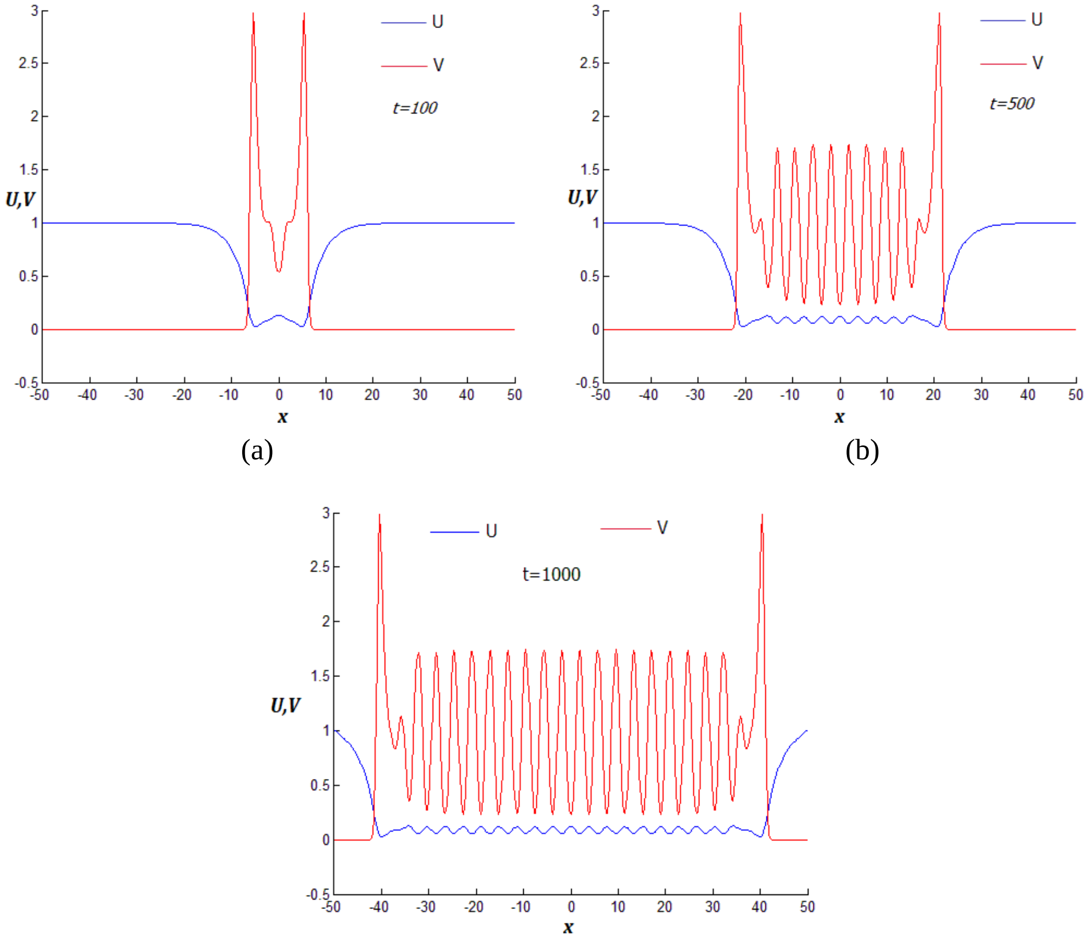

Figure 6. The replicating process of spot patterns for Gray-Scott model when (a) $t = 100$, (b) $t = 500$ and (c) $t = 1000$

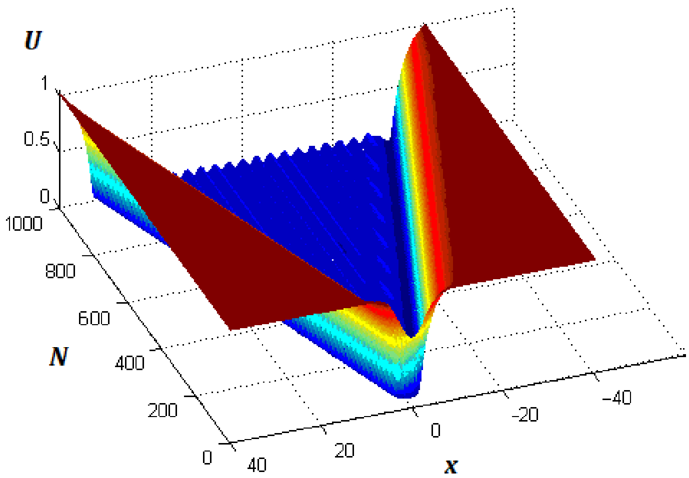

Figure 7. Graphical illustration of U for Gray-Scott model, when $N = 200, \Delta t = 0.01$

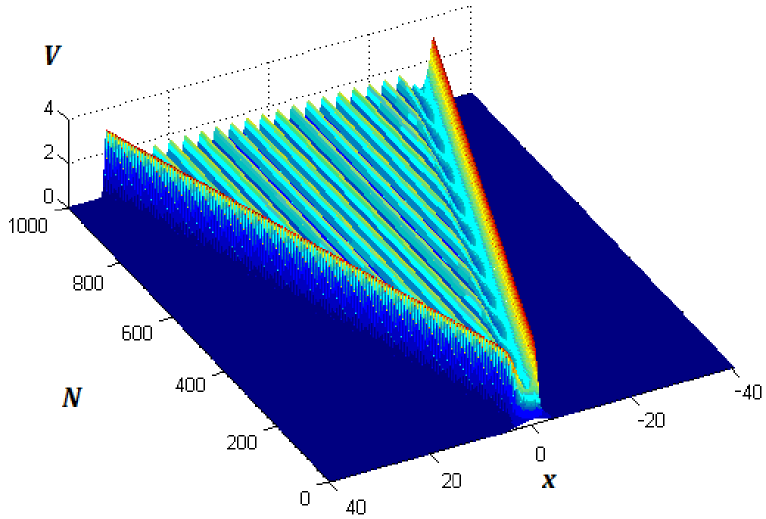

Figure 8. Graphical illustration of V for Gray-Scott model, when $N = 200, \Delta t = 0.01$

4. CONCLUSION

The continuum problem represented by the reaction-diffusion system is transformed into a discrete problem with a finite number of variables such that suggested method replaces the continuous problem with an algebraic system. The proposed method is well suited for approximating accurate solutions of the reaction-diffusion systems for pattern formation. For the validation of the suggested algorithm, approximate solutions of linear and nonlinear RD systems are shown on the models of certain chemical and biological problems. Firstly the method is conducted for getting numerical solution of the linear reaction diffusion system, for which the analytical solution exists. $L2$ norms of the computational solutions are quite satisfactory and are similar with the reported work of the polynomial quintic B-spline collocation method and better than the Crank-Nicolson-multigrid method when the same parameters are used. Nonlinear reaction-diffusion systems known as the Brusselator model, Schnakenberg model and Gray-Scott models are also simulated suitably. Solutions of the nonlinear problems, which have no analytical solutions in general, are given graphically. All of model solutions are represented fairly and can be compared with the equivalent graphs given in the studies [1-3, 19, 20, 32]. Also approximate solution of the Schnakenberg model with proposed method produced better error values. Use of the trigonometric quintic B-spline having continuity of order four allows us to have an approximate functions in order of four. Therefore, differential equations in order of four can be solved numerically by using the trigonometric B-spline functions to have solutions of continuity in order of four.

Computational cost of the algorithm depends on the gauss elimination method while solving the matrix system. As a computational cost, number of the basic operations can be calculated as $O((2N + 1)^2 \times \frac{t}{\Delta t})$. Since the resulting matrix is band matrix, it is solved by the Gauss elimination method, so the storage capacity is reduced and speed of the algorithm is accelerated. Therefore the method is easily implemented for such reaction-diffusion models. Consequently, the TQB collocation method produces fairly acceptable results for numerical investigation of RD systems. Thus, it is also recommended for finding solutions of other partial differential equations and fractional partial differential equations.

ACKNOWLEDGMENT

A part of this study was orally presented in the International Conference on Applied Mathematics and Analysis, ICAMA 2016, Ankara, Turkey.

CONFLICT OF INTEREST

The authors stated that there are no conflicts of interest regarding the publication of this article.

AUTHORSHIP CONTRIBUTIONS

The algorithm design of the non linear problem was suggested by Idiris Dağ. The numerical solutions of the problem, algorithm construction and coding as well as the writing of the article in English, were carried out by Aysun Tok Onarcan. Nihat Adar provided support during the coding phase and writing of the article.

REFERENCES

[1] Ruuth SJ. Implicit-explicit methods for reaction-diffusion problems in pattern formation. J Math Bio 1995; 34: 148-176.

[2] Madzvamuse A, Wathen AJ, Maini PK. A moving grid finite element method applied to a biological pattern generator. J Comp Phys 2003; 190: 478-500.

[3] Zegeling PA, Kok HP. Adaptive moving mesh computations for reaction-diffusion systems. J Comp App Math 2004; 168: 519-528.

[4] Ropp DL, Shadid JN, Ober CC. Studies of the accuracy of time integration methods for reaction-diffusion equations. J Comp Phys 2004; 194(2): 544-574.

[5] Ropp DL, Shadid JN. Stability of operator splitting methods for systems with indefinite operators: reaction-diffusion systems. J Comp Phys 2005; 203(2): 449-466.

[6] Chou CS, Zhang Y, Zhao R, Nie Q. Numerical Methods for Stiff Reaction-Diffusion Systems. Discrete and Continuous Dynamical Systems-Series B 2007;7: 515-525.

[7] Yadav OP, Jiwari R. A finite element approach for analysis and computational modelling of coupled reaction diffusion models. Numerical Methods for Partial Differential Equations 2019; 35 (2): 830-850.

[8] Mittal RC, Rohila R. Numerical Simulation of Reaction-Diffusion Systems by Modified Cubic B-spline Differential Quadrature Method. Chaos, Solitons and Fractals 2016; 92 (1): 1339-1351.

[9] Jiwari R, Singh S, Kumar A. Numerical simulation to capture the pattern formation of coupled reaction-diffusion models. Chaos, Solitons and Fractals 2017; 103: 422-439.

[10] Jiwari R, Gerisch A. A local radial basis function differential quadrature semidiscretisation technique for the simulation of time-dependent reaction-diffusion problems. Eng Comp 2016; 38 (6): 2666-2691.

[11] Schoenberg IJ. On Trigonometric Spline Interpolation. J Math Mech 1964;13: 795-826.

[12] Hamid NNA, Majid AA, Ismail AIM. Cubic Trigonometric B-spline Applied to Linear Two-Point Boundary Value Problems of Order Two. World Academy of Science, Engineering and Technology 2010; 47: 478-803.

[13] Gupta Y, Kumar MA Computer Based Numerical Method for Singular Boundary Value Problems. Int J Comp App 2011;1: 0975-8887.

[14] Zin SM, Abbas M, Majid AA, Ismail AIM. A New Trigonometric Spline Approach to Numerical Solution of Generalized Nonlinear Klien-Gordon Equation. PLoS one, 2014;9(5): e95774.

[15] Abbas M, Majid AA, Ismail AIM, Rashid A. Numerical Method Using Cubic Trigonometric B-Spline Technique for Nonclassical Diffusion Problems. Abstract and Applied Analysis, 2014; Article ID 849682.

[16] Yağmurlu NM, Karakaş AS. Numerical solutions of the equal width equation by trigonometric cubic B-spline collocation method based on Rubin–Graves type linearization. Num Meth Part Diff Eqs, 2020; 36(5): 1170-1183.

[17] Nikolis A. Numerical Solutions of Ordinary Differential Equations with Quadratic Trigonometric Splines. App Maths E-Notes 2004;4: 142-149.

[18] Nikolis A, Seimenis I. Solving Dynamical Systems with Cubic Trigonometric Splines. App Maths E-notes, 2005; 5: 116-123.

[19] Sahin A. Numerical solutions of the reaction-diffusion equations with B-spline finite element method. PhD, Eskişehir Osmangazi University, Eskişehir, Turkey, 2009.

[20] Ersoy O, Dag I. Numerical Solutions of the Reaction Diffusion System by Using Exponential Cubic B-spline Collocation Algorithms. Open Phys 2015; 13: 414-427.

[21] Onarcan AT, Adar N, Dag I. Trigonometric cubic B-spline collocation algorithm for numerical solutions of reaction–diffusion equation systems. Comp App Math 2018; 37: 6848–6869.

[22] Tok-Onarcan A, Adar N, Dag I. Wave simulations of Gray-Scott reaction-diffusion system. Math Meth in the App Sci 2019; 19: 5566–5581.

[23] Kaur N, Joshi V. Numerical solution to the Gray-Scott Reaction-Diffusion equation using Hyperbolic B-spline. J Phys: Conference Series 2022: 2267.

[24] Hepson ÖE, Yiğit G, Allahviranloo T. Numerical simulations of reaction–diffusion systems in biological and chemical mechanisms with quartic-trigonometric B-splines. Comp App Math 2021; 40(4): 1-23.

[25] Hepson ÖE, Numerical solutions of the Gardner equation via trigonometric quintic B-spline collocation method, Sakarya Üniversitesi Fen Bilimleri Enstitüsü Dergisi 2018; 22 (6): 1576–1584.

[26] Chandrasekharan Nair L, Awasthi A. Quintic trigonometric spline based numerical scheme for nonlinear modified Burgers' equation, Num Meth for Part Diff Eq 2019; 35(3): 1269–1289.

[27] Khater MMA, Nisar KS, Mohamed MS. Numerical investigation for the fractional nonlinear space-time telegraph equation via the trigonometric Quintic B-spline scheme. Math Meth in App Sci 2021; 44(6); 4598–4606.

[28] Alam MP, Kumar D, Khan A. Trigonometric quintic B-spline collocation method for singularly perturbed turning point boundary value problems. Int J Comp Math 2021;98(5): 1029–1048.

[29] Prigogine I, Lefever R. Symmetry Breaking Instabilities in Dissipative Systems. J Chem Phys 1968; 48:1695-1700.

[30] Schnakenberg J. Simple Chemical Reaction Systems with Limit Cycle Behavior. J Theo Bio 1979; 81: 389-400.

[31] Gray P, Scott SK. Autocatalytic Reactions in The Isothermal, Continuous Stirred Tank Reactor: Oscillations and Instabilities in the system A+2B 3B, B C. Chem Eng Sci, 1984;39: 1087-1097.

[32] Craster RV, Sassi R. Spectral Algorithms for Reaction-Diffusion Equations. Technical Report. Note del Polo 2006: No:99.

[33] Rubin SG, Graves Jr RA. A cubic spline approximation for problems in fluid mechanics. Technical Report, Nasa, Washington, 1975.

ESKİŞEHİR TECHNICAL UNIVERSITY JOURNAL OF SCIENCE AND TECHNOLOGY
A- APPLIED SCIENCES AND ENGINEERING

2023, 24(2), pp. 141-154, DOI: 10.18038/estubtda.1184918

RESEARCH ARTICLE

MODELLING OF DIFFERENT MOTHER WAVELET TRANSFORMS WITH ARTIFICIAL NEURAL NETWORKS FOR ESTIMATION OF SOLAR RADIATION

Kübra KAYSAL[1,*], Fatih Onur HOCAOĞLU [2]

[1,2] Electrical Engineering Department., Engineering Faculty, Afyon Kocatepe University, Afyonkarahisar, Turkey

ABSTRACT

In recent years, the interest in renewable energy sources has increased due to environmental damage and, the increasing costs of fossil fuel resources, whose current reserves have decreased. Solar energy, an environmentally friendly, clean and sustainable energy source, is one of the most important renewable energy sources. The amount of electrical energy produced from solar energy largely depends on the intensity of solar radiation. For this reason, it is essential to know and accurately predict the characteristics of the solar radiation intensity of the relevant region for the healthy sustainability of the existing solar energy systems and the systems planned to be installed. For this purpose, a two-stage forecasting model was developed using the hourly solar radiation intensity of 2014 in a region in Turkey. In the first stage of the study, the second month of each season was selected to investigate the seasonal effects of the region and large, medium, and small-scale events in the study area were examined using discrete wavelet transform. The performances of different mother wavelets in the Artificial Neural Network model with Wavelet Transform (W-ANN) are compared in the second stage. July, the most successful estimation result in seasonal solar radiation intensity was obtained. The most successful RMSE values for January, April, July and October were 65,9471W/m^2, 74,3183 W/m^2, 54,3868 W/m^2, 78,4085 W/m^2 respectively, the coiflet mother wavelet measured it.

Keywords: Artificial neural networks, Wavelet transform, Mother wavelets, Solar radiation estimation

1. INTRODUCTION

Energy has a vital role in the development of countries and in raising the welfare level of humanity. Various factors such as advancing technology, increasing population and industrialisation are increasing the energy need in the world. In the development of countries, an uninterrupted, cheap, and high-quality energy supply is needed. In daily life, energy is used in various ways such as kinetic, mechanical, electricity, heat, hydraulic, solar, and wind. These types of energy are obtained from various sources by different methods. Energy sources are obtained from fossil fuel and renewable energy sources [1,2]. Most of the world's energy needs are met by fossil fuels. In our country, a large part of the energy consumption is obtained from fossil fuels such as lignite and oil. In addition to the negative effects of these resources, which have high costs, on the country's economy, it is foreseen that their current reserves will be depleted shortly. In addition, considering the harmful effects of fossil fuel sources on the environment, such as air pollution, acid rain, and climate change, it is thought that renewable energy sources, which are cleaner and sustainable, will increase the share of production [3,4].

Solar energy, one of the renewable energy sources, is a low-cost, high-energy potential and environmentally friendly energy type. This energy, whose usage area is increasing day by day, has started to be the focus of researchers with various studies such as solar energy, electricity production estimation, hydrogen production, and increasing the efficiency of photovoltaic systems [5]. For this reason, it is envisaged that large-scale photovoltaic power plants will be widely established with developing technology and investment support. Solar radiation estimation is an essential factor of

*Corresponding Author: kubra543@hotmail.com
Received: 05.10.2022 Published: 21.06.2023

photovoltaic systems that are used effectively in energy production. While solar radiation directly affects efficiency, it has an essential place for investors in terms of proper planning, system installation, design and sustainability [6,7]. Solar energy varies according to regional, temporal and weather events. Due to this variable structure, problems such as voltage fluctuations and instability arise in the network and reduce the reliability of electricity generation from solar energy [8]. For this reason, establishing accurate and reliable models to predict solar radiation intensity has been a popular research topic from past to present and it continues to inspire researchers to develop various prediction models.

Gabralı [3] performed the prediction modelling of wind and solar energy potential with Wavelet Transform Artificial Neural Networks (W-ANN) in his study. In the study, first of all, the input data is divided into subcomponents by wavelet transform. The correlation values between the obtained sub-components were calculated, and the component with high correlation was given as the input of the Artificial Neural Network (ANN). The results obtained from the W-ANN model were successful compared to the ANN model created without transformation. Guermoui et al. [9] have estimated solar radiation using daily temperature data for the Algerian region. The study estimated solar radiation intensity using the support vector machine model corrected with 3-year temperature data. The results were found to be quite successful. Mohammadi et al. [10] used the Wavelet Transform-Support Vector Machine model for solar radiation intensity estimation in their study, in which they contributed to the literature. The success rate of the proposed hybrid model was 97.4%, higher than the other models. According to Falayi et al. [11] performed wavelet power spectrum analysis for Nigerian solar radiation studies. The results of the tests show that the aperture coefficient and sunshine duration stand out with high wavelet coefficients, while turbidity and cloudiness increase in low wavelet coefficients. According to the results, it was seen that cloudiness has a significant effect on solar radiation. Ferkous et al. [12] proposed the Wavelet-Gaussian Process Regression model for solar radiation estimation. For the analysis, 4 years of real-time solar radiation data from the Algerian region is used. Different types of mother wavelet models were established, and the results were compared. The best result in estimation was obtained with the coiflet1 mother wavelet. Belmahdi et al. [13] estimated one month ago solar radiation using time series models. Autoregressive Moving Average (ARMA) and Autoregressive Integrated Moving Average (ARIMA) models were used for forecasting. It has been determined that the ARIMA model is suitable for the city of Tetouan in estimating solar radiation. According to Rabehi et al. [14] created a prediction model using a new hybrid combination of these methods with enhanced Decision Trees, Multilayer Perceptrons, and Linear Regression in their study. The study used input data such as extraterrestrial radiation, daily minimum and maximum average temperatures, and sunshine duration ratio to estimate daily solar radiation. The multilayer sensor model has been identified as suitable for solar radiation estimation. In their study, Faisal et al. [15] made a radiation estimation using the solar radiation intensity data they measured from five different cities in Bangladesh. In analysis, three various networks have been developed, namely Recurrent Neural Network (RNN), Long-Short-Term Memory (LSTM), and Gated Repetitive Unit (GRU). The performance of the developed models was compared according to the Mean Absolute Percent Error (MAPE) performance criterion. As a result, GRU gave the best result among the three models, with an error value of 19.28%. Belmahdi et al. [16] compared the performance of various machine learning methods for solar radiation estimation. Global solar radiation data measured at Abdelmake Faculty of Science was used in the study. The most successful performance was obtained from Feed Forward Neural Networks (FFNN) and the ARIMA model among the various selected machine learning algorithms. Malik et al. [17] used ANN algorithms for solar radiation and wind speed estimation. The study discusses the benefits and limitations of various ANN models. As a result of the study, it has been seen that Levenberg Marquardt and Bayesian algorithms are very effective in estimating nonlinear properties such as solar radiation and wind speed. On the other hand, Monjoly et al. [18] estimated one hour after solar radiation using wavelet decomposition method, and various multiscaling decomposition models. As a result of the study calculated the rRMSE value for the Wavelet Decomposition and ANN hybrid prediction model as 7.86%, and the success value as 72.08%.

Some researchers have used a single estimation method for solar radiation estimation. For example, Wang et al. [19] used the ANN model to estimate the solar radiation intensity considering different weather conditions. In another study, Wang et al. [20] used a directly explicable neural network-based model to predict solar radiation intensity using meteorological, geographic, and time series data. Husein and Chung. [21] used the LSTM model for solar radiation estimation. Mutavhatsindi et al. [22] used Feedback Artificial Neural Network (FFNN), LSTM, and Support Vector Regression to estimate solar radiation intensity. Experiments proved that the FFNN model was more successful. Researchers have designed hybrid models to solve solar radiation prediction problems in recent years. Singla et al. [23] estimated solar radiation using deep learning methods based on Wavelet transform. As a result of the experiments, the Wavelet-Bidirectional LSTM deep learning model was found to be more successful. Meng et al. [24] proposed a new smart hybrid model for solar energy prediction using wavelet transform package and Generative Adversarial Networks (GANs). Guermoui et al. [25], a hybrid model of support vector machine and artificial bee colony algorithms, applied for global solar radiation estimation, and successful results were obtained. Huang et al. [26] used hybrid deep neural networks with wavelet transform for hourly solar irradiance estimation. The method yielded successful results.

In summary, single and hybrid forecasting methods are frequently used in solar radiation forecasting. However, all methods have advantages and disadvantages. Although single estimation methods give successful results in estimation, estimation accuracy is not as high as hybrid methods. Hybrid models are relatively robust, but it is difficult to determine the appropriate structure. An advanced prediction technology should be designed by examining the characteristic structure of solar radiation with variable characteristics very well. This study aims to investigate the potential of solar energy and predict solar radiation intensity using the Wavelet Transform Artificial Neural Network (W-ANN) model. The significance of energy resources for the advancement of energy and the development of nations is underscored. However, factors such as advancing technology, increasing population, and industrialization contribute to the growing demand for energy. Consequently, there is a pressing need for a continuous, cost-effective, and reliable energy supply. Solar energy is a cost-effective, high-potential, and environmentally friendly type of renewable energy. The utilization of this energy source is expanding day by day, and research related to solar energy is focused on various aspects such as solar energy generation, electricity production forecasting, hydrogen production, and improving the efficiency of photovoltaic systems. Solar radiation estimation is an important factor for effectively utilizing photovoltaic systems in power generation. Solar radiation, which directly impacts efficiency, holds a significant position for investors in terms of proper planning, system installation, design, and sustainability. It is known that current prediction models face challenges in terms of accuracy and reliability. Due to the variable nature of solar energy, issues such as voltage fluctuations and network instability arise, thereby reducing the reliability of electricity generation from solar energy. Hence, the development of precise and dependable models for estimating solar radiation intensity has been a popular research topic throughout history, motivating researchers to explore various prediction models.

This study aims to examine the solar radiation intensity characteristics seasonally for the design of solar energy systems in a particular region. Another aim of the study is to compare the performance of different types of mother wavelets in solar radiation intensity prediction for the Wavelet Transform Artificial Neural Network prediction model. For these purposes, one-year real-time solar radiation data were analysed with the help of wavelet transform. The solar radiation intensity data in the study area was arranged seasonally and the events affecting the potential of this energy were tried to be determined. In addition, hourly frequency short-term forecasting was carried out with solar radiation data. In the two-stage forecasting model, in the first stage, the data are analysed with different types of mother wavelet models, and divided into approximation and detail components. Obtained detail components were presented as input to the ANN model. MATLAB R2020a software was used to create models and test data. According to the results obtained, the most successful result for the W-ANN model was measured with the coiflet1 mother wavelet. This study was conducted to make an important contribution to solar radiation forecasting by evaluating the performance of different forecasting methods, and understanding seasonal variability for solar system design. In addition, he is investigating the use of advanced forecasting technologies such as wavelet transform and artificial neural networks in solar radiation estimation.

2. MATERIAL AND METHODS

2.1. Dataset

In this study, solar radiation intensity data from the Turkish Meteorology General Directorate (TMGM) measured between January 1, 2014 and December 31, 2014 belonging to the Van region were used. A total of 8760 real-time data at an hourly frequency were analysed with the help of various wavelet transforms, and trained with Artificial Neural Networks. 80% of the 8760 data were used as training data, and 20% were used as test data. When the hourly data given in Figure 1 are examined, it is observed that the solar radiation intensity does not have a certain trend, and shows sudden changes due to various reasons.

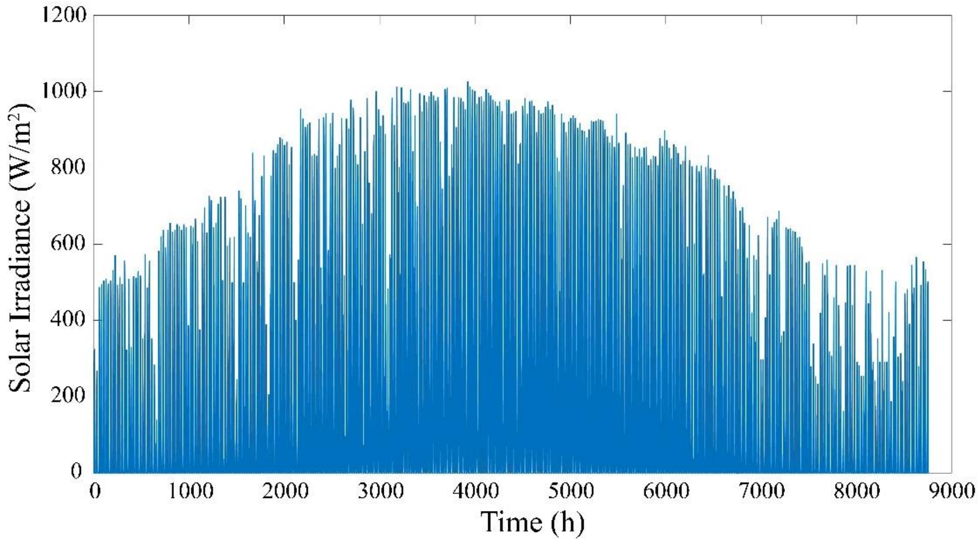

Figure 1. Hourly solar irradiance data between January 1, 2014, and December 31, 2014

2.2. Wavelet Transform

One of the widely known methods of signal processing is the Fourier transform. The most significant disadvantage of the Fourier transform is that time information is lost while obtaining information on the frequency axis. Time information in variable structured signals is essential for establishing and testing various systems. Unlike the Fourier transform, the wavelet transform allows a signal to be studied in both frequency and time axis. With the wavelet transform, it is possible to calculate both the high and low-frequency components of the signal in a specific time interval. In this way, the examination of the systems whose frequency changes over time, and the analysis of their instantaneous changes can be done very sensitively [27].

Wavelet transform decomposes a signal or data into wavelets at various stages. The most important parameter of this transformation is the mother wavelets. The signal is multiplied by a function called the master wavelet, which can be translated in time, and changed in width. Some mother wavelet functions used in wavelet transform are given in Figure 2.

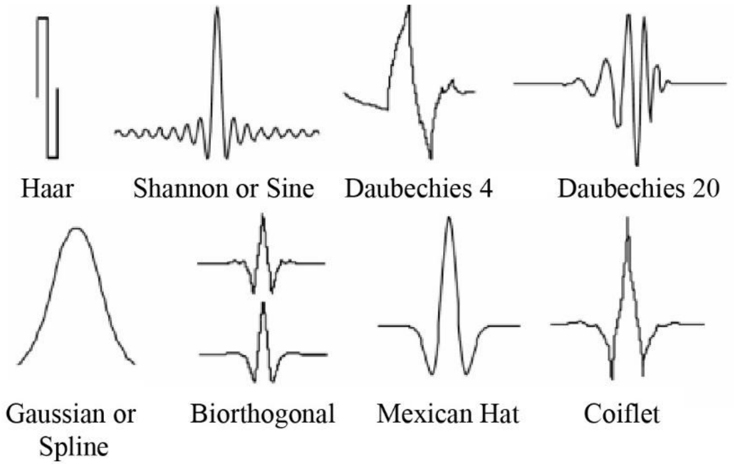

Figure 2. Various mother wavelets [28]

Discrete wavelet transform (DWT) has the advantage of calculating the wavelet coefficients at the selected scale and time interval. This way, the processing load caused by forming many coefficients will be reduced. The DWT function, which is re-expressed with the selected scale value, and used for the discrete wavelet transform, is given in equation 1 [29,30].

$$W_{m,n}\left(\frac{t-\tau}{s}\right) = s_0^{-m/2} W\left(\frac{t-n\tau_0 s_0^m}{s_0^m}\right) \quad (1)$$

In the equation, τ is the translation value, s is the scaling value, W is the mother wavelet transform function, m is the wavelet's translation, and n is the scaling parameter. s_0 is the shift step, and its value is greater than 1. τ_0 is the translation value in the time axis. The decomposition process of the signal repeats sequentially, and makes it possible to decompose it to the desired level [30]. The sequential iteration process is shown in Figure 3.

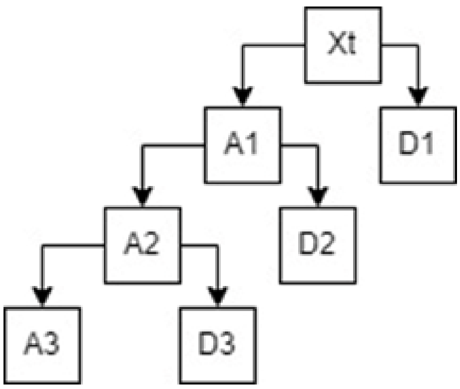

Figure 3. Sequential decomposition analysis

The decomposed signal (x_t) value is expressed in equation 2 according to the decomposition level.

$$\begin{aligned} x_t &= A_1 + D_1 \\ &= A_2 + D_2 + D_1 \\ &= A_3 + D_3 + D_2 + D_1 \end{aligned} \quad (2)$$

A low pass and high pass filter are used to decompose the time series signal. As a result, the signal is divided into one approximation (A) component, and as many detail (D) components as it is decomposed from the level. Low-frequency values in the signal give the approximation component, while high-frequency values give the detail components [31]. While low-frequency components reveal the seasonal changes in solar radiation intensity or the climatic character of the region, high-frequency components mostly reflect the characteristics such as suddenly changing cloudiness.

2.3. Artificial Neural Networks

Artificial neural networks are structures that have been developed inspired by the structure, and operation of the human brain. They are connected to each other by connections with various neuron structures and weights. ANNs are computer programs that mimic biological nerve cells. They can self-learn, memorise, and establish relationships between information [32]. A simple neural network consists of an input layer, a hidden layer, and an output layer. An example of ANN is given in Figure 4.

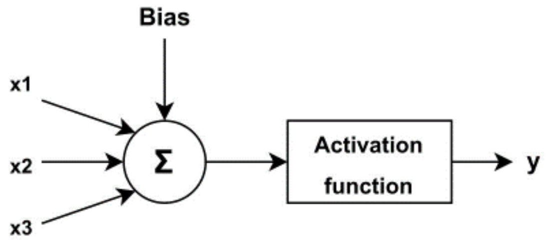

Figure 4. ANN Model

In an ANN model, each input value is multiplied by its own weight (w) and summed. The total value is applied to an activation function, and the output value is obtained. Starting from the explanation, equation 3 is obtained [33].

$$y = \sum_{i=1}^{N} x_i * w_i \tag{3}$$

In the equation, y represents the output value, x represents the input value, and w represents the weights. It is observed in various studies in the literature that pre-processing the input data increases the prediction success in ANN models [34]. To increase the prediction success in the study, a hybrid model was created by using wavelet transform and artificial neural networks together. In this context, a short-term estimation study was made for the solar radiation intensity in the study. In the W-ANN model, Haar, Coiflet (Coif1), Daubechies (Db1) and Symlets (Sym1) mother wavelet functions, which are frequently used in the literature, are used to evaluate the predictive performance of various mother wavelets used in wavelet transform [31].

3. APPLICATION AND RESULTS

In this section, a seasonal analysis of solar radiation intensity has been carried out to design solar energy systems in a particular region. Detail components obtained from various mother wavelet functions are presented as input to artificial neural networks, and short-term solar radiation intensity estimation is made.

3.1. Data Exploration

In the first stage, in order to reveal the seasonal effects of the solar radiation intensity data measured between January 1, 2014 and December 31, 2014, the second month of each season was selected, and analyzed on a monthly basis. April representing the spring, July representing the summer, October representing the autumn, and January representing the winter season were selected, and the events affecting the temporal change of solar radiation intensity were examined. Removing other months from the data reduces the processing load in wavelet transform and modelling process. In the second stage, to see the effects of different mother wavelet analyses on the prediction performance, discrete wavelet analysis was applied to the solar radiation intensity data for April, July, October and January with four different mother wavelet functions. In the third stage, the detail components of the signal, which are divided into approximation and detail components with different mother wavelet functions, are presented as input to the ANN model. In the ANN model, 80% of the input data was used as training data and 20% as test data.

Root Mean Square Error (RMSE) error criterion was used to evaluate the performance of W-ANN hybrid models. The RMSE formula is given in equation 4.

$$RMSE = \sqrt{\frac{\sum_{n=1}^{N}(y_n - \widehat{y_n})^2}{N}} \quad (4)$$

In the equation, y_n is the actual value observed in time in the data, and $\widehat{y_n}$ is the predicted value.

3.2. Wavelet Analysis Results

In the study, the second month of each season was chosen to represent the four seasons. April, July, October and January data are separated from the main data. Since the data is recorded in hourly periods, there are between 720 and 744 data records in a month, depending on the months with 30 or 31 days. No data loss was observed within months. The discrete wavelet transforms investigated large, medium and small-scale events in the study area. The original data s is represented by the approach component a and the detail component d. Of the detail components, $\boldsymbol{d_1}$ small, $\boldsymbol{d_2}$ medium and $\boldsymbol{d_3}$ describe large-scale events. Large-scale events have low frequency and long period, while small-scale events have high frequency and short period [3].

Figure 5 shows the detail and approximation components as a result of the discrete wavelet analysis of solar radiation intensity for April. There is a periodicity in solar radiation intensity throughout the month. The solar radiation intensity decreased on the 10th, 13th and 20th days of the month. The effect of all scale events can be mentioned during the month under review.

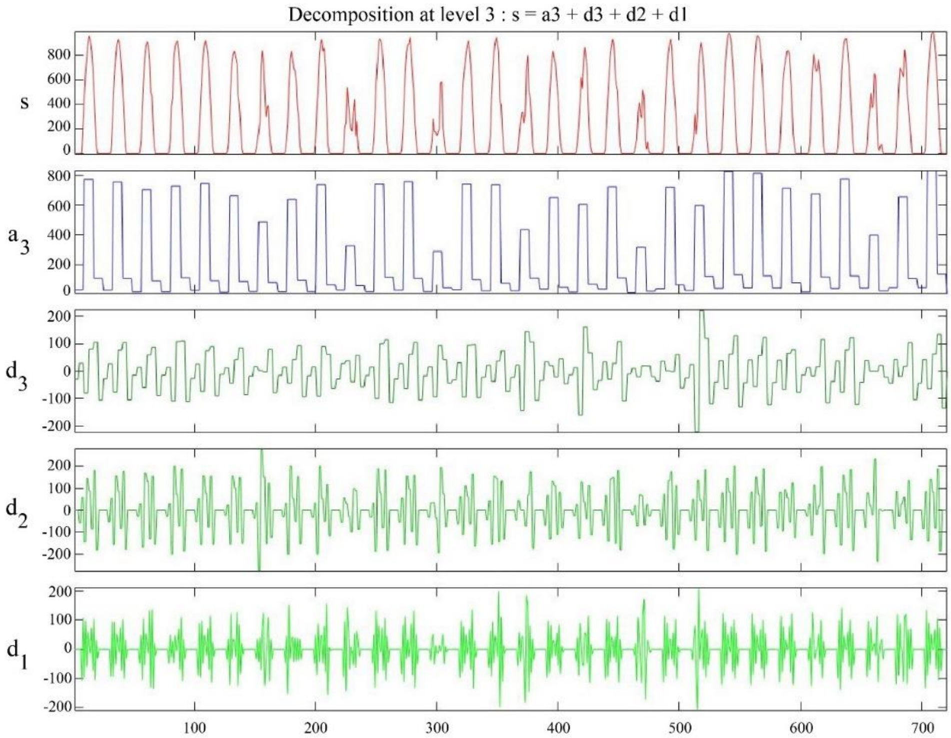

Figure 5. Discrete wavelet analysis of solar radiation intensity for April

Figure 6 shows the detail and approach components as a result of the discrete wavelet analysis of solar radiation intensity for July. On the 5th and 23rd days of the examined month, a decrease in solar radiation intensity occurred with the effect of large and small-scale events.

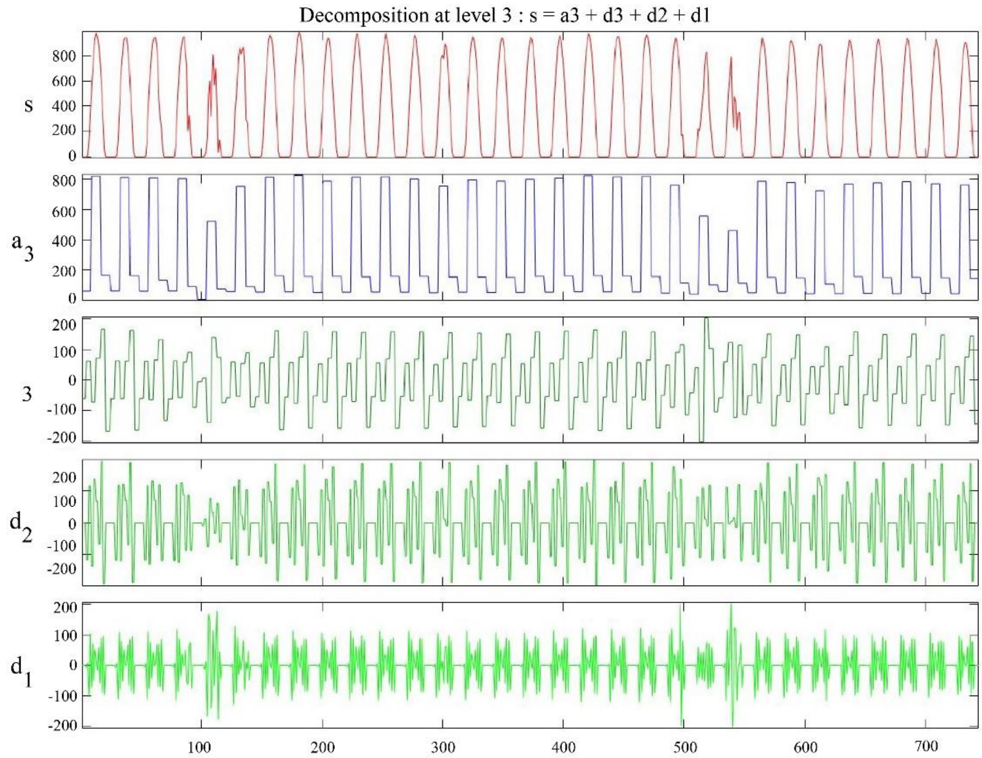

Figure 6. Discrete wavelet analysis of solar radiation intensity for July

Figure 7 shows the detail and approach components as a result of the discrete wavelet analysis of solar radiation intensity for October. It is seen that there is a decrease in the solar radiation intensity in the middle of the month examined and the events in all three scales have an effect.

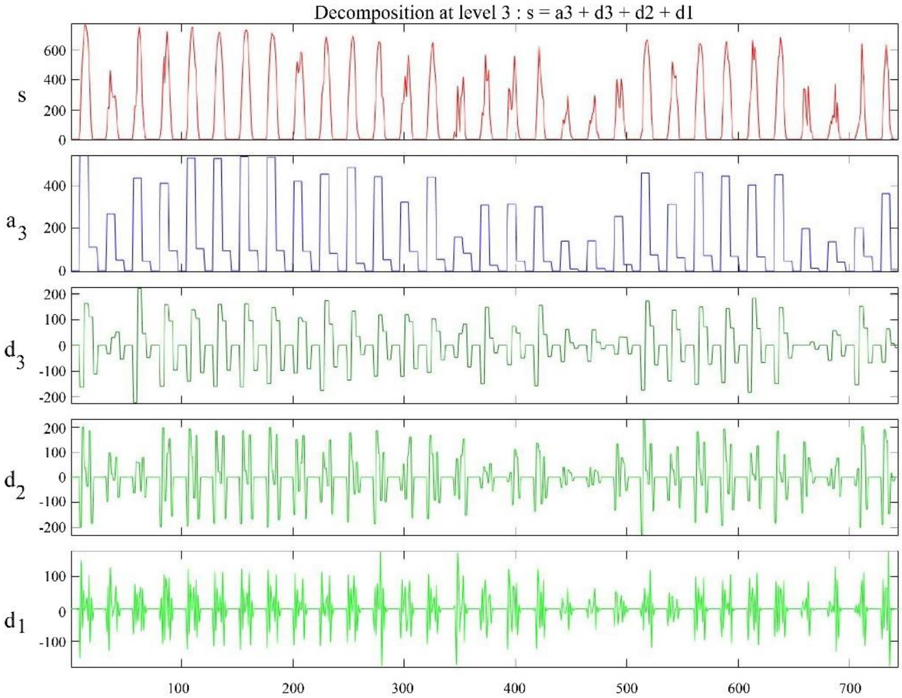

Figure 7. Discrete wavelet analysis of solar radiation intensity for October

Figure 8 shows the detail and approximation components as a result of the discrete wavelet analysis of solar radiation intensity for January. The effect of small-scale events can be seen on the first two days of the month and the 26th-28th days of the month.

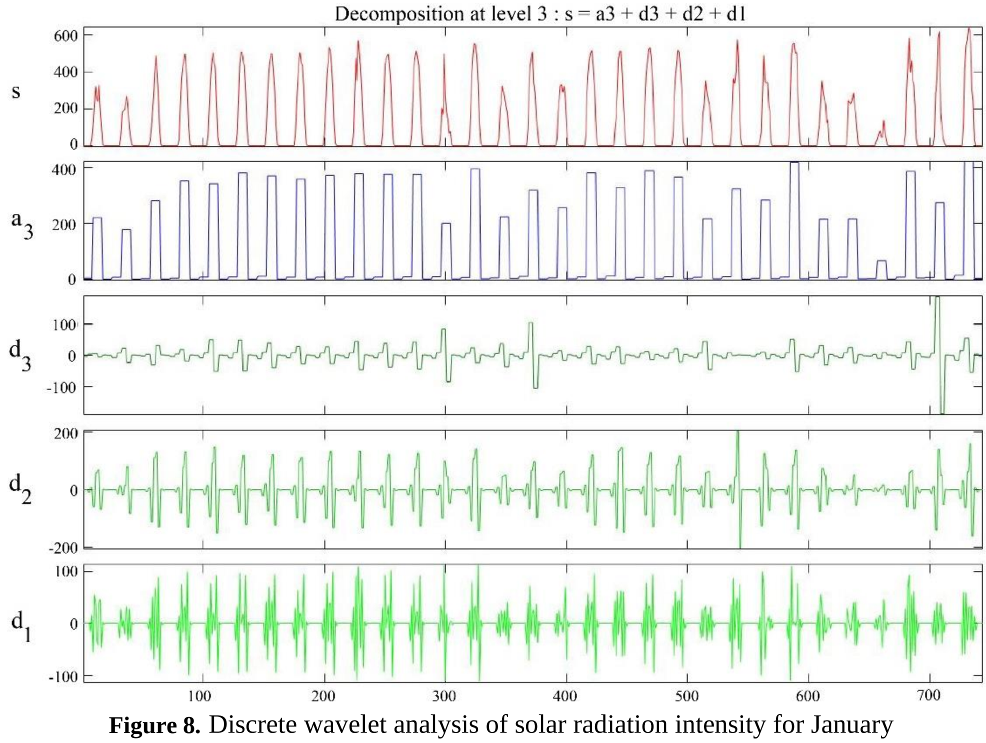

Figure 8. Discrete wavelet analysis of solar radiation intensity for January

3.3. W-ANN Estimation Results

In this study, the W-ANN model's data were first divided into subcomponents with four different mother wavelet transforms. The aim is to observe which mother wavelet gives more effective results in the ANN model. The data is subdivided, each from Level 5, using sym1, db1, haar, and coif1 mother wavelets. Each subcomponent was used as input for the ANN model. Thus, for each mother wavelet component, the short-term solar radiation intensity was estimated in the ANN model, and the most suitable mother wavelet type for the model was determined. In Figure 9-12, the Coif1 mother wavelet and the observation-forecast graphs of the months obtained from the ANN are given.

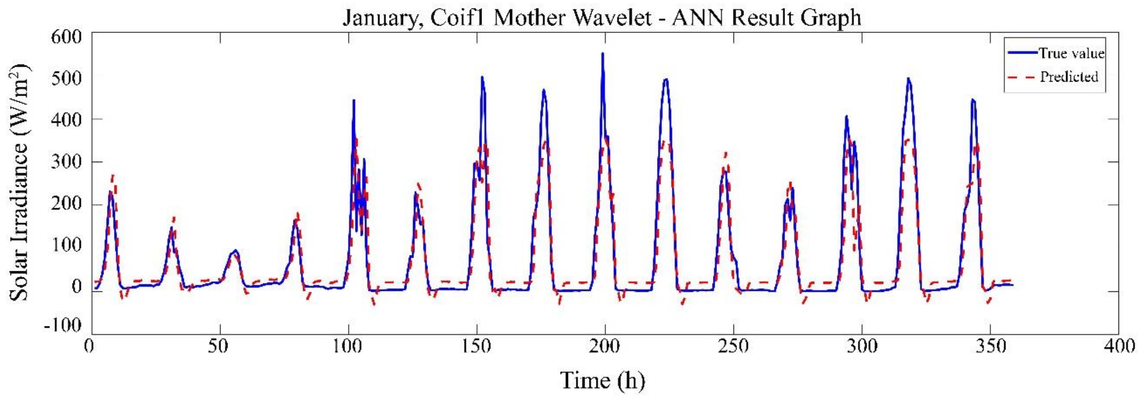

Figure 9. Coif1 mother wavelet ANN observation-predict graph for January

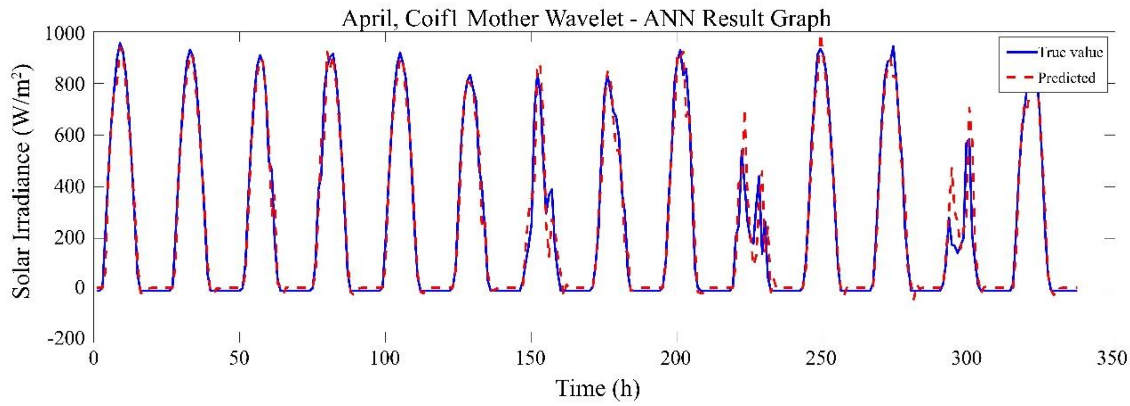

Figure 10. Coif1 mother wavelet ANN observation-predict graph for April

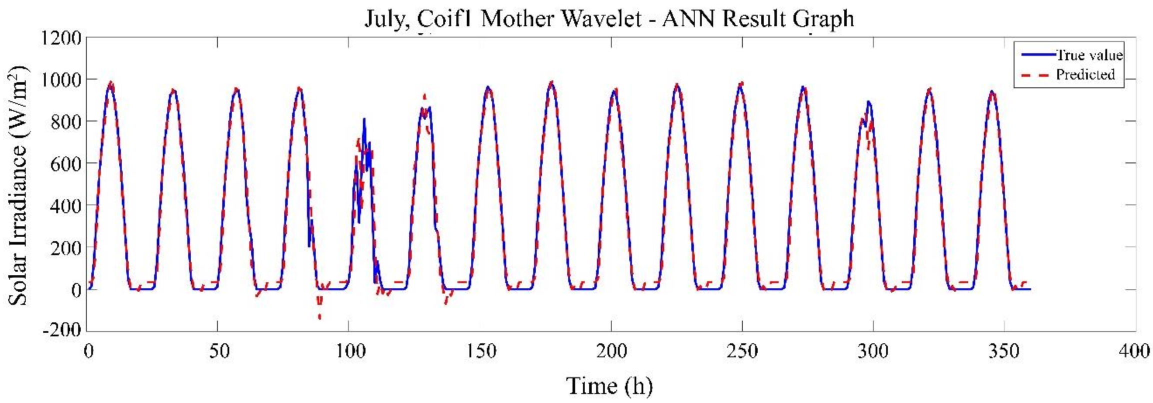

Figure 11. Coif1 mother wavelet ANN observation-predict graph for July

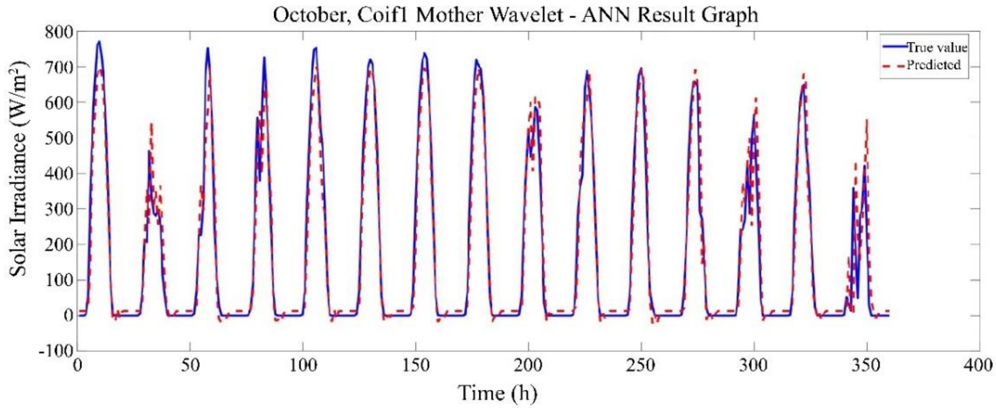

Figure 12. Coif1 mother wavelet ANN observation-predict graph for October

4. DISCUSSION

In this study, data separated from the fifth level to its sub-components with four different main wavelet transforms are presented as input to the ANN model. The short-term solar radiation was estimated with each main wavelet presented to the artificial neural network. The RMSE values of the model were calculated to determine the most suitable main wavelet type. The error values of the ANN models created with each mother wavelet are shown in Table 1. According to the results, in the estimation study of wavelet transform ANN models, the Coif1 mother wavelet was more successful for all selected months. The best results every month were obtained from July.

Table 1. Comparison of solar radiation (W/m^2), mother wavelet ANN error values

Months	Mother Wavelet-ANN Model RMSE Results (W/m^2)			
	Sym1	**Db1**	**Haar**	**Coif1**
January	67,9561	79,8354	74,3543	**65,9471**
April	74,5663	75,0166	85,9196	**74,3183**
July	61,3040	56,1864	58,2133	**54,3868**
October	84,1517	82,1218	80,1521	**78,4085**

The general results of the study are as follows:

1- In the study, periodic patterns of solar radiation intensity in four different seasons were examined using discrete wavelet analysis.
2- Solar radiation intensity data of April, July, October and January are separated, and detail and approximation components are obtained by wavelet analysis.
3- The detail components d1, d2 and d3 represent large, medium and small-scale events.
4- Periodicity was observed in solar radiation intensity in April, and decreases were detected on the 10th, 13th and 20th days.
5- In July, on the 5th and 23rd days, the solar radiation intensity decreased due to large and small-scale events.
6- In October, there was a decrease in solar radiation intensity around the middle of the month, and the effects of events at all scales were observed.
7- In January, the effects of small-scale events were observed on the first two days and on the 26th to 28th days.
8- According to the W-ANN prediction results, the Coif1 wavelet yielded more successful results compared to other wavelet types.
9- Among all months, the best prediction results were obtained for the month of July.

This study emphasises that the modelling should be done seasonally and monthly as much as possible to obtain reliable and successful results in solar radiation intensity estimation studies, since meteorological events vary seasonally. In addition, early warning systems against fluctuations in solar energy systems with variable characteristics can be developed by developing estimation models that can obtain reliable and accurate results with W-ANN models with different mother wavelet structures designed in the study. It is expected that the results obtained in this study will increase the efficiency of solar energy systems, and will also be a roadmap for the systems planned to be established for the active region and other regions with similar characteristics to this region in the future. These results show that discrete wavelet analysis and W-ANN model are an effective method to understand and predict the periodic patterns of solar radiation intensity in different seasons.

CONFLICT OF INTEREST

The authors stated that there are no conflicts of interest regarding the publication of this article.

AUTHORSHIP CONTRIBUTIONS

Kübra KAYSAL: Conceptualization, Formal analysis, Conception and design of study: analysis and/or interpretation of data, Drafting the manuscript, revising the manuscript critically for important intellectual content, Approval of the version of the manuscript to be published.**Fatih Onur HOCAOGLU:** Conceptualization, Formal analysis, Conception and design of study: analysis and/or interpretation of data, Drafting the manuscript, revising the manuscript critically for important intellectual content, Approval of the version of the manuscript to be published.

REFERENCES

[1] Acikgoz H. A novel approach based on integration of convolutional neural networks and deep feature selection for short-term solar radiation forecasting. Applied Energy 2022; 305: 117912.

[2] Mohsenzadeh Karimi S, Mirzaei M, Dehghani A, Galavi H, Huang YF. Hybrids of machine learning techniques and wavelet regression for estimation of daily solar radiation. Stochastic Environmental Research and Risk Assessment 2022; 1-15.

[3] Gabrali D. Modeling of wind and solar energy potential with artificial neural network and analysis with wavelet transformation. İstanbul Aydın University, Science Institute, Master's Thesis, 2019.

[4] Sun Y, Li H, Andlib Z, Genie MG. How do renewable energy and urbanization cause carbon emissions? Evidence from advanced panel estimation techniques. Renewable Energy 2022; 185: 996-1005.

[5] Akarslan E, Hocaoglu FO, Edizkan R. Novel short term solar irradiance forecasting models. Renewable Energy 2018; 123: 58-66.

[6] Sharifi SS, Rezaverdinejad V, Nourani V, Behmanesh J. Multi-time-step ahead daily global solar radiation5 forecasting: performance evaluation of wavelet-based artificial neural network model. Meteorology and Atmospheric Physics 2022; 134(3): 1-14.

[7] Qiu R, Li L, Wu L, Agathokleous E, Liu C, Zhang B, Sun S. Modeling daily global solar radiation using only temperature data: Past, development, and future. Renewable and Sustainable Energy Reviews 2022; 163: 112511.

[8] Hocaoğlu FO. Stochastic approach for daily solar radiation modeling. Solar Energy 2011; 85(2): 278-287.

[9] Guermoui M, Abdelaziz R, Gairaa K, Djemoui L, Benkaciali S. New temperature-based predicting model for global solar radiation using support vector regression. International Journal of Ambient Energy 2022; 43(1): 1397-1407.

[10] Mohammadi K, Shamshirband S, Tong CW, Arif M, Petković D, Ch S. A new hybrid support vector machine–wavelet transform approach for estimation of horizontal global solar radiation. Energy Conversion and Management 2015; 92: 162-171.

[11] Falayi EO, Adepitan JO, Oni OO, Faseyi MT. Wavelet power spectrum analysis applied for solar radiation investigations over Nigeria. Songklanakarin Journal of Science & Technology 2021; 43:4.

[12] Ferkous K, Chellali F, Kouzou A, Bekkar B. Wavelet-Gaussian Process Regression Model for Regression Daily Solar Radiation in Ghardaia, Algeria. Journal homepage: http://iieta. org/journals/i2m 2021; 20(2): 113-119.

[13] Belmahdi B, Louzazni M, El Bouardi A. One month-ahead forecasting of mean daily global solar radiation using time series models. Optik 2020; 219: 165207.

[14] Rabehi A, Guermoui M, Lalmi D. Hybrid models for global solar radiation prediction: a case study. International Journal of Ambient Energy 2020; 41: 31-40.

[15] Faisal AF, Rahman A, Habib MTM, Siddique AH, Hasan M, Khan MM. Neural networks based multivariate time series forecasting of solar radiation using meteorological data of different cities of Bangladesh. Results in Engineering 2022; 13: 100365.

[16] Belmahdi B, Louzazni M, El Bouardi A. Comparative optimization of global solar radiation forecasting using machine learning and time series models. Environmental Science and Pollution Research 2022; 29: 14871-14888.

[17] Malik P, Gehlot A, Singh R, Gupta LR, Thakur AK. A Review on ANN Based Model for Solar Radiation and Wind Speed Prediction with Real-Time Data. Archives of Computational Methods in Engineering 2022; 1:19.

[18] Monjoly S, André M, Calif R, Soubdhan T. Hourly forecasting of global solar radiation based on multiscale decomposition methods: A hybrid approach. Energy 2017; 119: 288-298.

[19] Wang F, Mi Z, Su S, Zhao H. Short-term solar irradiance forecasting model based on artificial neural network using statistical feature parameters. Energies 2012; 5(5):1355-1370.

[20] Wang H, Cai R, Zhou B, Aziz S, Qin B, Voropai N, Barakhtenko E. Solar irradiance forecasting based on direct explainable neural network. Energy Conversion and Management 2020; 226: 113487.

[21] Husein M, Chung IY. Day-ahead solar irradiance forecasting for microgrids using a long short-term memory recurrent neural network: A deep learning approach. Energies 2019; 12(10): 1856.

[22] Mutavhatsindi T, Sigauke C, Mbuvha R. Forecasting hourly global horizontal solar irradiance in South Africa using machine learning models. IEEE Access 2020; 8: 198872-198885.

[23] Singla P, Duhan M, Saroha S. A Hybrid Solar Irradiance Forecasting Using Full Wavelet Packet Decomposition and Bi-Directional Long Short-Term Memory (BiLSTM). Arabian Journal for Science and Engineering 2022; 1-27.

[24] Meng F, Zou Q, Zhang Z, Wang B, Ma H, Abdullah HM, Mohamed MA. An intelligent hybrid wavelet-adversarial deep model for accurate prediction of solar power generation. Energy Reports 2021; 7: 2155-2164.

[25] Guermoui M, Gairaa K, Boland J, Arrif T. A novel hybrid model for solar radiation forecasting using support vector machine and bee colony optimization algorithm: review and case study. Journal of Solar Energy Engineering 2021; 143(2).

[26] Huang X, Li Q, Tai Y, Chen Z, Zhang J, Shi J, Liu W. Hybrid deep neural model for hourly solar irradiance forecasting. Renewable Energy 2021; 171: 1041-1060.

[27] Farzanehdehkordi M, Ghaffaripour S, Tirdad K, Cruz AD, Sadeghian A. A wavelet feature-based neural network approach to estimate electrical arc characteristics. Electric Power Systems Research 2022; 208: 107893.

[28] Öner İV, Yeşilyurt MK, Yılmaz E. Wavelet Analysis Technique and Application Areas. Ordu University, Journal of Science and Technology 2017; 7: 42-56.

[29] Peng L, Wang L, Xia D, Gao. Effective energy consumption forecasting using empirical wavelet transform and long short-term memory. Energy 2022; 238: 121756.

[30] Osadchiy A, Kamenev A, Saharov V, Chernyi S. Signal processing algorithm based on discrete wavelet transform. Designs 2021; 5(3): 41.

[31] Nourani V, Komasi M, Mano A. A multivariate ANN-wavelet approach for rainfall–runoff modeling. Water resources management 2019; 23(14): 2877-2894.

[32] Alsafadi M, Filik ÜB. Hourly global solar radiation estimation based on machine learning methods in Eskısehır. Eskişehir Technical University Journal of Science and Technology A-Applied Sciences and Engineering 2020; *21*(2): 294-313.

[33] Kaysal A, Köroglu S, Oguz Y, Kaysal K. Artificial Neural Networks and Adaptive Neuro-Fuzzy Inference Systems Approaches to Forecast the Electricity Data for Load Demand, an Analysis of Dinar District Case. In 2018 2nd International Symposium on Multidisciplinary Studies and Innovative Technologies (ISMSIT) 2018; (pp. 1-6). IEEE.

[34] Partal T. Comparison of wavelet based hybrid models for daily evapotranspiration estimation using meteorological data. KSCE Journal of Civil Engineering 2016; 20(5): 2050-2058.

ESKİŞEHİR TECHNICAL UNIVERSITY JOURNAL OF SCIENCE AND TECHNOLOGY
A- APPLIED SCIENCES AND ENGINEERING

2023, 24(2), pp. 155-163, DOI: 10.18038/estubtda.1209564

RESEARCH ARTICLE

NONIC B-SPLINE APPROACH FOR ADVECTION DIFFUSION EQUATION

Emre KIRLI *

Department of Mathematics and Computer Science, Graduate School of Natural and Applied Sciences, Eskisehir Osmangazi University, Eskişehir, Türkiye

ABSTRACT

In this paper, a highly accurate method is introduced to achieve the numerical solution of the advection diffusion equation (ADE). This approach contains collocation technique based on nonic B-spline functions in the spatial-domain discretization and Adams Moulton scheme in the temporal-domain discretization. Two test problems are studied to validate effectiveness of the new presented method and efficiency of the approximate results are tested by calculating rate of temporal-convergence and error norm L_∞ for the suggested method. The obtained numerical results are compared in the tables by the other available studies in literature and it is observed that a better approximate solution is provided than the existing methods.

Keywords: Nonic B-spline, Advection diffusion equation, Collocation method

1. INTRODUCTION

ADE used to model a lot of real problems in physics and engineering is expressed in the following form:

$$w_t + \alpha w_x - \mu w_{xx} = 0, 0 \leq x \leq l \tag{1}$$

along with the boundary conditions (BCs)

$$\begin{matrix} w(0,t) = w(l,t) = 0 \\ w_x(0,t) = w_x(l,t) = 0 \end{matrix}, t \in [0,T] \tag{2}$$

and the initial condition (IC)

$$w(x,0) = \psi(x), 0 \leq x \leq l \tag{3}$$

where α and μ denote the steady uniform fluid velocity and the constant diffusion coefficient, respectively.

Numerous techniques have been implemented to ADE to solve it numerically so far including Finite difference method (FDM) [1-3], least-squares method [4], Taylor-Galerkin technique [5], cubic B-spline differential quadrature method (CBSDQM) [6], extended cubic B-spline collocation method (ECBSCM) [7], differential quadrature method based on quartic and quintic B-splines [8], extended cubic B-spline Galerkin method (ECBSGM) [9], Galerkin method [10] and collocation technique based on fourth-order cubic B-spline [11].

*Corresponding Author: emre.26@windowslive.com
Received: 24.11.2022 Published: 21.06.2023

The main purpose in this paper is to investigate the approximate solution of ADE by the new approach. In this approach, ADE is fully discretized by employing nonic B-spline collocation technique in spatial direction and Adams Moulton method in temporal direction. What is notable in this work is that the use of nonic B-spline functions that have not been utilized before to achieve the numerical solution of ADE. The rest structure of the paper is as follows. In section 2, the temporal and spatial discretizations of ADE are performed. In section 3, two test problems are examined to see the efficiency and accuracy of the present method. A brief summary about main findings of the suggested method is presented in section 4.

2. APPLICATION OF THE PROPOSED METHOD

In this work, the analytical solution of the unknown function at the grid points is represented by

$$w(x_r, t_n) = w_r^n, r = 0,1,\dots,M; \quad n = 0,1,2,\dots$$

where $x_r = rh$, $t_n = n\Delta t$ and the approximate value of w_r^n is denoted by W_r^n.

2.1. Time Discretization

Considering ADE of the form

$$w_t = \mu w_{xx} - \alpha w_x \tag{4}$$

and employing the following two-step method

$$w^{n+1} = w^n + \Delta t(\theta_1 w_t^{n+1} + \theta_2 w_t^n + \theta_3 w_t^{n-1}) \tag{5}$$

we have the temporal discretization of the Eq. (4). Choosing the coefficients in (5) as

$$\theta_1 = \frac{1}{2}, \theta_2 = \frac{1}{2}, \quad \theta_3 = 0$$

gives Crank-Nicolson (CN) method having order two in time and then choosing the coefficients in (5) as

$$\theta_1 = \frac{5}{12}, \theta_2 = \frac{2}{3}, \quad \theta_3 = -\frac{1}{12}$$

yields the third-order implicit Adams Moulton method which is going to be used to discretizate the temporal domain. Using Eq. (5), the temporal discretization of the Equation (4) is obtained as

$$\begin{aligned} w^{n+1} - \theta_1 \Delta t(\mu w_{xx}^{n+1} - \alpha w_x^{n+1}) \\ = w^n + \theta_2 \Delta t(\mu w_{xx}^n - \alpha w_x^n) + \theta_3 \Delta t(\mu w_{xx}^{n-1} - \alpha w_x^{n-1}) \end{aligned} \tag{6}$$

2.2. Nonic B-spline Collocation Method

Let the spatial domain $[0, l]$ be splitted into uniformly M finite elements at the knots

$$0 = x_0 < x_1 < \cdots < x_M = l$$

where $h = x_r - x_{r-1}, \quad r = 1, \dots, M$. On this partition, the nonic B-splines $\varphi_r, \quad r = -4, \dots, M+4,$ have the following form:

$$\varphi_r(x) = \frac{1}{h^9} \begin{cases} \phi_1, & x_{r-5} \le x < x_{r-4}, \\ \phi_2, & x_{r-4} \le x < x_{r-3}, \\ \phi_3, & x_{r-3} \le x < x_{r-2}, \\ \phi_4, & x_{r-2} \le x < x_{r-1}, \\ \phi_5, & x_{r-1} \le x < x_r, \\ \phi_6, & x_r \le x < x_{r+1}, \\ \phi_7, & x_{r+1} \le x < x_{r+2}, \\ \phi_8, & x_{r+2} \le x < x_{r+3}, \\ \phi_9, & x_{r+3} \le x < x_{r+4}, \\ \phi_{10}, & x_{r+4} \le x < x_{r+5}, \\ 0 & \text{otherwise} \end{cases} \tag{7}$$

where

$\phi_1 = (x - x_{r-5})^9,$
$\phi_2 = h^9 + 9h^8(x - x_{r-4}) + 36h^7(x - x_{r-4})^2 + 84h^6(x - x_{r-4})^3 + 126h^5(x - x_{r-4})^4$
$+126h^4(x - x_{r-4})^5 + 84h^3(x - x_{r-4})^6 + 36h^2(x - x_{r-4})^7 + 9h(x - x_{r-4})^8$
$-9(x - x_{r-4})^9,$
$\phi_3 = 502h^9 + 2214h^8(x - x_{r-3}) + 4248h^7(x - x_{r-3})^2 + 4536h^6(x - x_{r-3})^3$
$+2772h^5(x - x_{r-3})^4 + 756h^4(x - x_{r-3})^5 - 168h^3(x - x_{r-3})^6 - 216h^2(x - x_{r-3})^7$
$-72h(x - x_{r-3})^8 + 36(x - x_{r-3})^9,$
$\phi_4 = 14608h^9 + 36414h^8(x - x_{r-2}) + 34272h^7(x - x_{r-2})^2 + 11256h^6(x - x_{r-2})^3$
$-4032h^5(x - x_{r-2})^4 - 4284h^4(x - x_{r-2})^5 - 672h^3(x - x_{r-2})^6$
$+ 504h^2(x - x_{r-2})^7$
$+252h(x - x_{r-2})^8 - 84(x - x_{r-2})^9,$
$\phi_5 = 88234h^9 + 101934h^8(x - x_{r-1}) + 5544h^7(x - x_{r-1})^2 - 36456h^6(x - x_{r-1})^3$
$-10836h^5(x - x_{r-1})^4 + 5796h^4(x - x_{r-1})^5 + 2856h^3(x - x_{r-1})^6$
$-504h^2(x - x_{r-1})^7 - 504h(x - x_{r-1})^8 + 126(x - x_{r-1})^9,$
$\phi_6 = 156190h^9 - 88200h^7(x - x_r)^2 + 23940h^5(x - x_{r-1})^4 - 4200h^3(x - x_r)^6$
$+603h(x - x_r)^8 - 126(x - x_r)^9,$
$\phi_7 = 88234h^9 - 101934h^8(x - x_{r+1}) + 5544h^7(x - x_{r+1})^2 + 36456h^6(x - x_{r+1})^3$
$-10836h^5(x - x_{r+1})^4 - 5796h^4(x - x_{r+1})^5 + 2856h^3(x - x_{r+1})^6$
$+504h^2(x - x_{r+1})^7 - 504h(x - x_{r+1})^8 + 84(x - x_{r+1})^9,$
$\phi_8 = 14608h^9 - 36414h^8(x - x_{r+2}) + 34272h^7(x - x_{r+2})^2 - 11256h^6(x - x_{r+2})^3$
$-4032h^5(x - x_{r+2})^4 + 4284h^4(x - x_{r+2})^5 - 672h^3(x - x_{r+2})^6$
$- 504h^2(x - x_{r+2})^7$
$+252h(x - x_{r+2})^8 - 36(x - x_{r+2})^9,$
$\phi_9 = 502h^9 - 2214h^8(x - x_{r+3}) + 4248h^7(x - x_{r+3})^2 - 4536h^6(x - x_{r+3})^3$
$+2772h^5(x - x_{r+3})^4 - 756h^4(x - x_{r+3})^5 - 168h^3(x - x_{r+3})^6 + 216h^2(x - x_{r+3})^7$
$-72h(x - x_{r+3})^8 + 9(x - x_{r+3})^9,$
$\phi_{10} = [h - (x - x_{r+4})]^9.$
The set of nonic B-spline functions

$$\{\varphi_{-4}(x), \varphi_{-3}(x), \ldots, \varphi_{M+3}(x), \varphi_{M+4}(x)\}$$

generates a basis over the spatial domain $[0, l]$. The global approximate solution $W(x,t)$ corresponding to the analytical solution $w(x,t)$ is expressed as a combination of separable solution of the nonic B-spline spatial terms $\varphi_j(x)$ and temporal terms $\delta_j(t)$ as

$$W(x,t) = \sum_{j=-4}^{M+4} \delta_j \varphi_j \tag{8}$$

where temporal term $\delta_j(t)$ is going to be determined by means of the collocation procedure. Since each subinterval $[x_{r-1}, x_r]$ is covered by ten B-splines, the approximate solution and its first two derivatives at the knots x_r are calculated in terms of temporal terms $\delta_j(t)$ using (7) and (8) as

$$\begin{aligned} W_r &= \delta_{r-4} + 502\delta_{r-3} + 14608\delta_{r-2} + 88234\delta_{r-1} + 156190\delta_r + 88234\delta_{r+1} + 14608\delta_{r+2} + 502\delta_{r+3} + \delta_{r+4}, \\ W_r' &= \frac{9}{h}(-\delta_{r-4} - 246\delta_{r-3} - 4046\delta_{r-2} - 11326\delta_{r-1} + 11326\delta_{r+1} + 4046\delta_{r+2} + 246\delta_{r+3} + \delta_{r+4}), \\ W_r'' &= \frac{72}{h^2}(\delta_{r-4} + 118\delta_{r-3} + 952\delta_{r-2} + 154\delta_{r-1} - 2450\delta_r + 154\delta_{r+1} + 952\delta_{r+2} + 118\delta_{r+3} + \delta_{r+4}). \end{aligned} \tag{9}$$

Substituting (9) into (6), the fully-discretization of ADE is obtained as

$$\begin{aligned} &\delta_{r-4}^{n+1}(1 + a_1 - a_2) + \delta_{r-3}^{n+1}(502 + 118a_1 - 246a_2) + \delta_{r-2}^{n+1}(14608 + 952a_1 - 4046a_2) + \\ &\delta_{r-1}^{n+1}(88234 + 154a_1 - 11326a_2) + \delta_r^{n+1}(156190 - 2450a_1) + \delta_{r+1}^{n+1}(88234 + 154a_1 + 11326a_2) + \\ &\delta_{r+2}^{n+1}(14608 + 952a_1 + 4046a_2) + \delta_{r+3}^{n+1}(502 + 118a_1 + 246a_2) + \delta_{r+4}^{n+1}(1 + a_1 + a_2) \\ &= W_r^n + a_3(W'')_r^n + a_4(W')_r^n + a_5(W'')_r^{n-1} + a_6(W')_r^{n-1}, \quad 0 \le r \le M \end{aligned} \tag{10}$$

where

$$a_1 = -\theta_1 \Delta t \mu \frac{72}{h^2}, \quad a_2 = \theta_1 \Delta t \alpha \frac{9}{h}, \quad a_3 = \theta_2 \Delta t \mu \frac{72}{h^2},$$

$$a_4 = -\theta_2 \Delta t \alpha \frac{9}{h}, \quad a_5 = \theta_3 \Delta t \mu \frac{72}{h^2}, \quad a_6 = -\theta_3 \Delta t \alpha \frac{9}{h}.$$

Hence, we get a linear system (10) consisting of $M + 1$ algebraic equations in $M + 9$ unknowns $(\delta_{-4}^{n+1}, \ldots, \delta_{N+4}^{n+1})$. Using BCs (2) and the following additional BCs

$$\begin{aligned} w_{xx}(0,t) &= 0 \quad w_{xx}(l,t) = 0 \\ w_{xxx}(0,t) &= 0 \quad w_{xxx}(l,t) = 0, \end{aligned}$$

the variables

$$\delta_{-4}^{n+1}, \delta_{-3}^{n+1}, \delta_{-2}^{n+1}, \delta_{-1}^{n+1}, \delta_{M+1}^{n+1}, \delta_{M+2}^{n+1}, \delta_{M+3}^{n+1} \text{ and } \delta_{M+4}^{n+1}$$

are eliminated from the above system. Thus, the system is reduced to solvable matrix system of $(M + 1) \times (M + 1)$ dimension. In order to commence iterative computation, the initial vector

$$\delta^0 = (\delta_{-4}^0, \ldots, \delta_{M+4}^0)^T$$

is first computed using ICs, BCs and additional BCs. After getting the initial vector δ^0 , the unknown vector

$$\delta^1 = (\delta^1_{-4}, \dots, \delta^1_{M+4})$$

is obtained by making use of CN method. Thus, the unknown vectors

$$\delta^{n+1} = (\delta^{n+1}_{-4}, \dots, \delta^{n+1}_{M+4})^T (n = 1,2, \dots)$$

at any desired time level can be computed repeatedly by solving the recurrence relation two precious δ^n and δ^{n-1}.

3. NUMERICAL EXPERIMENTS

In this section, two test problem are examined to illustrate the efficiency and applicability of the suggested method. Accuracy of solution is tested by measuring error norm L_∞

$$L_\infty = \max_m |w_m - W_m| \tag{11}$$

and the order of temporal convergence is calculated by the formula

$$\text{order}=\frac{log\left|\frac{(L_\infty)_{\Delta t_i}}{(L_\infty)_{\Delta t_{i+1}}}\right|}{log\left|\frac{\Delta t_i}{\Delta t_{i+1}}\right|} \tag{12}$$

where $(L_\infty)_{\Delta t_i}$ is the error norm L_∞ for time step Δt_i.

3.1. Problem 1

Consider pure advection problem obtained by taking $\mu = 0$. The analytical solution of this problem is given by

$$w(x,t) = 10\, exp\left(-\frac{(x - \tilde{x}_0 - \alpha t)^2}{2\rho^2}\right). \tag{13}$$

The numerical computation is performed by choosing flow velocity $\alpha = 0.5 m/s$, initial peak location $\tilde{x}_0 = 2km$, $\rho = 264$ in the spatial domain $[0,9000]$ until the terminating time $t = 9600s$. In this case, the wave which is initially located at $\tilde{x}_0 = 2km$ with its peak moves to the right along a channel maintaining its initial shape and size by the time $t = 9600s$. The suggested program is running until the time $t = 9600s$ and the figures of initial solution and waves at various time levels are presented in Figure 1 with $h = 60, \Delta t = 1$. It can be observed from Figure 1 that wave preserves its initial state while moving to the right. Thus, the initial wave moves 4.8 km from the initial position and the peak of the wave remains stable 10 in progress of time. The graph of absolute error at $t = 9600s$ is also given in Figure 2 which shows that the influence of BCs can be neglected.

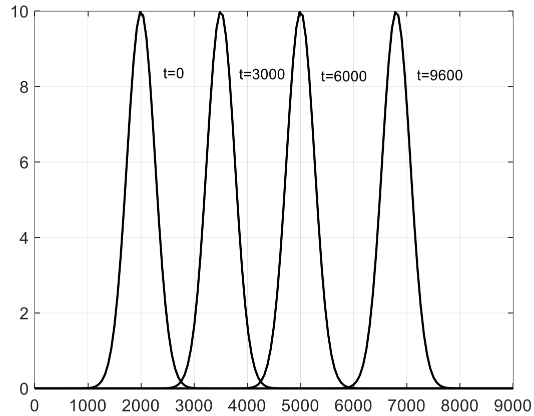

Figure 1. Waves at $t = 0,3000,6000,9600$.

The error norms L_∞ are listed in Table 1 to make a comparison with previous studies given in [4,7,9]. The obtain results confirm that the suggested method gives better results then the other methods. Also, the order of temporal convergence is calculated for $h = 100$ and different temporal steps Δt_i . The calculated order of convergence along with error norm is listed in Table 2. As expected from the theoretical results, the order of the temporal convergence is three.

Table 1. Comparison of L_∞ at time $t = 9600$

Method	h	Δt	L_∞
Proposed	200	50	4.56×10^{-2}
Proposed	100	50	1.93×10^{-2}
Proposed	50	50	1.94×10^{-2}
[9]	200	50	2.18×10^{-1}
[9]	100	50	1.90×10^{-1}
[9]	50	50	1.90×10^{-1}
[7]	200	50	1.29
[7]	100	50	3.25×10^{-1}
[7]	50	50	1.98×10^{-1}
[4]	200	50	5.18×10^{-1}
[4]	100	50	3.76×10^{-1}
[4]	50	50	3.73×10^{-1}

Table 2. The error norms and temporal order of convergence with $h = 100$ at $t = 9600$

Δt_i	Order	L_∞
100	-	1.63×10^{-1}
50	3.07	1.95×10^{-2}
25	3.01	2.41×10^{-3}
12.5	3.00	3.01×10^{-4}

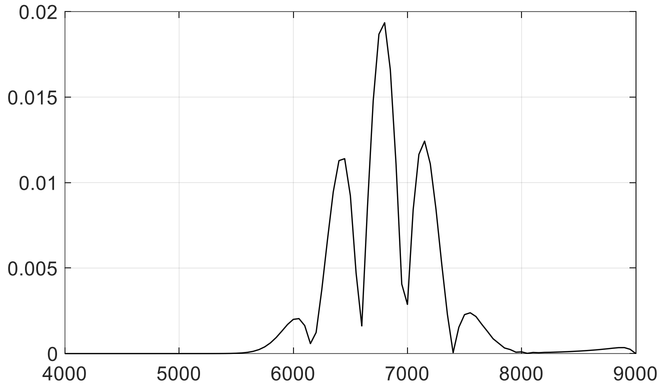

Figure 2. Absolute error for Problem 1 with h=$\Delta t = 50$.

3.2. Problem 2

The analytical solution of this problem, modeling fade out of an initial bell shaped concentration of height 1, is

$$w(x,t) = \frac{1}{\sqrt{4t+1}} exp\left(-\frac{(x-\tilde{x}_0-\alpha t)^2}{\mu(4t+1)}\right) \tag{13}$$

The initial wave forms the peak of which is initially located at $\tilde{x}_0$, moves to the right along x axis as time progresses.

The computation is carried out by taking the parameters $\alpha = 0.8$ m/s and $\mu = 0.005$ m^2/s . Table 3 gives the comparison of L_∞ error norms with $\Delta t = 0.0125$. It can be seen from the Table 3 that our method produces better results than the methods given in Method I [6] and [9]. But the result of Method II [6] is a bit better than the result of the present method for $h = 0.025$. The order of convergence and L_∞ error norms are listed Table 4. It is seen from Table 4 that when time step size is reduced from 0.01 to 0.00125, the order of temporal convergence approaches to three.

Table 3. Comparison of L_∞ at time $t = 5$ with $0 \le x \le 9$

h	Proposed	[9]	Method I [6]	Method II [6]
0.2	1.36×10^{-1}	1.33×10^{-1}	1.25×10^{-1}	1.36×10^{-1}
0.1	4.01×10^{-3}	4.23×10^{-3}	6.96×10^{-3}	1.46×10^{-2}
0.05	3.94×10^{-5}	8.43×10^{-4}	1.21×10^{-4}	2.89×10^{-4}
0.025	3.98×10^{-5}	8.43×10^{-4}	3.07×10^{-4}	1.81×10^{-5}

Table 4. The error norms and temporal order of convergence with $h = 0.01$ at $t = 5$.

Δt_i	Order	L_∞
0.01	-	2.04×10^{-5}
0.005	3.00	2.55×10^{-6}
0.0025	3.00	3.19×10^{-7}
0.00125	3.00	3.98×10^{-8}

Figure 3 shows the behaviour of numerical solutions up to time $t = 5$ over the spatial interval [0,9] with $h = \Delta t = 0.001$. Figure 4 gives the graph of the absolute error with $h = 0.01, \Delta t = 0.00125$ at time $t = 5$. It can be seen from Figure 4 that maximum error appears at about the peak of the final wave. Thus, it can be said that the there is no problem in applying BCs.

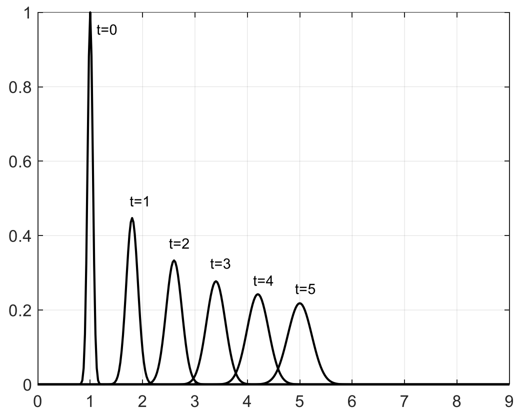

Figure 3. Waves at $t = 0,1,2,3,4,5$.

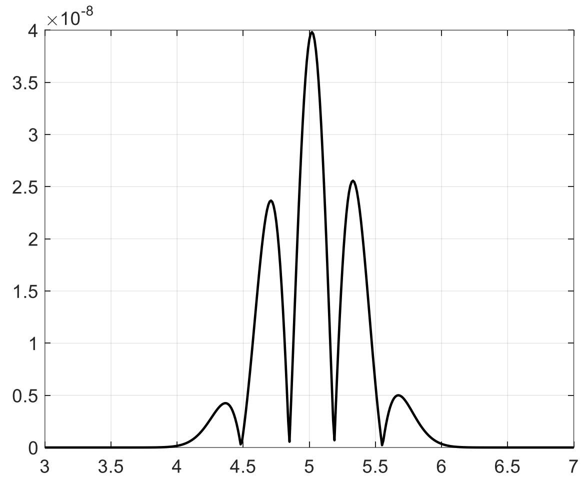

Figure 4. Absolute error for Problem 2 with $h = 0.01, \Delta t = 0.00125$ at $t = 5$.

4. CONCLUSION

In this paper, nonic B-spline collocation technique in collaboration with Adams Moulton method has been proposed to get approximate solution of ADE. To show the effectiveness of the present method, two test problems are used by computing error norms L_∞ and compared with the results existing in the literature. The results obtained by the present method is found to be better than the existed studies given in [4,6,7,9]. The order of temporal convergence is calculated numerically, which agrees with theoretical rate. Consequently, nonic B-spline functions can be applied to obtain approximate solution of the high order nonlinear partial differential equations.

CONFLICT OF INTEREST

The author stated that there are no conflicts of interest regarding the publication of this article.

REFERENCES

[1] Dehghan M. Weighted finite difference techniques for the one-dimensional advection-diffusion equation. Appl Math Comput 2004; 147: 307-319.

[2] Sari M, Güraslan G, Zeytinoglu A. High-Order finite difference schemes for solving the advection-diffusion equation. Math Comput Appl 2010; 15 (3): 449-460.

[3] Mohebbi A, Dehghan M. High-order compact solution of the one-dimensional heat and advection-diffusion equations. Appl Math Model 2010; 34: 3071-3084.

[4] Dağ İ, Irk D, Tombul M. Least-squares finite element method for the advection diffusion equation. Appl Math Comput 2006; 173: 554-565.

[5] Dağ İ, Canıvar A, Şahin A. Taylor-Galerkin method for advection-diffusion equation. Kybernetes 2011; 40: 762-777.

[6] Korkmaz A, Dağ İ. Cubic B-spline differential quadrature methods for the advection-diffusion equation. Int J Numer Method H, 2012; 22:1021-1036.

[7] Irk D, Dağ İ, Tombul M. Extended cubic B-spline solution of the advection-diffusion equation. KSCE Journal of Civil Engineering 2015; 19(4): 929-934.

[8] Korkmaz A, Dağ İ. Quartic and quintic B-spline methods for advection diffusion equation. Appl Math Comput 2016; 274: 208-219.

[9] Zorşahin Görgülü M, Dağ İ, Dogan S, Irk D. A numerical solution of the Advection-Diffusion equation by using extended cubic B-Spline functions. AUBTD-A 2018; 19(2): 347-355.

[10] Zorşahin Görgülü M, Irk D. The Galerkin finite element method for advection diffusion equation. Sigma J Eng & Nat Sci 2019; 37(1): 119-128.

[11] Mittal, RC, Rohila, R. The numerical study of advection-diffusion equations by the fourth-order cubic B-spline collocation method. Math Sci 2020; 14: 409-423.